Phenomenology of Higgs bosons in the various extensions of the Standard Model

Takashi Kasai

DOCTOR OF SCIENCE

Department of Accelerator Science
School of Mathematical and Physical Science
The Graduate University for Advanced Studies

2000

Abstract

In the Standard Model (SM) of the perticle physics, the existence of the Higgs boson is predicted as a consequence of including mass of the particles. Experimental search for the Higgs boson has been continued at the Run-II of the Tevatron experiment. If the Higgs boson is discovered, we can test the SM and distinguish models of new physics at high energy scales by checking the mass and various properties of the Higgs boson. The purpose of this paper is to clarify allowed properties of the Higgs boson in various models beyond the SM, e.g. two-Higgs-doublet model (2HDM) with a softly-broken discrete symmetry, Zee-Model which requires the existence of a SU(2) charged Higgs singlet in order to generate the small neutrino mass, and Minimal Super-symmetric Standard Model (MSSM). The possible range of the Higgs boson mass (m_h) for each model is obtained by demanding the considered theory to be a valid effective theory all the way up to some cut-off energy scale (Λ). In the SM, the allowed Higgs boson mass is 143-175 GeV, if the cut-off scale is taken as the Planck scale (10^{19} GeV) and $m_t = 175$ GeV. For both of the 2HDM and the Zee-Model, the mass upper bound is same as that of the SM, whereas the lower bound is considerably reduced. It is given by about 100 GeV in the decoupling regime where only one neutral Higgs boson is light as compared to the other physical states of the Higgs boson. In the mixing regime, m_h is no longer bounded from below. Thus, if the Higgs boson is discovered with the mass around 100 GeV in near future, the 2HDM and the Zee-Model with very high cut-off scale are another candidates of models which predict such light Higgs boson along with the MSSM of which mass upper bound is about 120 GeV. The 2HDM and the Zee-Model might be distinguished each other by the partial decay width of $h \to \gamma\gamma$ or the charged Higgs boson decay into a lepton pair.

Contents

Chapter 1

Introduction

The Standard Model (SM) of the particle [1] was successful in giving mass to some gauge bosons and fermions through the mechanism of electroweak gauge-symmetry breaking. In consequence, the existence of the Higgs boson was predicted. After the discovery of the top quark, the Higgs sector is the last remaining part yet to be confirmed in the SM. Experimental search for the Higgs boson has been continued at the Fermilab Tevatron experiments. Current experimental lower bound of Higgs boson mass is given by CERN LEP-II experiments; the Higgs boson with the mass less than about 110 GeV has been excluded, if its production cross section and decay modes are similar to that of the SM Higgs boson[2]. The Run-II of the Tevatron can be sensitive to a SM-like Higgs boson with mass up to about 180 GeV, provided that the integrated luminosity of the collider is large enough (about $30\,\mathrm{fb}^{-1}$) [3]. Furthermore, the primary goal of the CERN LHC experiments is to guarantee the discovery of a SM-like Higgs boson for its mass as large as about 1 TeV[4], which is the upper bound of the SM Higgs boson mass. (For a Higgs boson mass beyond this value, the SM is no longer a consistent low-energy effective theory.)

Discovery of the Higgs particle is important not only in confirming the mechanism of the electroweak gauge-symmetry breaking but also in providing us useful information on physics beyond the SM. When the Higgs boson is discovered, its mass and various decay properties will be measured to test the SM and to distinguish models of new physics at high energy scales. In this thesis we discuss the properties of the Higgs boson in various extensions of the SM.

The most interesting property of the Higgs boson is its mass value. For each model, we can obtain the mass bounds by demanding the considered theory to be a valid effective theory all the way up to some cut-off energy scale (Λ); by using renormalization group equations (RGE's) and requiring the vacuum stability and the validity of perturbation theory below a given cut-off scale Λ, we can determine the lower and the upper bounds of the Higgs boson mass as a function of Λ, respectively.

Allowed region of the Higgs boson and the top quark masses in the SM was examined in ref. [5]. The prediction of the SM Higgs boson mass is $143 - 175$ GeV, if the SM is precisely valid and any new particles do not appear up to Planck scale. If the Higgs boson is discovered with small mass as currently searched, it suggests that there is new physics beyond the SM at high energy scale and the SM appears as a low energy effective theory.

The Minimal Super-symmetric Standard Model (MSSM) is most popular in the particle models beyond the SM. In the MSSM, the Higgs boson self couplings is determined by SUSY relation at $m_{\rm stop}$. Therefore, the mass range do not depend on Λ. The theoretical upper bound on the lightest CP-even Higgs boson mass is given by about 120 GeV for $m_t = 175$ GeV and $m_{\rm stop} = 1$ TeV [6, 7, 8].

We investigate also the lightest CP-even Higgs-boson mass for the two-Higgs-doublet model (2HDM) with soft-breaking terms [10]. The upper bound of the lightest Higgs boson mass is almost the same as that in the SM. Whereas the lower bound is much reduced in comparison with that in the SM. For example in the decoupling regime where only one neutral Higgs boson is light as compared to the other physical states of Higgs bosons, for $\Lambda = 10^{19}$ GeV and $m_t = 175$ GeV, while the upper bound is about 175 GeV, which is almost the same as that in the SM, the lower bound is given by 100 GeV. This is considerably smaller than the similar lower bound in the SM. For the region of the small soft-breaking mass, the lower and upper bounds are proportional to the soft-breaking mass and these are no longer bounded from below in the case without the soft-breaking mass.

Next, the Higgs boson mass bounds for the Zee-Model is investigated [11]. This model is an extension of the SM to incorporate the small masses of the neutrinos suggested by data [12]. In this model, the three different flavor neutrinos are massless at the tree level, and their small masses are induced radiatively through one-loop diagrams. The Higgs

sector of the Zee-model is similar to that of the 2HDM except for the existence of an additional weak-singlet charged Higgs field, so that the physical scalar-bosons include two CP-even, one CP-odd and two pairs of charged Higgs bosons. We show that the upper and lower mass bounds for h are almost the same as those in the 2HDM.

For the Zee-Model, although the allowed mass range is same as that of the 2HDM, the singlet charged Higgs boson can significantly modify the partial decay width of $h \rightarrow$ via radiative corrections, and its collider phenomenology can also be drastically different from that of the charged Higgs bosons in the usual 2HDMs.

This thesis is organized as follows. In Chapter 2, we review the Higgs sector in the SM, and the mass bounds in the MSSM is also mentioned. In Chapter 3, we discuss mass bounds of the Higgs boson for the 2HDM. In Chapter 4, mass bound and other phenomenology of Higgs bosons for the Zee-model are discussed. In Chapter 5, we present our conclusion. Relevant RGE's and so on are collected in Appendix.

Chapter 2

Higgs boson

2.1 The Higgs mechanism

The Higgs mechanism is proposed in order to explain the existence of massive gauge particles, like W-boson and Z-boson [13].

In the QED, the massless gauge boson which interacts with the fermions is lead by requiring the $U(1)$ local gauge invariance on the kinetic term of the fermion. The QED Lagrangian is written as,

$$\mathcal{L}_{QED} = i^{-} \ ^{\mu} D_{\mu} \ - m^{-} \ - \frac{1}{4} F_{\mu\nu}^{2}, \tag{2.1}$$

where $D_\mu = \partial_\mu - ieA_\mu$ and is the fermion field and A_μ is the $U(1)$ gauge field. This Lagrangian is invariant under the local $U(1)$ gauge transformation,

$$(x) \ \rightarrow \ e^{i\alpha(x)} \ (x) \tag{2.2}$$

$$A(x) \ \rightarrow \ A(x) + \frac{1}{e}\partial_\mu \alpha(x). \tag{2.3}$$

But if we try to introduce the gauge boson mass term $\mathcal{L}_{m_A} = \frac{1}{2} m_A^2 A_\mu A^\mu$ for the extension to the massive gauge boson case, it unfortunately causes a problem of a violation of the $U(1)$ local gauge symmetry.

In the SM, without such a violation of the gauge symmetry, the gauge bosons gain mass through the Higgs mechanism which introduce the Higgs field ϕ. We first consider

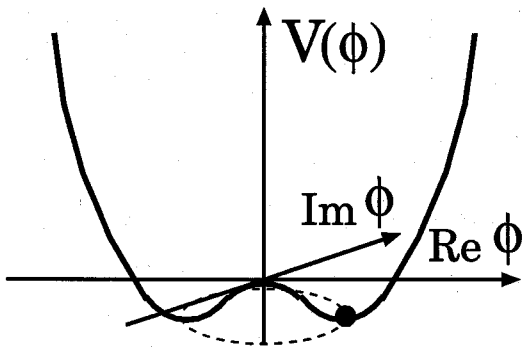

Figure 2.1: Higgs potential V. The ϕ has expectation value at the minimum of V.

$U(1)$ case. The Lagrangian of the Higgs sector is

$$\mathcal{L}_\phi = |D_\mu \phi|^2 - V(\phi), \tag{2.4}$$

where V is the Higgs potential. V is assumed to be

$$V(\phi) = m^2 |\phi|^2 + \lambda |\phi|^4, \tag{2.5}$$

where $m^2 < 0$, $\lambda > 0$. The shape of V is shown as Figure 2.1. This Lagrangian is invariant under the $U(1)$ local gauge transformation,

$$\phi \to e^{i\alpha(x)} \phi. \tag{2.6}$$

Because the potential has the minimum at $\phi = -\frac{m^2}{2\lambda}$, the symmetry around $\phi = 0$ is spontaneously broken and the ϕ has the vacuum expectation value,

$$\langle \phi \rangle \equiv \frac{v}{\sqrt{2}} = -\frac{m^2}{2\lambda}. \tag{2.7}$$

We can set v as real without loss of generality. By substituting $\phi = \frac{1}{\sqrt{2}}(v + x + iy)$ into the Higgs sector in the Lagrangian (eq. (2.4)), we obtain

$$\mathcal{L}_{kin} = \frac{1}{2}(\partial_\mu x)^2 + \frac{1}{2}(\partial_\mu y)^2 - evA_\mu \partial^\mu y + \frac{1}{2}e^2 v^2 A_\mu A^\mu + \cdots \tag{2.8}$$

$$V = \frac{1}{2}\left(2\lambda v^2\right) x^2 + \cdots, \tag{2.9}$$

where $\mathcal{L}_{kin}$ is the kinetic term of ϕ. From the kinetic terms, we extract the mass term of the gauge boson

$$\mathcal{L}_{mass_A} = \frac{1}{2} m_A^2 A_\mu A^\mu, \tag{2.10}$$

where

$$m_A^2 = ev. \tag{2.11}$$

And in the V, we find the mass term of field x. Its mass square is

$$m_h^2 = 2\lambda v^2. \tag{2.12}$$

The field x represents the physical Higgs boson of which mass is $\sqrt{2\lambda v^2}$. On the other hand, although the field y represents the massless Goldstone boson [14], we can delete the field y by suitable gauge transformation.

Thus, through the Higgs mechanism, the gauge boson can have mass without conflict with the gauge symmetry. After the spontaneous symmetry breaking, one component of the complex field ϕ becomes the physical Higgs boson and another becomes a longitudinal polarization of the massive gauge boson A_μ.

2.2 The Higgs sector in the Standard Model

In this section, the Higgs sector in the SM[1] is reviewed. In order to give a unified description of the electro-magnetic and the weak force, $SU(2)\times U(1)$ local gauge symmetry on the Lagrangian is assumed in the SM. Although for the color interaction the $SU(3)$ local gauge symmetry is also assumed in the SM, we neglect this sector in the discussion below, for simplicity.

In the SM the total Lagrangian $\mathcal{L}_{SM}$ is written as

$$\mathcal{L}_{SM} = \mathcal{L}_{kin} - V(\phi) + \mathcal{L}_{Yukawa} \tag{2.13}$$

where $\mathcal{L}_{kin}$ is kinetic terms which are given by

$$\begin{aligned}
\mathcal{L}_{kin} &= |D_\mu \phi|^2 \\
&\quad + i\overline{q_L}\ {}^{\mu}D_\mu q_L + i\overline{u_R}\ {}^{\mu}D_\mu u_R + i\overline{d_R}\ {}^{\mu}D_\mu d_R \\
&\quad + i\overline{l_L}\ {}^{\mu}D_\mu l_L + i\overline{\mathrm{e_R}}\ {}^{\mu}D_\mu \mathrm{e_R} \\
&\quad - \sum_{a=SU(2)U(1)} \frac{1}{4} F_{\mu\nu}^{a^2}.
\end{aligned} \tag{2.14}$$

In the above equation, q_L is the left-handed quark doublet with an implicit generation index while u_R and d_R denote the right-handed singlet quarks. Similarly, l_L and e_R denote the left-handed and right-handed leptons in three generations. The covariant derivative D_μ is taken as

$$D_\mu = \partial_\mu - ig_2 A_\mu^a T^a - ig_1 B_\mu \frac{Y}{2} \tag{2.15}$$

where, T^a and Y are generator of $SU(2)$ and $U(1)$ respectively. The $F_{\mu\nu}^a$ is defined as,

$$F_{\mu\nu}^a = \partial_\mu A_\nu^a - \partial_\nu A_\mu^a + g f^{abc} A_\mu^b A_\nu^c. \tag{2.16}$$

Higgs potential $V(\phi)$ is assumed as follows,

$$V(\phi) = m^2 |\phi|^2 + \lambda |\phi|^4, \tag{2.17}$$

where λ and m^2 are real parameters. We assume $m^2 < 0$ and $\lambda > 0$. The Higgs doublet consists of two components as $\phi = \begin{pmatrix} \phi^0 \\ \phi^- \end{pmatrix}$, and $\tilde{\phi} \equiv (i\tau_2)\,\phi^*$.

The Lagrangian is invariant under the gauge transformation

$$\phi \rightarrow e^{i\alpha(x)^a T^a + i\beta(x) Y} \phi \tag{2.18}$$

$$\rightarrow e^{i\alpha(x)^a T^a + i\beta(x) Y} \tag{2.19}$$

$$A_\mu^a \rightarrow A_\mu^a + \frac{1}{g_2}\partial_\mu \alpha^a(x) + f^{abc} A_\mu^b \alpha^c(x) \tag{2.20}$$

$$B_\mu \rightarrow B_\mu + \frac{2}{g_1}\partial_\mu \beta(x) \tag{2.21}$$

where $SU(2)$ and $U(1)$ charges of the particles are shown in Table 2.1.

Assuming that the ϕ has the vacuum expectation value

$$\langle \phi \rangle = \frac{1}{\sqrt{2}} \begin{pmatrix} v \\ 0 \end{pmatrix}, \tag{2.22}$$

the gauge bosons gain mass, meanwhile the Higgs boson appears. By substituting the vacuum expectation value $\langle \phi \rangle$ into the kinetic term of ϕ, the mass term of the weak boson $W^\pm$, Z is lead. The charged vector boson $W^\pm$ has mass

$$M_W = \frac{1}{2} v g_2 \tag{2.23}$$

and the neutral vector boson Z has mass

$$m_Z = \frac{1}{2} v \sqrt{g_1^2 + g_2^2}. \tag{2.24}$$

In the Higgs potential, the Higgs boson mass square is found as

$$m_h^2 = 2\lambda v^2. \tag{2.25}$$

Before the spontaneous symmetry breaking, the ϕ consists of four components. After it, one component becomes physical Higgs boson and remaining three components become longitudinal polarization of the massive gauge boson W_μ^+, W_μ^- and Z_μ. In the above, the vacuum expectation value v is about 246 GeV, which is lead from the measurement of the Fermi coupling.

$\mathcal{L}_{Yukawa}$ is the Yukawa coupling term. In the $SU(2) \times U(1)$ theory, the fermion mass term of the QED, *i.e.* $-m\overline{\quad} = -m\overline{\quad}\left\{\frac{1}{2}(1- \ _5) + \frac{1}{2}(1+ \ _5)\right\} = -m\left(\overline{\quad}_R \ _L + \overline{\quad}_L \ _R\right)$ violates the gauge symmetry, because $\ _L$ is a $SU(2)$ doublet whereas $\ _R$ is a $SU(2)$ singlet. In the SM, so that the gauge invariance of the fermion mass term is conserved, the interaction between the fermion and the Higgs field is introduced. The coupling is called the Yukawa coupling. The Yukawa coupling terms in the SM are given by,

$$\mathcal{L}_{\text{Yukawa}} = \overline{d_{R_i}} \left(y_D V_{CKM}^\dagger\right)_{ij} \tilde{\phi}^\dagger q_{L_j} + \overline{u_{R_i}} (y_U)_{ii} \phi^\dagger q_{L_i} + \overline{e_{R_i}} (y_E)_{ii} \tilde{\phi}^\dagger l_{L_i} + h.c., \tag{2.26}$$

where y_U,y_D,y_E are diagonal Yukawa matrices and V_{CKM} is the Cabibbo-Kobayashi-Maskawa (CKM) matrix. By introducing the vacuum expectation value of ϕ, the Yukawa coupling terms tern into the fermion mass terms.

$$\mathcal{L}_{m_f} = \overline{d_{R_i}} \left(y_D V_{CKM}^\dagger\right)_{ij} d_{L_j} + \overline{u_{R_i}} (y_U)_{ii} u_{L_i} + \overline{e_{R_i}} (y_E)_{ii} e_{L_i} + h.c., \tag{2.27}$$

Later, we shall only keep the top Yukawa coupling constants $y_t = (y_U)_{33}$ in our numerical evaluation of the RGE's.

Thus, through the Higgs mechanism, the gauge boson can have mass without conflict with the gauge symmetry in the SM, and the existence of the Higgs boson is predicted.

Table 2.1: SU(2) and U(1) charges of particles in the SM where $Q = T^3 + \frac{Y}{2}$

	Q	T	T^3	Y
ν_L	0	$\frac{1}{2}$	$\frac{1}{2}$	-1
e_L	-1	$\frac{1}{2}$	$-\frac{1}{2}$	-1
e_R	-1	0	0	-2
u_L	$\frac{2}{3}$	$\frac{1}{2}$	$\frac{1}{2}$	$\frac{1}{3}$
d_L	$-\frac{1}{3}$	$\frac{1}{2}$	$-\frac{1}{2}$	$\frac{1}{3}$
u_R	$\frac{2}{3}$	0	0	$\frac{4}{3}$
d_R	$-\frac{1}{3}$	0	0	$-\frac{2}{3}$
ϕ^0	0	$\frac{1}{2}$	$\frac{1}{2}$	-1
ϕ^-	-1	$\frac{1}{2}$	$-\frac{1}{2}$	-1

2.3 The Higgs boson search

Let me summarize current states of the experimental Higgs boson search. Although the electroweak gauge symmetry breaking mechanism in the SM is successful in giving a supreme description of the electro-magnetic and the weak interaction, the Higgs sector is still unexplored experimentally. After the discovery of the top quark, the Higgs sector is the last remaining part yet to be confirmed in the SM. If the Higgs boson is discovered, we obtain the evidence of the SM. Experimental search for the Higgs boson has been continued at the Fermilab Tevatron experiments.

In the LEP-II experiments, the Higgs boson with the mass less than about 110 GeV has been excluded, if its production cross section and decay modes are similar to that of the SM Higgs boson[2]. Recently, the ALEPH collaboration reported the Higgs boson candidates of which mass is 114 GeV. The LEP experiment had searched the Higgs boson mainly produced by the Higgs-strahlung process $e^+e^- \to Zh$, and there are small contribution from the WW and ZZ fusion process $e^+e^- \to \bar{\nu}\nu h$, $e^+e^- \to e^+e^- h$. It decays by the process, $h \to q\bar{q}$, $h \to l\bar{l}$, W^+W^-, ZZ and $h \to$. The production and decay rate are seen in ref. [17].

The Run-II of the Tevatron can be sensitive to a SM-like Higgs boson with mass

up to about 180 GeV, should the integrated luminosity of the collider be large enough (about $30\,\mathrm{fb}^{-1}$) [3]. In the Tevatron, the Higgs boson can be produced through mainly $p\bar{p} \to hZ$, hW process. The produced Higgs boson decays mainly into fermion pair, like $h \to b\bar{b}$.

The several years later, the LHC will arise. The primary goal of the CERN LHC experiments is to guarantee the discovery of a SM-like Higgs boson for its mass as large as about 1 TeV[4], which is the upper bound of the SM Higgs boson mass to be a consistent low-energy effective theory. The JLC is also being planned.

The SM Higgs boson mass bound is also obtained from precision measurements of the electroweak ρ parameter. Adding the radiative correction to the ρ parameter and comparing it with experimental data, we can obtain the Higgs boson mass bound. Recently, the LEP Electroweak Working group reports that the SM Higgs mass upper bound is 215 GeV [15].

2.4 The mass bounds on the Higgs boson in the SM

In this section theoretical bounds on the Higgs boson mass in the SM are discussed [5]. Although the mass of the Higgs boson is a free parameter in the minimal SM, the allowed mass range of the Higgs boson (h) can be determined by demanding the considered theory to be a valid effective theory all the way up to some cut-off energy scale (Λ).

The analysis of the Higgs boson mass is done as follows. We first assume the free parameter of the theory m_h at a low energy scale. The Higgs boson self coupling constant λ is determined by the tree level mass formula (2.25). Then we run the λ to higher energy scale up to Λ. The cut-off energy scale Λ is the energy scale that the new physics appears. For example, if the SM is precisely valid and the new particle do not appear up to Planck scale (m_{pl}), Λ is set as $m_{pl} \sim 10^{19}$.

According to the renormalization theory, the values of the Higgs boson self coupling constant runs with energy scale (Figure 2.2). The running is calculated numerically by solving renormalization group equations (RGE's). The one-loop RGE's for the SM are shown in Appendix A. In this analysis Yukawa coupling constants except top-Yukawa

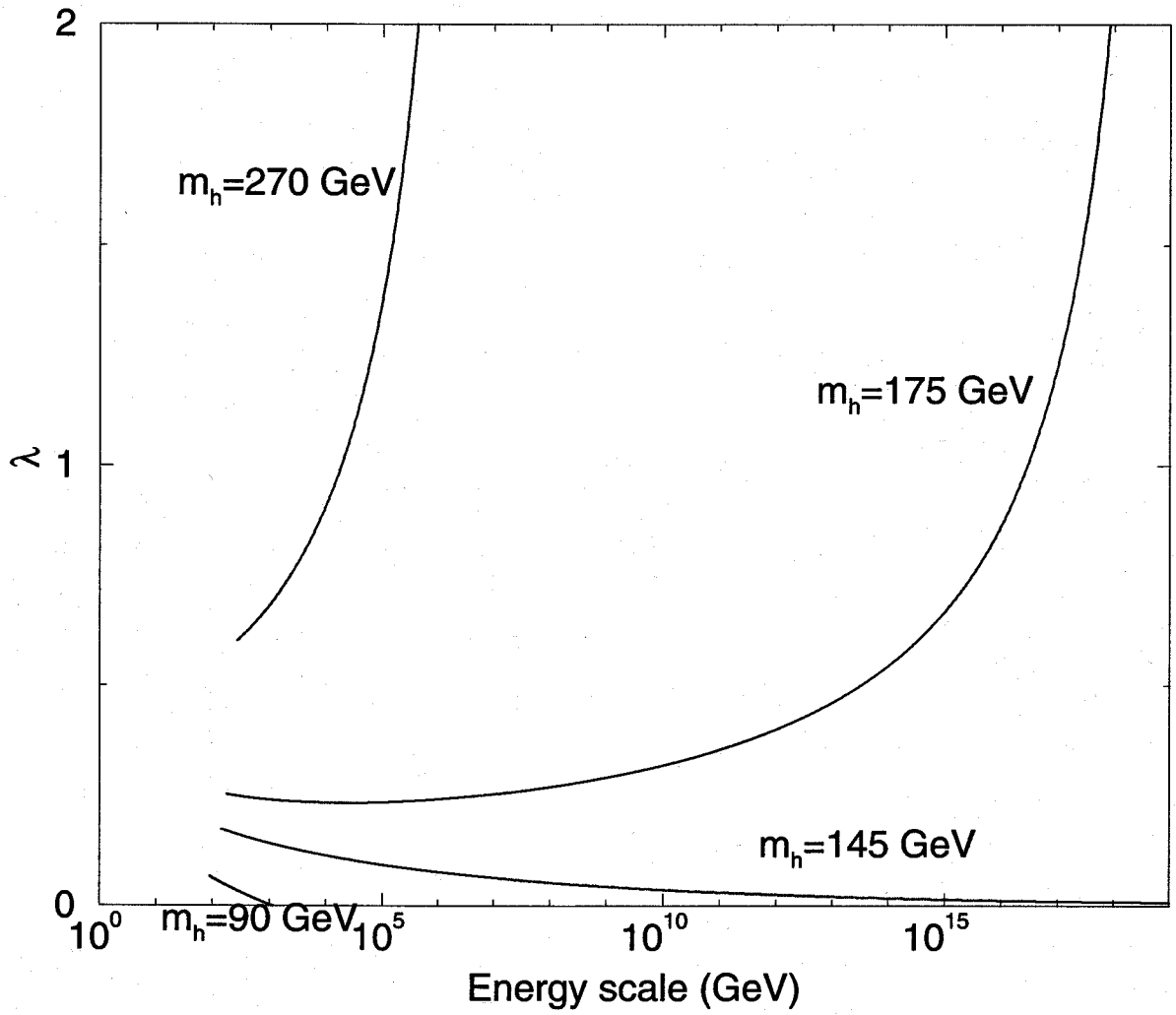

Figure 2.2: Running of λ for the several values of m_h.

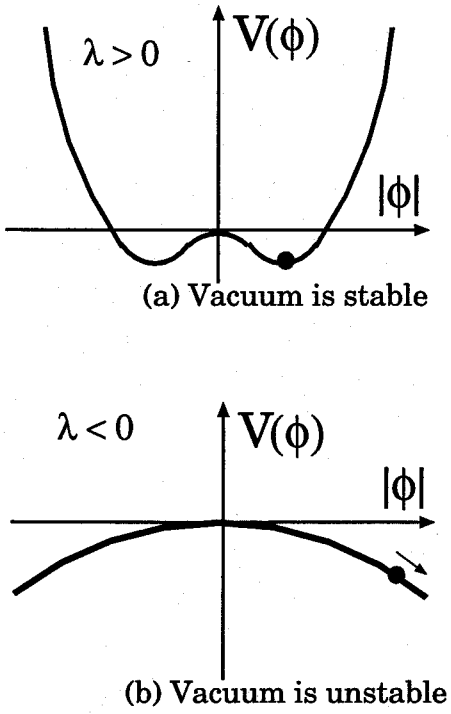

Figure 2.3: The vacuum stability condition. If $\lambda > 0$, the vacuum stays in a stable point (a). But in the case of $\lambda < 0$, the vacuum is unstable (b).

coupling constant y_t are neglected because of their tiny effects.

At each energy scale up to Λ, it is required that the theory is valid. In order to check this, we check whether the Higgs boson self coupling constant (λ) satisfies two conditions: the applicability of perturbation theory and the vacuum stability condition. First, we discuss the condition of the applicability of perturbation theory. If λ is too large, the theory is not reliable. So, we assume the condition,

$$\lambda < 4\pi. \tag{2.28}$$

This condition gives an upper bound on m_h.

Second, the vacuum stability condition is lead by the requirement that the Higgs potential V have a minimum so that the vacuum has stable points as seen in Figure 2.3 (a). If $\lambda < 0$, the vacuum go to $\phi \to \infty$ and do not have a stable point as shown in Figure 2.3 (b). This condition implies,

$$\lambda > 0. \tag{2.29}$$

This condition gives a lower bound on m_h.

Imposing these conditions, m_h is bounded. If m_h is too big, λ^2 term in RGE of λ (eq. A.1) which comes from the Higgs boson loop, grow λ to $+\infty$ as energy scale becomes higher. As a result, λ blows up soon and the allowed cut-off is small. On the other hand, if m_h is too small, y_t^4 term which comes from top-quark loop, reduce λ into negative value, and λ becomes negative soon. Also in this case, the allowed cut-off becomes small.

Thus allowed region of the Higgs boson in the SM is examined [5]. For example, for the Plank scale $m_{Pl} \sim 10^{19}$ GeV as Λ, the lower and the upper bounds become about 145 - 175 GeV at $m_t = 175$ GeV, respectively. More detailed results is shown in Table 3.1. The allowed mass range is depend on m_t. If we take m_t larger, the allowed range of m_t shift to higher, because large λ dismiss strong $-y_t^4$ term effect. The shift of lower bound is larger than that of the upper bound.

This has been reexamined by taking into account the two-loop beta function in [33].

2.5 The mass bounds on the Higgs boson in the MSSM

In this section, we study the allowed range of the lightest Higgs boson mass in the Minimal Super-symmetric Standard Model (MSSM) [7]. The MSSM is most popular in the models beyond the SM, because of the unification of three gauge couplings [16].

There are two Higgs doublets in the MSSM. The tree-level Higgs potential with the soft breaking terms is written as

$$\begin{aligned} V_{SUSY} &= \frac{1}{8}g_2^2\left(\overline{H_1}\tau_a H_1 + \overline{H_2}\tau_a H_2\right)^2 + \frac{1}{8}g_1^2\left(\overline{H_1}H_1 - \overline{H_2}H_2\right)^2 \\ &\quad + m_1^2\overline{H_1}H_1 + m_2^2\overline{H_2}H_2 \\ &\quad - m_3^2\left(H_1H_2 + \overline{H_1H_2}\right). \end{aligned} \tag{2.30}$$

By introducing the vacuum expectation value, five types of Higgs boson appear: h, H, A, $H^{\pm}$ the same as the ordinary 2HDM.

In the MSSM, Higgs boson self coupling constants are determined by the gauge coupling constants, and this relation is broken below the SUSY breaking scale m_{SUSY} by the radiative effect, where we assume that all the supersymmetry (SUSY) particles have mass

close to SUSY breaking scale $m_{SUSY} \simeq m_{stop}$ and also assume $m_{stop} > m_W$, M. In the previous inequality, the soft breaking mass M 3.8 is equal to the CP-odd Higgs boson mass m_A in the MSSM.

We can obtain the values of the coupling constants at the low energy scale by solving the RGE's numerically. Assuming that all the Higgs bosons but h have mass close to M, we use the RGE's of the ordinary 2HDM between m_{stop} and M, and the RGE's of the SM below the energy scale M. The relations between the Higgs boson self coupling constants of the MSSM and the those of the 2HDM at the SUSY breaking scale are follows.

$$\lambda_1 = \frac{1}{4}\left(g_1^2 + g_2^2\right) \tag{2.31}$$

$$\lambda_2 = \frac{1}{4}\left(g_1^2 + g_2^2\right) \tag{2.32}$$

$$\lambda_3 = \frac{1}{4}\left(g_2^2 - g_1^2\right) \tag{2.33}$$

$$\lambda_4 = -\frac{1}{2}g_2^2 \tag{2.34}$$

$$\lambda_5 = 0 \tag{2.35}$$

At the electro-weak scale, the lightest Higgs boson mass is calculated by the tree level mass formula in SM (2.25).

For each allowed sets of two vacuum expectation values, we repeat the analysis about any $\tan\beta$ and can determine allowed range of the Higgs boson mass as a function of M. If $m_{stop} = 1$ TeV, the upper bound of m_h is about 120 GeV (fig. 2.4). This is lighter than that of the SM by 20 GeV if its cut-off is 10^{19} GeV. If the Higgs boson is discovered and its mass is $110 - 120$ GeV, the MSSM will be favored as the primary candidate model beyond the SM.

Also, in extended versions of the SUSY SM, we can obtain upper bounds, if we demand that all dimensionless coupling constants remain perturbative up to the GUT scale [9].

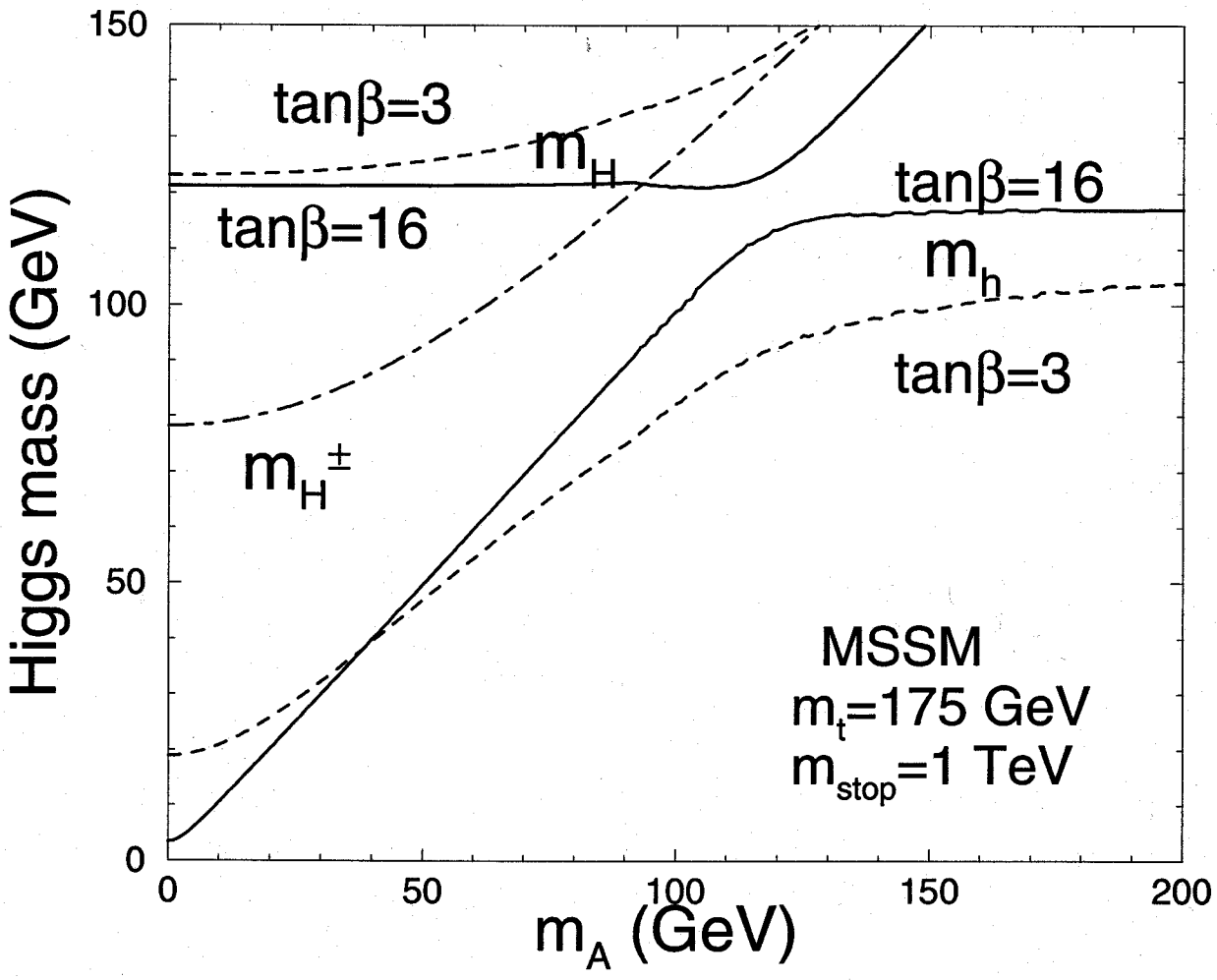

Figure 2.4: The Higgs boson masses in the MSSM as a function of m_A. m_h and m_H are plotted with $\tan\beta = 3$ (dashed line) and 16 (solid line). $m_{H^\pm}$ (dot-dashed line) do not depend on $\tan\beta$.

Chapter 3

Mass bounds in the two-Higgs-doublet-model

In this chapter, the lightest CP-even Higgs-boson mass for the two-Higgs-doublet model (2HDM) is investigated[10]. The 2HDM is the most simple extension of the SM. Imposing the discrete symmetry for suppressing the flavor changing neutral current (FCNC), The 2HDM is classified in two types; namely, one where only one Higgs doublet has Yukawa couplings with the quarks and leptons (Model I), and the other where the one Higgs doublet interacts only with the down-type quarks and leptons and the second one only with up-type quarks (Model II). We can determine mass bounds as a function of a cut-off scale Λ by a similar method as used in the SM. The lower bound of the lightest Higgs boson mass is much reduced in comparison with that in the SM. For example in the decoupling regime where only one neutral Higgs boson is light as compared to the other physical states of Higgs bosons and for $\Lambda = 10^{19}$ GeV and $m_t = 175$ GeV, while the upper bound is about 175 GeV, which is almost the same as in the SM, the lower bound is given by 100 GeV. This is considerably smaller than the similar lower bound in the SM which is 145 GeV. For the region of the small soft-breaking mass, the lower and upper bounds depend on the soft-breaking mass and there is no longer bounded from below in the case without the soft-breaking mass. In Model II 2HDM the constraint from $b \to s$ branching ratio excludes the small mass region of the neutral Higgs boson.

3.1 The two-Higgs-doublet-model

The 2HDM includes two Higgs doublets φ_1, φ_2. The Higgs potential of the 2HDM is given as [17]

$$\begin{aligned} V_{\rm 2HDM}(\varphi_1,\varphi_2) &= m_1^2\left|\varphi_1\right|^2 + m_2^2\left|\varphi_2\right|^2 - m_3^2\left(\varphi_1^\dagger\varphi_2 + \varphi_2^\dagger\varphi_1\right) \\ &+\frac{\lambda_1}{2}\left|\varphi_1\right|^4 + \frac{\lambda_2}{2}\left|\varphi_2\right|^4 + \lambda_3\left|\varphi_1\right|^2\left|\varphi_2\right|^2 \\ &+\lambda_4\left|\varphi_1^\dagger\varphi_2\right|^2 + \frac{\lambda_5}{2}\left\{\left(\varphi_1^\dagger\varphi_2\right)^2 + \left(\varphi_2^\dagger\varphi_1\right)^2\right\}. \end{aligned} \tag{3.1}$$

For simplicity, we take all the self-coupling constants and the mass parameters in (3.1) to be real. m_3^2 terms are the soft-breaking terms for the discrete symmetry discussed below. In the 2HDM, a discrete symmetry is often assumed in order to suppress the flavor changing neutral current (FCNC) in a natural way [18]. There are two types of discrete symmetry. According to the discrete symmetry, the 2HDM is classified in two types.

$$\begin{aligned} \text{Model I} &: \phi_1 \to -\phi_1 \\ \text{Model II} &: \phi_1 \to -\phi_1,\ d_R \to -d_R,\ \mathrm{e_R} \to -\mathrm{e_R} \end{aligned}$$

By imposing the discrete symmetry, the Yukawa interactions are restricted. In Model II φ_1 has couplings with down-type quarks and leptons and φ_2 has couplings with up-type quarks, and only φ_2 has couplings with fermions in Model I. For Model I,

$$\mathcal{L}_{Yukawa-I} = \overline{d_{R_i}}\left(y_D V_{CKM}^\dagger\right)_{ij}\widetilde{\phi_2}^\dagger q_{L_j} + \overline{u_{R_i}}\left(y_U\right)_{ii}\phi_2^\dagger q_{L_i} + \overline{\mathrm{e_{R_i}}}\left(y_E\right)_{ii}\widetilde{\phi_2}^\dagger l_{L_i} + h.c., \tag{3.2}$$

and for Model II,

$$\mathcal{L}_{Yukawa-II} = \overline{d_{R_i}}\left(y_D V_{CKM}^\dagger\right)_{ij}\widetilde{\phi_1}^\dagger q_{L_j} + \overline{u_{R_i}}\left(y_U\right)_{ii}\phi_2^\dagger q_{L_i} + \overline{\mathrm{e_{R_i}}}\left(y_E\right)_{ii}\widetilde{\phi_1}^\dagger l_{L_i} + h.c., \tag{3.3}$$

where y_U,y_D,y_E are diagonal Yukawa matrices and V_{CKM} is the Cabibbo-Kobayashi-Maskawa (CKM) matrix. $\phi_m = \begin{pmatrix} \phi_m^0 \\ \phi_m^- \end{pmatrix}$ and $\widetilde{\phi_m} \equiv (i\tau_2)\,\phi_m^*$ with $m = 1, 2$. In this analysis, we also include soft-breaking terms for the discrete symmetry in the Higgs potential.[1] Inclusion

[1]There have been several works on the Higgs mass bounds in the 2HDM with and without the soft-breaking term [19, 20, 21, 22, 23, 24].

of these terms does not induce the FCNC problem, because these mass terms do not produce FCNC in tree level and the effect is negligible. On the contrary, these terms may be necessary to avoid the domain wall problem [25].

It is useful to work on the following basis by rotating the doublets φ_1 and φ_2 with $Y = -1$ as

$$\begin{pmatrix} \varphi_1 \\ \varphi_2 \end{pmatrix} = \begin{pmatrix} \cos\beta & -\sin\beta \\ \sin\beta & \cos\beta \end{pmatrix} \begin{pmatrix} \Phi \\ \chi \end{pmatrix}, \tag{3.4}$$

where Φ and χ are parameterized as

$$\Phi = \begin{pmatrix} \frac{1}{\sqrt{2}}(v + \phi_1 + i\phi_2) \\ \phi^- \end{pmatrix}, \quad \chi = \begin{pmatrix} \frac{1}{\sqrt{2}}(\chi_1 + iA) \\ H^- \end{pmatrix}, \tag{3.5}$$

where v, ϕ_1, ϕ_2, χ_1 and A are real parameters, and down component ϕ^-, H^- are complex fields. In this expression, the mixing angle β and the vacuum expectation value $v \sim 246$ GeV are given by $\tan\beta = \langle\varphi_2\rangle/\langle\varphi_1\rangle$ and $v/\sqrt{2} = \sqrt{\langle\varphi_1\rangle^2 + \langle\varphi_2\rangle^2}$ respectivery.

From the above Higgs potential (3.1), it is straightforward to derive masses of the Higgs bosons assuming that there is no CP nor charge violation at vacuum. The masses of the physical charged Higgs boson ($H^\pm$) and CP-odd Higgs boson (A) are expressed as

$$m_{H^\pm}^2 = M^2 - \frac{\lambda_4 + \lambda_5}{2} v^2, \tag{3.6}$$

$$m_A^2 = M^2 - \lambda_5 v^2, \tag{3.7}$$

where M is a dimensionful free parameter related to the soft-breaking mass m_3 and defined by

$$M = \frac{m_3}{\sqrt{\cos\beta \sin\beta}}. \tag{3.8}$$

As for the CP-even neutral Higgs modes, ϕ_1 and χ_1 are not yet mass-eigenstates. The mass eigenstates h and H are obtained by diagonalizing the mass matrix;

$$\frac{1}{2}(\phi_1, \chi_1) \begin{pmatrix} M_{11}^2 & M_{12}^2 \\ M_{12}^2 & M_{22}^2 \end{pmatrix} \begin{pmatrix} \phi_1 \\ \chi_1 \end{pmatrix} = \frac{1}{2}(h, H) \begin{pmatrix} m_h^2 & 0 \\ 0 & m_H^2 \end{pmatrix} \begin{pmatrix} h \\ H \end{pmatrix}, \tag{3.9}$$

where

$$M_{11}^2 = v^2 \left(\lambda_1 \cos^4\beta + \lambda_2 \sin^4\beta + \frac{\lambda}{2} \sin^2 2\beta \right),$$

$$
\begin{aligned}
M_{12}^2 &= \frac{v^2}{2}\sin 2\beta\left(-\lambda_1\cos^2\beta+\lambda_2\sin^2\beta+\lambda\cos 2\beta\right), \\
M_{22}^2 &= v^2\left(\lambda_1+\lambda_2-2\lambda\right)\sin^2\beta\cos^2\beta+M^2,
\end{aligned}
$$

and $\lambda = \lambda_3+\lambda_4+\lambda_5$. The mass of the lighter (heavier) CP-even Higgs boson h (H) is given by

$$
m_{h,H}^2 = \frac{1}{2}\left\{M_{11}^2+M_{22}^2 \mp \sqrt{(M_{11}^2-M_{22}^2)^2+4M_{12}^4}\right\}. \tag{3.10}
$$

For the case of $v^2 \ll M^2$, they can be expressed as

$$
m_h^2 = v^2\left(\lambda_1\cos^4\beta+\lambda_2\sin^4\beta+\frac{\lambda}{2}\sin^2 2\beta\right)+\mathcal{O}(\frac{v^4}{M^2}), \tag{3.11}
$$

$$
m_H^2 = M^2+v^2\left(\lambda_1+\lambda_2-2\lambda\right)\sin^2\beta\cos^2\beta+\mathcal{O}(\frac{v^4}{M^2}). \tag{3.12}
$$

Notice that the free parameter M characterizes properties of the Higgs bosons in this model. In the case of $M^2 \gg \lambda_i v^2$, the masses of all the Higgs bosons but h become close to M. In this region, these heavy Higgs bosons decouple from the low-energy observable due to the decoupling theorem [26] and below the scale M the model is effectively regarded as the SM with one Higgs doublet. On the other hand, if $M^2 \sim \lambda_i v^2$, the masses are controlled by the self-coupling constants, and thus the heavy Higgs bosons do not decouple and the lightest CP-even Higgs boson can have a different property from the SM Higgs boson [27]. We can see such a property of the Higgs boson masses in Figure 3.1.

3.2 Higgs boson mass bounds through RGE analysis in 2HDM

In this section, we discuss bounds on the Higgs boson mass for 2HDM through RGE analysis. For each set of parameters defined at the electroweak scale, the running coupling constants are calculated numerically through RGE's at the one-loop level. We require that any of the dimensionless coupling constants does not blow up below a given cut-off scale Λ, and the coupling constants satisfy the vacuum stability condition, to be discussed later. We vary the input parameters at the electroweak scale and determine the possible range of the lightest CP-even Higgs boson mass as a function of Λ.

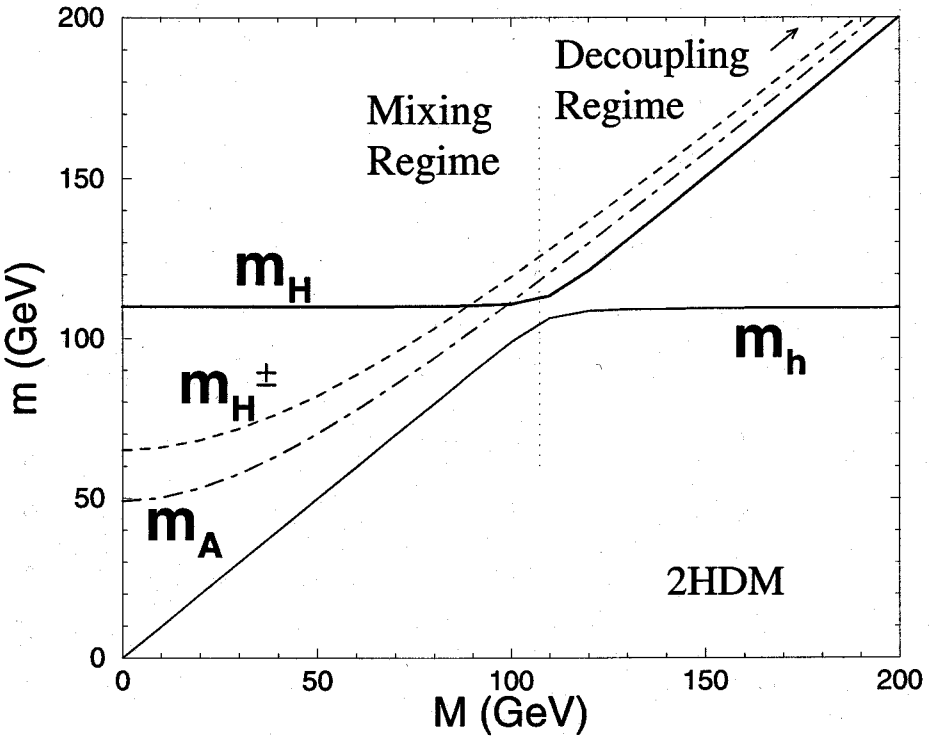

Figure 3.1: The Higgs boson masses as a function of M. Other parameters (λ_i and $\tan\beta$) are fixed in certain values. $M \gg 100$ GeV is a decoupling regime and $M \sim 100$ GeV is a mixing regime.

Let us discuss the conditions for validity of perturbation theory and the vacuum stability. For the first condition, we require that the running coupling constants of the Higgs self-couplings and the Yukawa couplings do not blow up below a certain energy scale Λ;

$$^{\forall}\lambda_i(\mu) < 8\pi,\ y_t^2(\mu) < 4\pi\,, \tag{3.13}$$

for a renormalization scale μ less than Λ.[2] For the requirement of the vacuum stability, we assume that the quartic interaction terms in the potential do not give negative contribution for all directions of scaler fields at each energy scale up to Λ. This condition leads to

$$\begin{aligned} &\lambda_1(\mu) > 0,\ \ \lambda_2(\mu) > 0, \\ &\sqrt{\lambda_1(\mu)\lambda_2(\mu)} + \lambda_3(\mu) + \min\left[0, \lambda_4(\mu)+\lambda_5(\mu), \lambda_4(\mu)-\lambda_5(\mu)\right] > 0, \end{aligned} \tag{3.14}$$

for $\mu < \Lambda$. We also require that the tree-level Higgs potential at the weak scale does not have any global minimum except for the one we consider. In particular, we assume that there is no CP nor charge breaking at the global minimum.[3] These conditions imposed on the coupling constants at a high energy region are transmitted into constraints on the coupling constants at the electroweak scale and then on the masses of Higgs bosons.

In our analysis, we use the 1-loop RGE's for the SM and the 2HDM which are found in Appendix A, or for example, in ref. [21, 28]. We only consider the top-Yukawa coupling contribution as the Yukawa interaction. The running top mass is defined as $\overline{m_t}(\mu) = \frac{1}{\sqrt{2}} y_t(\mu) v \sin\beta$ and it is related to the pole mass m_t by $\overline{m_t}(m_t) = m_t(1 - \frac{4}{3\pi}\alpha_s(m_t))$. Note that only the running of λ_2 in eq. (A.3) has a quartic power contribution of the top-Yukawa coupling constant y_t. This affects on λ_2 as a negative factor: the large y_t tends to make the vacuum unstable along the direction of $\langle\varphi_2\rangle$[4].

[2]This condition corresponds to the conditions $\lambda_{SM}(\mu) < 4\pi$ and $y_t^{SM}(\mu) < 4\pi$ with coupling normalization of $m_{H_{SM}} = \sqrt{2\lambda_{SM}}v$ and $m_t = \frac{1}{\sqrt{2}} y_t^{SM} v$ in the SM case. The above condition becomes the same as the SM condition in the decoupling limit of our 2HDM for large $tan\beta$ because in this case $\lambda_2(\mu) \sim 2\lambda_{SM}(\mu)$ and $y_t(\mu) \sim y_t^{SM}(\mu)$.

[3]The vacuum stability condition here is slightly different from that in ref. [23], where they have put $\lambda_4(\mu) + \lambda_5(\mu) < 0$ and $\lambda_5(\mu) < 0$ below $\mu < \Lambda$ in addition to (3.14) in the model with $M^2 = 0$. In the case of $M^2 \sim 0$, our condition is essentially the same as that in ref. [23], because we then have $\lambda_4 + \lambda_5 < 0$ and $\lambda_5 < 0$ at the electroweak scale from the positiveness of the squared-masses of $\chi^{\pm}$ and χ_2 and we can show that these inequalities tend to be preserved at higher energy scale according to the 2HDM RGE's.

In the decoupling case where $M^2 \gg \lambda_i v^2$, there can be a sizable correction on the lightest CP-even Higgs boson mass at a low energy scale. In order to include this effect, instead of calculating the λ_i's at the weak scale from the RGE and using the tree-level mass formulas, we adopt the following procedure. We determine the λ_i at the scale M by using the 2HDM RGE in the region between Λ and M, and then calculate the CP-even Higgs boson mass according to the tree-level formulas. Since the effective theory below M is just the SM with one Higgs doublet, we use the SM RGE from M to m_h to evaluate the lightest Higgs boson mass. Although this procedure is not really justified for $M^2 \sim \lambda_i v^2$, we calculate the mass in this way because the correction from the SM RGE is numerically very small in such case.

There are important phenomenological constraints on the 2HDM. From the low-energy electroweak precision tests, the ρ parameter should be closed to unity, which means that the custodial $SU(2)_V$ symmetry should not be badly broken in the Higgs sector. We evaluate the 2HDM contribution to the ρ parameter according to refs. [29]. Taking account of the experimental data up to 95% CL [30], we here set the condition $\Delta\rho_{\rm 2HDM} = -0.0020 - 0.00049\frac{m_t - 175{\rm GeV}}{5{\rm GeV}} \pm 0.0027$ for our analysis, where $\Delta\rho_{\rm 2HDM}$ is the extra contribution of the 2HDM to the ρ parameter.[4]

Another experimental constraint is obtained from the $b \to s$ measurement [31]. It is known that there is very strong constraint on the charged-Higgs boson mass from this process in the case of Model II, while Model I is not strongly constrained (Figure 3.2). We calculate the $b \to s$ branching ratio with the next-to-leading order QCD correction [32] and use its constraint to determine the allowed region of the parameter space.

In the actual analysis, we first fix parameter sets of m_h, $\tan\beta$ and M. Since the Higgs potential contains three masses and five coupling constants, the number of free parameters is four with fixing $v = 246$ GeV for each set of the parameter choice. We examine four-dimensional parameter space of λ_1, λ_3, λ_4 and λ_5 under the experimental constraints above and obtain a maximum scale Λ where one of the conditions (3.13) and (3.14) is broken.

[4]We here set the reference value of the SM Higgs mass into 100 GeV. We also include uncertainties from the strong coupling constant and the electromagnetic coupling constant at the Z pole for our evaluation of the ρ parameter.

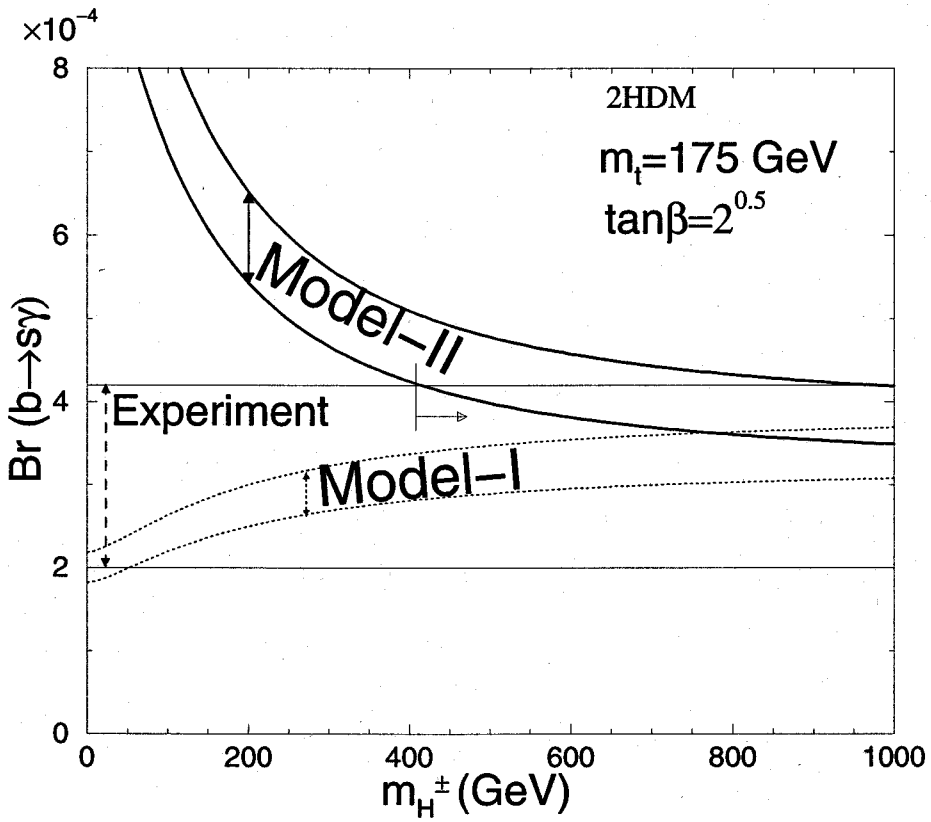

Figure 3.2: $b \to s$ branching ratio as a function of $m_{H^\pm}$ with $\tan\beta = \sqrt{2}$, $m_t = 175$ GeV. In the Model I, any $m_{H^\pm}$ do not conflict with experimental value. But in the Model II, $m_{H^\pm} < 400$ GeV is excluded. The more $\tan\beta$ becomes high, the more constraint relaxed. If m_t is higher than 175 GeV, more large $m_{H^\pm}$ is excluded.

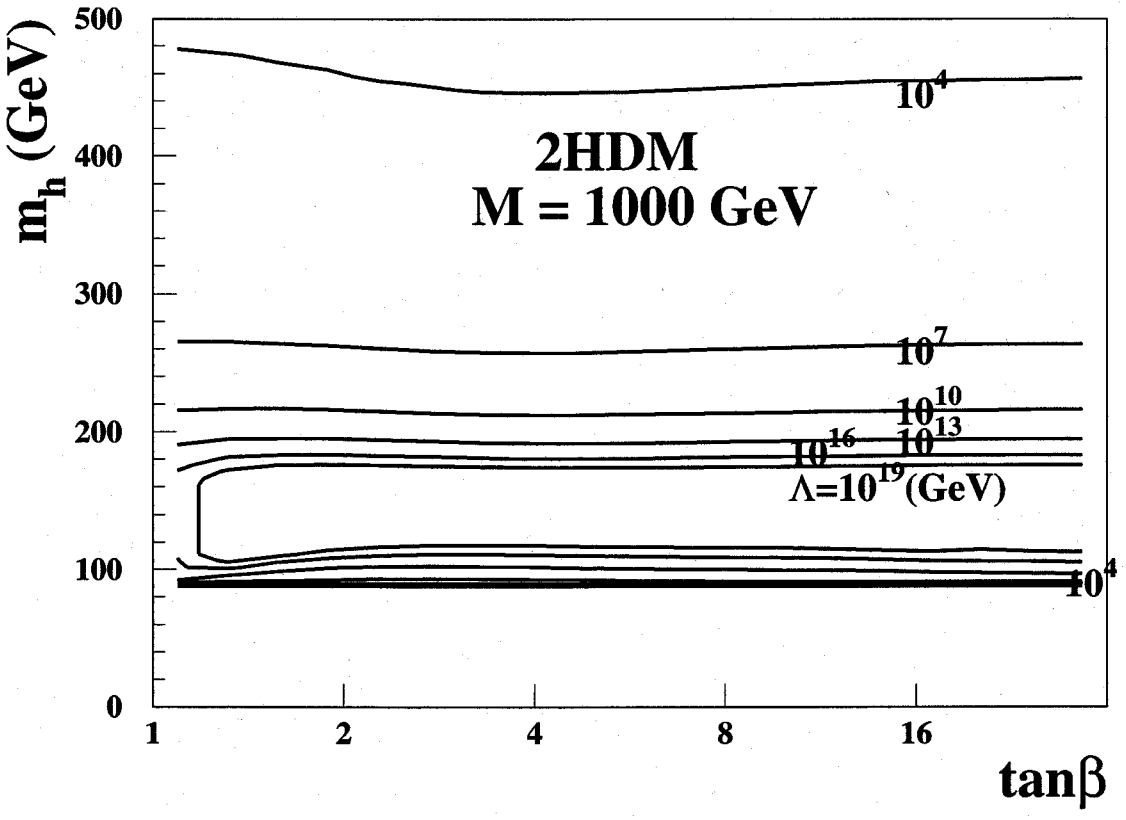

Figure 3.3: The allowed region of the lightest CP even Higgs boson mass as a function of $\tan\beta$ for different values of the cut-off scale (Λ) for $M = 1000$ GeV in the 2HDM. The top mass is taken to be 175 GeV. For each Λ ($= 10^{19}, 10^{16}, 10^{13}, 10^{10}, 10^{7}, 10^{4}$ GeV) the inside of the contour is allowed. There is no difference between Model I and Model II in this figure.

We also put $m_Z = 91.19$ GeV and $\alpha_S(m_Z) = 0.118$. The mass of the top quark is fixed as 175 GeV in our main analysis and later the dependence on m_t is discussed.

Let us first consider the case of the decoupling regime ($v^2 \ll M^2$). All the Higgs bosons but h are all heavy and their masses are almost degenerate around M. Fig. 3.3 shows that the contour plot of each Λ ($= 10^{19}, 10^{16}, 10^{13}, 10^{10}, 10^{7}, 10^{4}$ GeV) for $M = 1000$ GeV on the m_h-$\tan\beta$ plane. The $\tan\beta$ dependence is not so sensitive except for the small $\tan\beta$ region where the top-Yukawa coupling constant blows up at a low energy scale. For the smaller values of m_h, λ_2 tends to become negative because of the negative effect of y_t^4-term in the RGE for λ_2. On the other hand, for a large value of m_h, λ_2 blows up at a low energy scale. There is no difference between Model I and Model II in the decoupling

regime, because the constraint from $b \to s$ is not important in this case.

The qualitative result may be understood by looking at the RGE's. From eq. (3.11), m_h^2 is approximately given by $\lambda_2 v^2$ for $\tan\beta \gg 1$, and the RGE for λ_2 is given by

$$16\pi^2 \mu \frac{d\lambda_2}{d\mu} = 12\lambda_2^2 - 3\lambda_2(3g^2 + g'^2) + \frac{3}{2}g^4 + \frac{3}{4}(g^2 + g'^2)^2 + 12\lambda_2 y_t^2 - 12y_t^4 + A, \quad (3.15)$$

where $A = 2\lambda_3^2 + 2(\lambda_3 + \lambda_4)^2 + 2\lambda_5^2 > 0$. When we fix the coupling normalization by $m_H^{SM} = \sqrt{\lambda_{SM}} v$, the SM RGE for λ_{SM} is obtained by substituting λ_{SM} and y_t^{SM} to λ_2 and y_t in eq. (3.15) and neglecting the A term in the RHS. Thus the difference is only in the existence of the positive term A in eq. (3.15). This term works to improve the stability of vacuum to some extent, and the lower bound is expected to be reduced in the 2HDM.

Next we see the case of the mixing regime ($M = 100$ GeV $\sim m_z$), where the heavy Higgs masses are realized only by the large λ_i's ($i = 1 - 5$) and their mixing. In this case, the data from the low energy experiment strongly constrain the model. The contour plots for each Λ on m_h-$\tan\beta$ plane in Model I and Model II are shown in figs. 3.4(a) and 3.4(b), respectively. We can see in figs. 3.4(a) and 3.4(b) that there is an allowed region for $\Lambda = 10^{19}$ GeV in Model I, while the largest Λ is less than 10^4 GeV in Model II because the $b \to s$ measurement gives a strong constraint for Model II 2HDM. Note that the allowed region in fig. 3.4(a) lies around $m_h \sim m_Z$ ($\sim M$) for large $\tan\beta$. This is because that, in the region of $M^2 < \lambda_2 v^2$, the mass of the lighter CP-even Higgs boson h comes from $M_{22} \sim M$ and the heavier Higgs boson H has the mass of $M_{11} \sim \sqrt{\lambda_2} v$. On the other hand, in the decoupling regime, the situation is reversed and the h boson has the mass of $M_{11} \sim \sqrt{\lambda_2} v$.

We repeated the above analysis for various values of M and obtained the upper and lower bounds of the lightest CP-even Higgs boson masses for various cut-off scales, which are shown in the contour plots in the m_h-M plane in figs. 3.5, (a) and (b) for Model I and II, respectively. In fig 3.5(a), the qualitative behavior of the allowed region is understood from the above argument on the mass matrix. For the region of $M^2 \ll \lambda_2 v^2$, the allowed region of m_h lies around $m_h \sim M$, and that becomes along $\sqrt{\lambda_2} v$ and no longer depends on M for $M^2 \gg \lambda_2 v^2$. Though there are the upper bounds of m_h for each Λ, m_h is not bounded from below by our condition. Our results at $M = 0$ are consistent to those in [23]. If we take account of the experimental result of $b \to s$, m_h is bounded from below

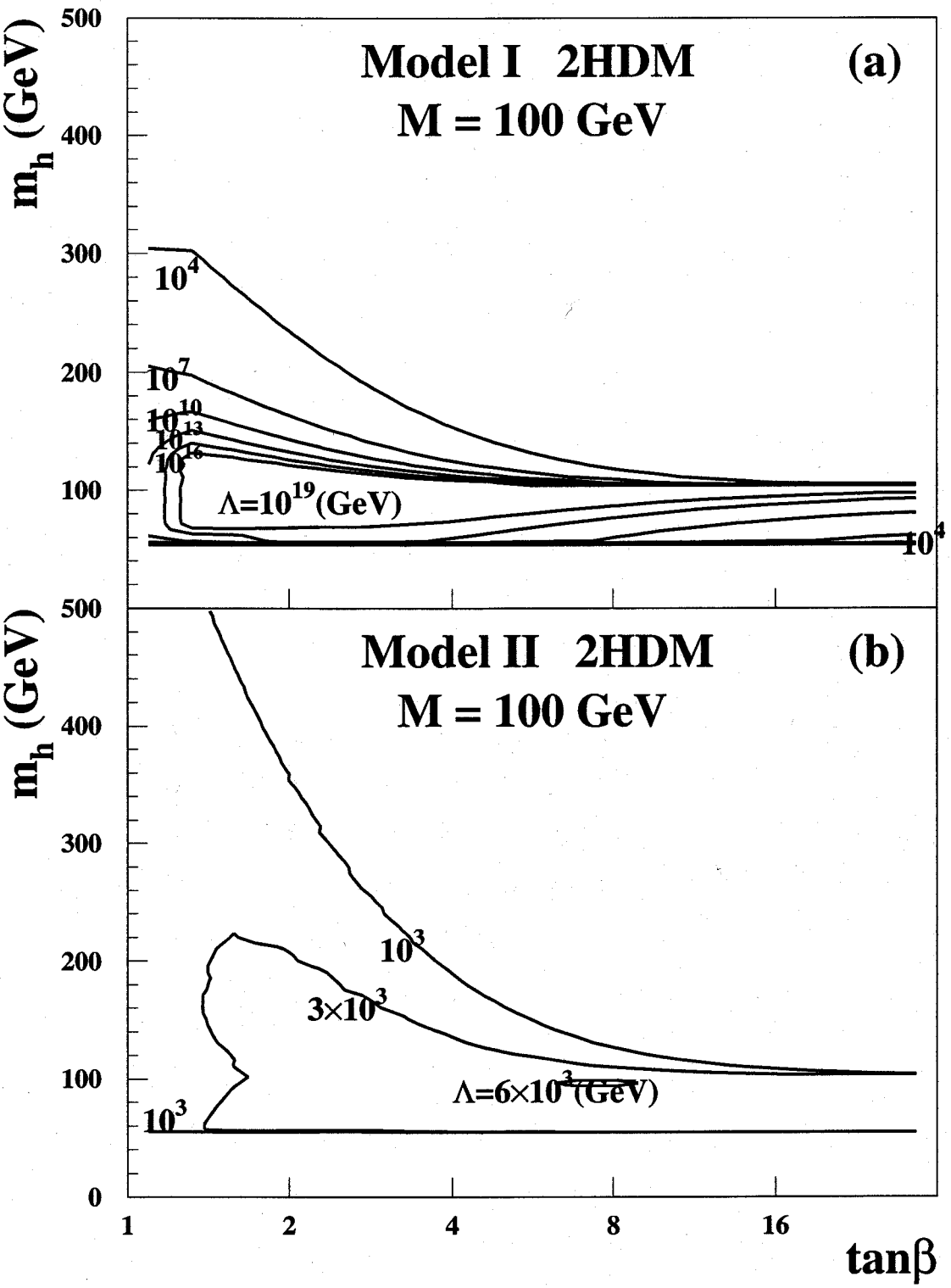

Figure 3.4: The allowed region of the lightest CP even Higgs boson mass as a function of $\tan\beta$ for different values of Λ for $M = 100$ GeV in the Model I (a) and Model II (b) 2HDM. The top mass is taken to be 175 GeV. For the Model II lines for $\Lambda = 1000$ and 3000 GeV are shown.

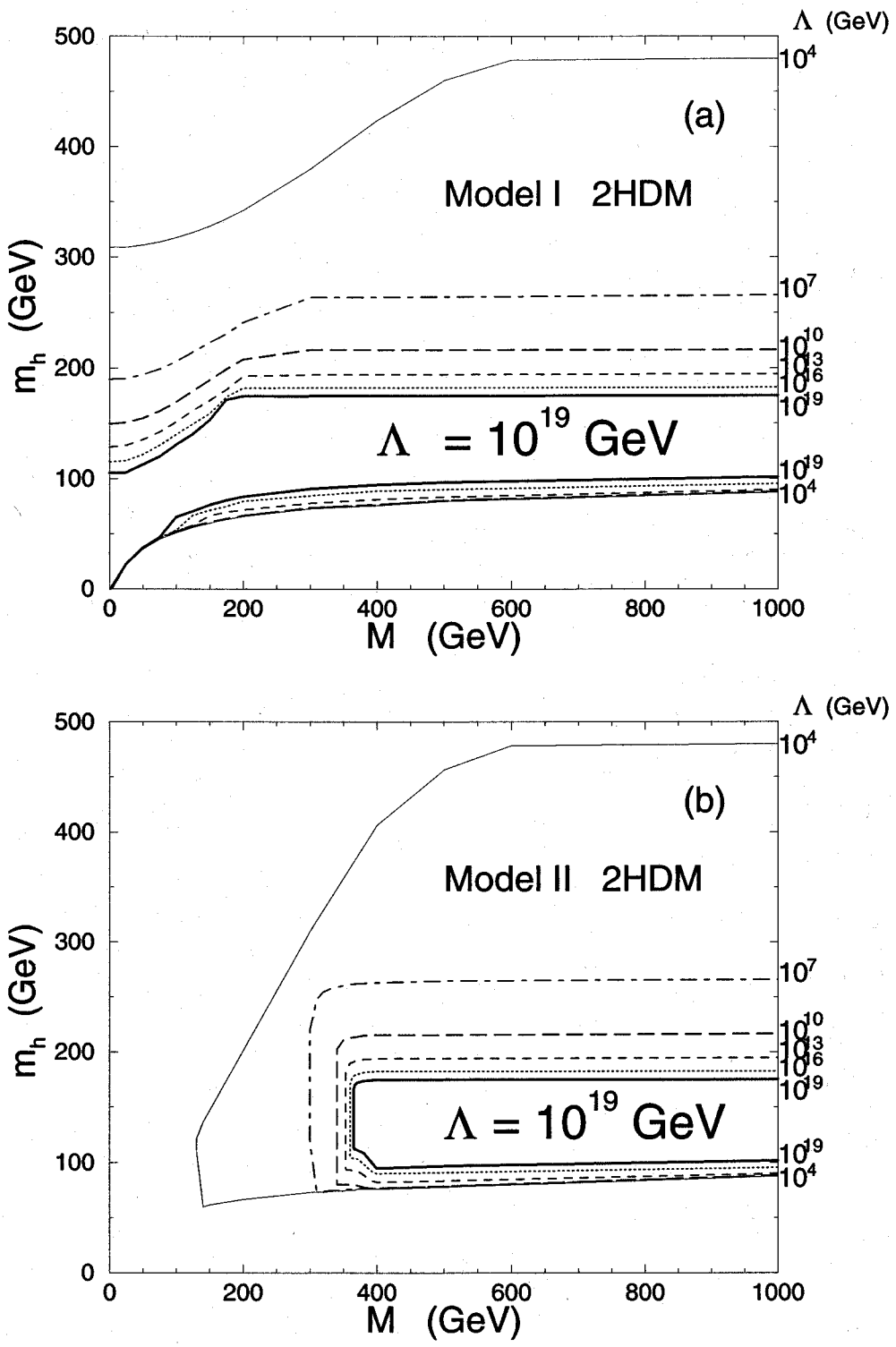

Figure 3.5: The upper and lower bounds of the lightest CP even Higgs boson mass as a function of M for different values of Λ in the Model I (a) and Model II (b) 2HDM for $m_t = 175$ GeV.

in the case of Model II as seen in fig. 3.5(b) because the small M region ($M \lesssim 350$ GeV) necessarily corresponds to the light charged Higgs boson mass and is excluded by the $b \to s$ constraint.[5]

Finally, we show the figure in which the results in the SM and the 2HDM (Model I and II) are combined on m_h-M plane (fig. 3.6). For a reference, the upper and lower bounds of the lightest CP-even Higgs mass in the MSSM are also given for the case that the stop mass is 1 TeV. These lines are calculated by a similar method described in ref. [7]: namely we use the SUSY relation for Higgs self-coupling constants at the 1 TeV scale and use the 2HDM RGE between 1 TeV and M, and the SM RGE between M and m_h scale. In this figure, M is the CP-odd Higgs boson mass in the case of the MSSM. It is easy to observe from this figure that the difference of the bounds among the SM, the 2HDM(I) and the 2HDM(II). We here choose, as an example, $\Lambda = 10^{19}$ GeV for the results in the SM and the 2HDM at $m_t = 175$ GeV. While the upper bounds in these models are all around 175 GeV, the lower bounds are completely different; about 145 GeV in the SM, about 100 GeV in the Model II and no bound in Model I.

In order to see the top quark mass dependence of the above results, we have repeated the analysis for $m_t = 170$ GeV and 180 GeV. It turns out that the lower bound has sizable dependence of the top mass whereas the upper bound does not change very much. For example, the lower line for $\Lambda = 10^{19}$ GeV in the 2HDM shown in fig. 3.6 shifts to lower (upper) by 9 GeV for $m_t = 170$ (180) GeV at $M = 1000$ GeV, but the corresponding shift for the upper line is about 3 (4) GeV. In Table 1, we list the m_t dependence of the lightest CP-even Higgs mass bounds for each value of Λ in the SM and the 2HDM for $M = 1000$ GeV and for $M = 200$ GeV (Model I). In the mixing regime of Model II, for smaller m_t, the $b \to s$ constraint is relaxed and the lower bound is reduced further.

We also comment on a question how much our results are improved if a higher order analysis is made in the effective potential method. In the SM, the next-to-leading order

[5]For the estimation of theoretical uncertainties we added in quadratures the errors from the various input parameters. If we use more conservative way to add theoretical uncertainties for the $b \to s$ evaluation, the bound on the charged Higgs boson or on the M in Model II becomes rather smaller[32]. The lower bound of m_h due to the $b \to s$ constraint is then reduced by a few GeV according to the change of the allowed region of M.

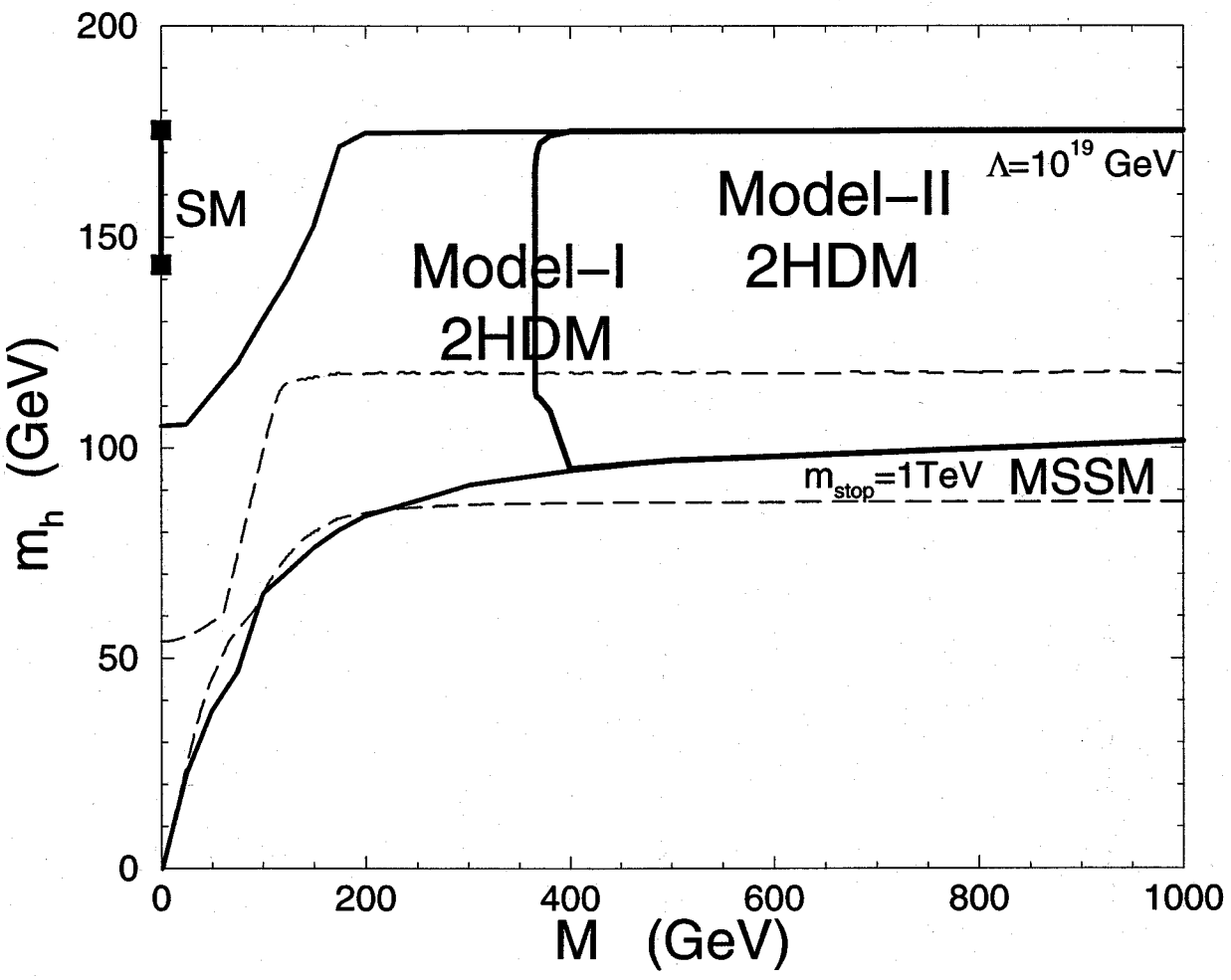

Figure 3.6: The upper and the lower bounds of the lightest CP even Higgs boson mass in the Model I and II 2HDM and the SM Higgs boson mass for $\Lambda = 10^{19}$ GeV. The upper and lower bounds of the lightest CP even Higgs boson mass in the MSSM are also shown for the case that stop mass is 1 TeV. In this case M corresponds to the CP-odd Higgs boson mass in the MSSM.

Table 3.1: A list of the lower and upper bounds of the lightest CP-even Higgs mass in GeV for each m_t (170, 175, 180 GeV) and Λ (= 10^{19}, 10^{16}, 10^{13}, 10^{10}, 10^{7}, 10^{4} GeV) in the SM as well as the 2HDM for $M = 1000$ GeV and for $M = 200$ GeV (Model I). Model I and II give the same bounds for $M = 1000$ GeV.

	Λ (GeV)	$m_t = 170$ GeV	$m_t = 175$ GeV	$m_t = 180$ GeV
Standard Model		133 - 172	143 - 175	153 - 179
2HDM ($M = 1000$GeV)	10^{19}	93 - 172	102 - 175	111 - 179
2HDM I ($M = 200$GeV)		79 - 171	84 - 175	91 - 179
		133 - 180	142 - 182	152 - 186
	10^{16}	89 - 180	96 - 183	104 - 186
		73 - 179	80 - 182	85 - 185
		132 - 192	141 - 194	150 - 197
	10^{13}	85 - 193	90 - 195	97 - 197
		68 - 191	72 - 193	77 - 195
		129 - 215	138 - 216	147 - 217
	10^{10}	85 - 216	89 - 216	93 - 218
		64 - 208	67 - 208	70 - 207
		122 - 264	130 - 264	138 - 264
	10^{7}	84 - 266	88 - 266	93 - 265
		64 - 238	67 - 241	69 - 241
		101 - 460	107 - 458	113 - 458
	10^{4}	84 - 480	88 - 480	92 - 478
		63 - 343	66 - 342	68 - 342

analysis of the effective potential shows that the lower bound reduces by about 10 GeV ($\Lambda = 10^{19}$ GeV) [33]. It may be then expected that a similar reduction of the lower bound would occur in the 2HDM by doing such higher order analysis.

3.3 Summary of 2HDM analysis

By the similar method as used in the SM, we have analyzed the upper and the lower bounds of the lightest CP-even Higgs boson mass in the 2HDM with a softly-broken discrete symmetry. While the upper bound has been found to be almost the same as in the SM, the lower bound turns out to be much reduced. In particular in the decoupling regime, both Model I and Model II give the lower bounds of about 100 GeV for $\Lambda = 10^{19}$ GeV, which is lower by 40 GeV than the SM result. In this regime, the properties of the lightest Higgs boson such as the production cross section and the decay branching ratios are almost the same as the SM Higgs boson. In this analysis, we have not explicitly considered constraint from the Higgs boson search at LEP II, but if the Higgs boson is discovered with the mass around 100 GeV at Tevatron or LHC experiment in near future and its property is quite similar to the SM Higgs boson, the 2HDM with very high cut-off scale is another candidate of models which predict such light Higgs boson along with the MSSM of which mass upper bound is less than 120 GeV, and its extensions.

Chapter 4

Phenomenology of Higgs bosons in the Zee-Model

In this chapter the Higgs boson mass bounds for the Zee-Model is investigated [11]. From the observations of atmospheric and solar neutrinos, there are increasing evidences for neutrino oscillations [34]. If this is a correct interpretation, the SM has to be extended to incorporate the small masses of the neutrinos suggested by data. There have been several ideas proposed in literature to generate small neutrino masses. The Zee-model is one of such attempts [12, 35, 36, 37, 38]. In this model, the three different flavor neutrinos are massless at the tree level, and their small masses are induced radiatively through one-loop diagrams. For such a mass-generation mechanism to work, it is necessary to extend the Higgs sector of the SM to contain at least two weak-doublet fields and one weak-singlet charged scalar field [12]. Although many studies have been done to examine the interaction of the leptons and the Higgs bosons in the Zee-model [39], the scalar (Higgs) sector of the model remains unexplored in detail. In this chapter we study the Higgs sector of the Zee-model to clarify its impact on the Higgs search experiments, either at the CERN LEP-II, the Run-II of the Fermilab Tevatron, the CERN Large Hadron Collider (LHC), or future linear colliders (LC's).

The Higgs sector of the Zee-model is similar to that of the 2HDM except for the existence of an additional weak-singlet charged Higgs field, so that the physical scalar-bosons include two CP-even, one CP-odd and two pairs of charged Higgs bosons. In this

chapter, we shall first determine the upper and lower bounds for the lightest CP-even Higgs boson mass (m_h) as a function of the cut-off scale Λ of the Zee-model, using RGE's.[1] We show that the upper and lower mass bounds for h are almost the same as those in the 2HDM. We also study the possible range of the Higgs-boson self-coupling constants at the electroweak scale as a function of Λ. By using these results, we examine effects of the additional loop contribution of the singlet charged Higgs boson to the partial decay width of $h \rightarrow$. We show that, by taking $\Lambda = 10^{19}$ GeV, the deviation of the decay width from the SM prediction can be about -20% or nearly +10% for m_h between 125 GeV and 140 GeV when the mass of the isospin singlet charged Higgs boson is taken to be around 100 GeV. The magnitude of the deviation becomes larger for lower cutoff scales and smaller masses of the singlet charged Higgs boson. If we choose $\Lambda = 10^4$ GeV and the singlet charged Higgs boson mass to be 100 GeV, the positive deviation can be greater than +30% (+40%) for $m_h = 125$ GeV (140 GeV). Such a deviation from the SM prediction could be tested at the LHC and the option of LC [41, 42, 43]. We also discuss phenomenology of the singlet charged Higgs boson at present and future collider experiments, which is found to be completely different from that of the ordinary 2HDM-like charged Higgs bosons. To detect such a charged Higgs boson at LEP-II experiments, experimentalists have to search for their data sample with $e^{\pm}$ or $\mu^{\pm}$ plus missing energy, in contrast to the usual detection channels: either $\tau\nu$ or cs decay modes.

This chapter is organized as follows. In Sec. 4.1, we introduce the Higgs sector of the Zee-model and review the neutrino masses and mixing in this model which are consistent with the atmospheric and solar neutrino observations. Numerical results on the possible range of the mass and coupling constants of the Higgs bosons are given in Sec. 4.2. In Sec. 4.3, we discuss the one-loop effect of the extra-Higgs bosons in the Zee-model to the partial decay width of $h \rightarrow$ and its impacts on the neutral Higgs-boson search at high-energy colliders. The phenomenology of the charged Higgs boson that comes from the additional singlet field is discussed in Sec. 4.4.

[1]For the model with see-saw mechanism for neutrino mass generation the Higgs mass bound has been studied as a function of cut-off scale in Ref. [40].

4.1 Zee-model

To generate small neutrino mass radiatively, the Zee-model contains a $SU(2)_L$ singlet charged scalar field ω^-, in addition to two $SU(2)_L$ doublet fields ϕ_1, and ϕ_2. The Zee-Model Lagrangian is written as:

$$\mathcal{L} = \mathcal{L}_{kin} + \mathcal{L}_{ll\omega} + \mathcal{L}_{Yukawa} - V(\phi_1, \phi_2, \omega^-)\,, \tag{4.1}$$

where

$$\begin{aligned}
\mathcal{L}_{kin} &= |D_\mu \phi_1|^2 + |D_\mu \phi_2|^2 + \left|D_\mu \omega^-\right|^2 \\
&\quad + i\overline{q_L}\ {}^{\mu}D_\mu q_L + i\overline{u_R}\ {}^{\mu}D_\mu u_R + i\overline{d_R}\ {}^{\mu}D_\mu d_R \\
&\quad + i\overline{l_L}\ {}^{\mu}D_\mu l_L + i\overline{e_R}\ {}^{\mu}D_\mu e_R \\
&\quad - \sum_{a=SU(3),SU(2),U(1)} \frac{1}{4} F_{\mu\nu}^{a^2},
\end{aligned} \tag{4.2}$$

$$\mathcal{L}_{ll\omega} = f_{ij}\overline{l_{i_L}}(i\tau_2)(l_{j_L})^C \omega^- + f_{ij}\overline{l_{i_L}}^C(i\tau_2) l_{j_L}\omega^+, \tag{4.3}$$

where i, j $(= 1, 2, 3)$ are the generation indices, and

$$\begin{aligned}
V_{\text{Zee}}(\phi_1, \phi_2, \omega^-) &= m_1^2 |\phi_1|^2 + m_2^2 |\phi_2|^2 + m_0^2 \left|\omega^-\right|^2 \\
&\quad - m_3^2(\phi_1^\dagger \phi_2 + \phi_2^\dagger \phi_1) - \mu \widetilde{\phi_1}^T i\tau_2 \widetilde{\phi_2}\,\omega^- + \mu \phi_2^T i\tau_2 \phi_1\,\omega^+ \\
&\quad + \frac{1}{2}\lambda_1 |\phi_1|^4 + \frac{1}{2}\lambda_2 |\phi_2|^4 + \lambda_3 |\phi_1|^2 |\phi_2|^2 \\
&\quad + \lambda_4 \left|\phi_1^\dagger \phi_2\right|^2 + \frac{\lambda_5}{2}\left[\left(\phi_1^\dagger \phi_2\right)^2 + \left(\phi_2^\dagger \phi_1\right)^2\right] \\
&\quad + \sigma_1 \left|\omega^-\right|^2 |\phi_1|^2 + \sigma_2 \left|\omega^-\right|^2 |\phi_2|^2 + \frac{1}{4}\sigma_3 \left|\omega^-\right|^4 .
\end{aligned} \tag{4.4}$$

In the above equations, q_L is the left-handed quark doublet with an implicit generation index while u_R and d_R denote the right-handed singlet quarks. Similarly, l_L and e_R denote the left-handed and right-handed leptons in three generations. The charge conjugation of a fermion field is defined as ${}^C \equiv C\overline{}^T$, where C is the charge conjugation matrix $(C^{-1}\ {}^{\mu}C = -\ {}^{\mu T})$ with the super index T indicating the transpose of a matrix. Also, $\phi_m = \begin{pmatrix} \phi_m^0 \\ \phi_m^- \end{pmatrix}$ and $\widetilde{\phi_m} \equiv (i\tau_2)\,\phi_m^*$ with $m = 1, 2$. Without loss of generality, we have

taken the anti-symmetric matrix f_{ij} and the coupling μ to be real in the equations (4.3) and (4.4). In order to suppress flavor changing neutral current (FCNC) at the tree level, a discrete symmetry, with $\phi_1 \to \phi_1$, $\phi_2 \to -\phi_2$, $\omega^+ \to +\omega^+$, is imposed to the Higgs sector of the Lagrangian, which is only broken softly by the m_3^2 term and the μ term. Under the discrete symmetry there are two possible Yukawa-interactions; that is, for Model-I

$$\mathcal{L}_{Yukawa-I} = \overline{d_{R_i}} \left(y_D V_{CKM}^\dagger\right)_{ij} \widetilde{\phi_2}^\dagger q_{L_j} + \overline{u_{R_i}} (y_U)_{ii} \phi_2^\dagger q_{L_i} + \overline{e_{R_i}} (y_E)_{ii} \widetilde{\phi_2}^\dagger l_{L_i} + h.c., \quad (4.5)$$

and for Model-II,

$$\mathcal{L}_{Yukawa-II} = \overline{d_{R_i}} \left(y_D V_{CKM}^\dagger\right)_{ij} \widetilde{\phi_1}^\dagger q_{L_j} + \overline{u_{R_i}} (y_U)_{ii} \phi_2^\dagger q_{L_i} + \overline{e_{R_i}} (y_E)_{ii} \widetilde{\phi_1}^\dagger l_{L_i} + h.c., \quad (4.6)$$

where y_U,y_D,y_E are diagonal Yukawa matrices and V_{CKM} is the Cabibbo-Kobayashi-Maskawa (CKM) matrix. Later, we shall only keep the top Yukawa coupling constants $y_t = (y_U)_{33}$ in our numerical evaluation of the RGE's.[2] In that case, there is no difference between the Yukawa couplings of the Model-I and the Model-II models. Finally, for simplicity, we assume that all λ_i and m_i^2 are real parameters.

Let us now discuss the Higgs sector. The $SU(2)_L \times U(1)_Y$ symmetry is broken to $U(1)_{em}$ by $\langle\phi_1\rangle$ and $\langle\phi_2\rangle$, the vacuum expectation values of ϕ_1 and ϕ_2. (They are assumed to be real so that there is no spontaneous CP violation.) The number of physical Higgs bosons are two CP-even Higgs bosons (H,h), one CP-odd Higgs boson (A) and two pairs of charged Higgs boson ($S_1^\pm$, $S_2^\pm$). We take a convention of $m_H > m_h$ and $m_{S_1} > m_{S_2}$. In the basis where two Higgs doublets are rotated by the angle β, with $\tan\beta = \frac{\langle\phi_2^0\rangle}{\langle\phi_1^0\rangle}$, the mass matrices for the physical states of Higgs bosons are given by

$$M_N^2 = \begin{bmatrix} \left(\lambda_1 \cos^4\beta + \lambda_2 \sin^4\beta + \frac{\lambda}{2}\sin^2 2\beta\right) v^2 & \left(\lambda_2 \sin^2\beta\,.\;\lambda_1 \cos^2\beta + \lambda\cos 2\beta\right) \frac{\sin 2\beta}{2} v^2 \\ \left(\lambda_2 \sin^2\beta\,.\;\lambda_1 \cos^2\beta + \lambda\cos 2\beta\right) \frac{\sin 2\beta}{2} v^2 & M^2 + \left(\lambda_1 + \lambda_2\,.\;2\lambda\right) \frac{\sin^2 2\beta}{4} v^2 \end{bmatrix}, \quad (4.7)$$

for CP-even Higgs bosons,

$$M_A^2 = M^2 - \lambda_5 v^2, \quad (4.8)$$

for CP-odd Higgs boson, and

$$M_S^2 = \begin{bmatrix} M^2 - \frac{\lambda_4+\lambda_5}{2} v^2 & -\frac{\mu v}{\sqrt{2}} \\ -\frac{\mu v}{\sqrt{2}} & m_0^2 + \left(\frac{\sigma_1}{2}\cos^2\beta + \frac{\sigma_2}{2}\sin^2\beta\right) v^2 \end{bmatrix}, \quad (4.9)$$

[2]Our analysis will thus be valid in the cases where the effect of the bottom Yukawa coupling sufficiently small; i.e. in the region of not too large $\tan\beta$.

for charged Higgs bosons. Here, $\lambda \equiv \lambda_3 + \lambda_4 + \lambda_5$ and $M^2 \equiv m_3^2/\sin\beta\cos\beta$. The vacuum expectation value v ($\sim$ 246 GeV) is equal to $\sqrt{2}\sqrt{\langle\phi_1^0\rangle^2 + \langle\phi_2^0\rangle^2}$. Mass eigenstates for the CP-even and the charged Higgs bosons are obtained by diagonalizing the mass matrices (4.7) and (4.9), respectively. The original Higgs boson fields, ϕ_1, ϕ_2, ω^-, can be expressed in terms of the physical states and the Nambu-Goldstone modes (G^0 and $G^\pm$) as

$$\phi_1^0 = \frac{1}{\sqrt{2}}\left(v\cos\beta + H\cos\alpha - h\sin\alpha + i(G^0\cos\beta - A\sin\beta)\right), \tag{4.10}$$

$$\phi_1^- = G^-\cos\beta - (S_1^-\cos\chi - S_2^-\sin\chi)\sin\beta, \tag{4.11}$$

$$\phi_2^0 = \frac{1}{\sqrt{2}}\left(v\sin\beta + H\sin\alpha + h\cos\alpha + i(G^0\sin\beta + A\cos\beta)\right), \tag{4.12}$$

$$\phi_2^- = G^-\sin\beta + (S_1^-\cos\chi - S_2^-\sin\chi)\cos\beta, \tag{4.13}$$

$$\omega^- = S_1^-\sin\chi + S_2^-\cos\chi, \tag{4.14}$$

where the angle α and χ are defined from the matrices which diagonalize the 2×2 matrices M_N^2 and M_S^2, respectively. Namely,

$$\begin{pmatrix} \cos(\alpha\,.\,\beta) & \sin(\alpha\,.\,\beta) \\ .\,\sin(\alpha\,.\,\beta) & \cos(\alpha\,.\,\beta) \end{pmatrix} M_N^2 \begin{pmatrix} \cos(\alpha\,.\,\beta) & .\,\sin(\alpha\,.\,\beta) \\ \sin(\alpha\,.\,\beta) & \cos(\alpha\,.\,\beta) \end{pmatrix} = \begin{pmatrix} m_H^2 & 0 \\ 0 & m_h^2 \end{pmatrix} \tag{4.15}$$

$$\begin{pmatrix} \cos\chi & \sin\chi \\ .\,\sin\chi & \cos\chi \end{pmatrix} M_S^2 \begin{pmatrix} \cos\chi & .\,\sin\chi \\ \sin\chi & \cos\chi \end{pmatrix} = \begin{pmatrix} m_{S_1}^2 & 0 \\ 0 & m_{S_2}^2 \end{pmatrix} \tag{4.16}$$

where $m_H^2 > m_h^2$ and $m_{S_1}^2 > m_{S_2}^2$. The mixing angles α and χ then satisfy

$$\tan 2\alpha = \frac{M^2 - (\lambda_3+\lambda_4+\lambda_5)\,v^2}{M^2 - (\lambda_1\cos^2\beta - \lambda_2\sin^2\beta)\frac{v^2}{\cos 2\beta}}\tan 2\beta, \tag{4.17}$$

$$\tan 2\chi = \frac{-\sqrt{2}\mu v}{M^2 - m_0^2 - \left(\lambda_4+\lambda_5+\sigma_1\cos^2\beta + \sigma_2\sin^2\beta\right)\frac{v^2}{2}}, \tag{4.18}$$

which show that α and χ approaches to $\beta - \frac{\pi}{2}$ and zero, respectively[3], when M^2 is much greater than v^2, μ^2 and m_0^2; i.e., in the decoupling regime, where the massive Higgs bosons from the extra weak-doublet are very heavy due to the large M so that they are decoupled from the low energy observables.

Although neutrinos in this model are massless at the tree level, the loop diagrams involving charged Higgs bosons, as shown in Fig. 4.1, can generate the Majorana mass

[3]Recall that we assumed $m_H > m_h$.

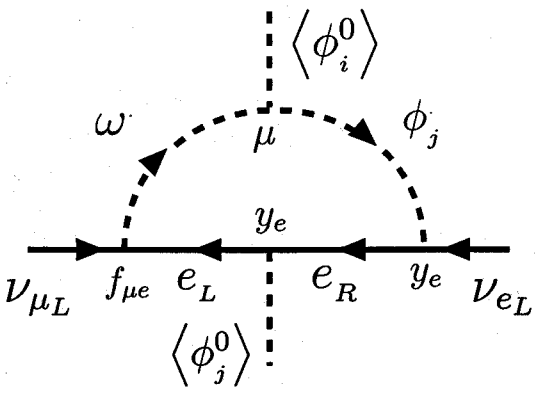

Figure 4.1: A representative diagram that generates the neutrino mass. For Model-I, $i = 1$, $j = 2$, and for Model-II, $i = 2$, $j = 1$.

terms for all three-flavor neutrinos. It was shown [12] that at the one loop order, the neutrino mass matrix is real and symmetric with vanishing diagonal elements, in the basis where the charged lepton Yukawa-coupling constants are diagonal in the lepton flavor space. More explicitly, we have

$$M_\nu = \begin{pmatrix} 0 & m_{12} & m_{13} \\ m_{12} & 0 & m_{23} \\ m_{13} & m_{23} & 0 \end{pmatrix}, \tag{4.19}$$

with

$$m_{ij} = f_{ij}(m_{e_j}^2 - m_{e_i}^2)\mu \cot\beta \frac{1}{16\pi^2} \frac{1}{m_{S_1}^2 - m_{S_2}^2} \ln \frac{m_{S_1}^2}{m_{S_2}^2}, \tag{4.20}$$

where m_{e_i} $(i = 1, 2, 3)$ is the charged lepton mass for Model-I. For Model-II, $\cot\beta$ should be replaced by $\tan\beta$. Note that Eq. (4.20) is valid for $m_{S_i} \gg m_{e_j}$.

The phenomenological analysis of the above mass matrix in the Zee-model was given in Ref. [36, 37]. It was concluded that, in the Zee-model, the bi-maximal mixing is the only possibility to reconcile the atmospheric and the solar neutrino data. Here we gave a brief summary of their results, for completeness. Let us denote the three eigenvalues for the neutrino mass matrix, cf. Eq. (4.19), as m_{ν_1}, m_{ν_2} and m_{ν_3}, which satisfy $m_{\nu_1} + m_{\nu_2} + m_{\nu_3} = 0$. The possible pattern of the neutrino mass spectrum which is allowed in the Zee-model is $|m_{\nu_1}| \simeq |m_{\nu_2}| \gg |m_{\nu_3}|$, with $m_{\nu_1}^2 - m_{\nu_3}^2 \simeq m_{\nu_2}^2 - m_{\nu_3}^2 = \Delta m_{atm}^2$, and $\left|m_{\nu_1}^2 - m_{\nu_2}^2\right| = \Delta m_{solar}^2$, where $\Delta m_{atm}^2 = O(10^{-3})$ eV^2 from the atmospheric neutrino data, and $\Delta m_{solar}^2 = O(10^{-5})$

eV^2 (MSW large angle solution) or $O(10^{-10})$ eV^2 (vacuum oscillation solution) from the solar neutrino data.[4] Thus, we have $|m_{\nu_1}| \simeq |m_{\nu_2}| \simeq \sqrt{\Delta m^2_{atm}}$ ($m_{\nu_1} \simeq -m_{\nu_2}$) and $|m_{\nu_3}| \simeq \frac{\Delta m^2_{solar}}{2\sqrt{\Delta m^2_{atm}}}$. The approximate form of the neutrino mass matrix is given by

$$M_\nu = \begin{pmatrix} 0 & \pm\sqrt{\frac{|m_{\nu_1} m_{\nu_2}|}{2}} & \mp\sqrt{\frac{|m_{\nu_1} m_{\nu_2}|}{2}} \\ \pm\sqrt{\frac{|m_{\nu_1} m_{\nu_2}|}{2}} & 0 & -m_{\nu_1} - m_{\nu_2} \\ \mp\sqrt{\frac{|m_{\nu_1} m_{\nu_2}|}{2}} & -m_{\nu_1} - m_{\nu_2} & 0 \end{pmatrix}, \tag{4.21}$$

where the upper (lower) sign corresponds to $m_h < 0$ (> 0) case, and the corresponding Maki-Nakagawa-Sakata (MNS) matrix[44], which diagonalizes the neutrino mass matrix, is

$$U = \begin{pmatrix} \sqrt{\frac{|m_{\nu_2}|}{|m_{\nu_1}|+|m_{\nu_2}|}} & \sqrt{\frac{|m_{\nu_1}|}{|m_{\nu_1}|+|m_{\nu_2}|}} & 0 \\ -\frac{1}{\sqrt{2}}\sqrt{\frac{|m_{\nu_1}|}{|m_{\nu_1}|+|m_{\nu_2}|}} & \frac{1}{\sqrt{2}}\sqrt{\frac{|m_{\nu_2}|}{|m_{\nu_1}|+|m_{\nu_2}|}} & \frac{1}{\sqrt{2}} \\ \frac{1}{\sqrt{2}}\sqrt{\frac{|m_{\nu_1}|}{|m_{\nu_1}|+|m_{\nu_2}|}} & -\frac{1}{\sqrt{2}}\sqrt{\frac{|m_{\nu_2}|}{|m_{\nu_1}|+|m_{\nu_2}|}} & \frac{1}{\sqrt{2}} \end{pmatrix}. \tag{4.22}$$

In the above equations, we took the limiting case where $U_{13} = 0$ and $U_{32} = U_{23} = \frac{1}{\sqrt{2}}$.[5] From Eqs. (4.20) and (4.21), we obtain

$$\left|\frac{f_{12}}{f_{13}}\right| \simeq \frac{m_\tau^2}{m_\mu^2} \simeq 3 \times 10^2, \tag{4.23}$$

$$\left|\frac{f_{13}}{f_{23}}\right| \simeq \frac{\sqrt{2}\Delta m^2_{atm}}{\Delta m^2_{solar}} \simeq \begin{cases} 10^2 & \text{(for the MSW large angle solusion)} \\ 10^7 & \text{(for the vacuum oscillation solusion)} \end{cases}. \tag{4.24}$$

Therefore, the magnitudes of the three coupling constants should satisfy the relation $|f_{12}| \gg |f_{13}| \gg |f_{23}|$. This hierarchy among the couplings f_{ij} is crucial for our later discussion on the phenomenology of the singlet charged Higgs bosons.

For a given value of the parameters m_{S_1}, m_{S_2}, $\tan\beta$ and μ, the coupling constants f_{ij} can be calculated from Eq. (4.20). For example, for $m_{S_1} = 500\,\text{GeV}$, $m_{S_2} = 100\,\text{GeV}$, $\tan\beta = 1$, and $\mu = 100\,\text{GeV}$ and $m_{12} = 3 \times 10^{-2}\,\text{eV}$, we obtain $|f_{12}| \sim 3 \times 10^{-4}$. As in this example, when S_1^- is rather heavy and the lighter charged Higgs boson S_2^- is

[4]Due to the structure of the mass matrix, cf. Eq. (4.19), only the hierarchy pattern $|m_{\nu_1}| \simeq |m_{\nu_2}| \gg |m_{\nu_3}|$, rather than $|m_{\nu_1}| \simeq |m_{\nu_2}| \ll |m_{\nu_3}|$, is realized in the Zee-model [36, 37].

[5]This limit corresponds to $\theta_2 = \frac{\pi}{4}$ and $\theta_3 = 0$ in the notation of Ref. [44].

almost a weak singlet, i.e. the mixing angle χ approaches to zero, it is unlikely to have an observable effect from the Zee-model to the low energy data[39]; e.g., the muon life-time, the universality of tau decay into electron or muon, the rare decay of $\mu \to e\gamma$, the universality of W-boson decay into electron, muon or tau, and the decay width of Z boson. When $|f_{ij}|$ are small, we do not expect a large rate in the lepton flavor violation decay of a light neutral Higgs boson, such as $h \to \mu^{\pm}e^{\mp}$ (the largest one), $h \to e^{\pm}\tau^{\mp}$, or $h \to \mu^{\pm}\tau^{\mp}$ (the smallest one). On the contrary, as to be discussed in Section 4.3, the decay width of $h \to \gamma\gamma$ can significantly deviate from the SM value.

Finally, the phenomenological constraints on f_{12} were derived in Ref. [38]. From the consistency of the muon decay rate and electroweak precision test they found

$$\frac{f_{12}^2}{\overline{M}^2} < 7 \times 10^{-4} G_F \,, \tag{4.25}$$

where G_F is the Fermi constant, and

$$\frac{1}{\overline{M}^2} = \frac{\sin^2\chi}{m_{S_1}^2} + \frac{\cos^2\chi}{m_{S_2}^2}. \tag{4.26}$$

This means that the f_{ij} cannot be $O(1)$ unless the charged Higgs boson masses are at the order of 10 TeV.

4.2 Higgs boson mass and couplings through RGE's

In this section, we determine the bounds on the mass of the lightest CP-even Higgs boson as a function of the cut-off scale of the Zee-model by analyzing the set of RGE's. We also study the allowed ranges of the coupling constants, especially σ_1 and σ_2 in Eq. (4.4). In Sec. 4.3, they will be used to evaluate how much the partial decay width of $h \to \gamma\gamma$ can deviate from its SM value due to the one-loop contribution from the singlet charged Higgs boson.

The mass bounds are determined in the following manner. For each set of parameters defined at the electroweak scale, the running coupling constants are calculated numerically through RGE's at the one-loop level. We require that any of the dimensionless coupling constants does not blow up below a given cut-off scale Λ, and the coupling constants satisfy the vacuum stability condition, to be discussed later. We vary the input parameters at the

electroweak scale and determine the possible range of the lightest CP-even Higgs boson mass as a function of Λ. In a similar manner, we can also study the allowed ranges of various Higgs boson self-coupling constants at the electroweak scale as well as the correlation between the size of the Higgs boson mass and of the self-coupling constants.

We derived the one-loop RGE's for the Zee-model, and listed them in the Appendix B for reference. For simplicity, in the RGE's, we have neglected all the Yukawa coupling constants (y_u, y_d, y_e) but the top Yukawa coupling y_t.[6] Although we have kept the new coupling constants f_{ij} in the RGE's given in the Appendix B, we have neglected f_{ij} in the numerical calculation, because the magnitudes of these coupling constants are numerically small and do not affect the results unless the singlet-charged scalar-boson mass is larger than a few TeV [cf. Eq. (4.25)]. The dimensionless coupling constants relevant to our numerical analysis are the three gauge-coupling constants g_1, g_2, g_3, the top Yukawa-coupling constant y_t, and eight scalar self-coupling constants, λ_i $(i = 1 - 5)$ and σ_i $(i = 1 - 3)$. There are five dimensionful parameters in the Higgs potential, namely m_1^2, m_2^2, m_3^2, m_0^2 and μ. Instead of m_1^2, m_2^2, m_3^2, we take v, $\tan\beta$, and $M^2 \equiv m_3^2/\sin\beta\cos\beta$, as independent parameters, where v (~ 246 GeV) characterizes the weak scale and M the soft-breaking scale for the discrete symmetry.

In the actual numerical calculation we first fix $\tan\beta$ and M. For a given mass (m_h) for the lightest CP-even Higgs boson, we solve one of λ_i, which is chosen to be λ_3 here, in terms of other λ_i. We then numerically evaluate all dimensionless coupling constants according to the RGE's. From m_h to M we use the SM RGE's, which are matched to the Zee-model RGE's at the soft-breaking scale M. [7]

We requires the following two conditions to be satisfied for each scale Q up to a given cut-off scale Λ.

1. Applicability of the perturbation theory implies

[6] In the model with the type-II Yukawa interaction, the bottom-quark Yukawa interaction can become important for a large $\tan\beta$.

[7] The parameter m_0 and μ are only relevant to the charged scalar mass matrix. In principle, the numerical results depend on these parameters through the renormalization of various coupling constants between m_h and the charged scalar mass scale. Since these effects are expected to be small, we calculate the RGE's as if all the scalar-bosons except for h decouple at the scale M.

$$\lambda_i(Q) < 8\pi, \quad \sigma_i(Q) < 8\pi, \quad y_t^2(Q) < 4\pi\,. \tag{4.27}$$

2. The vacuum stability conditions must be satisfied. The requirement that quartic terms of the scalar potential do not have a negative coefficient in any direction leads to the following conditions at each renormalization scale Q:

(a)

$$\lambda_1(Q) > 0, \quad \lambda_2(Q) > 0, \quad \sigma_3(Q) > 0\,. \tag{4.28}$$

(b)

$$\sigma_1(Q) + \sqrt{\frac{\lambda_1(Q)\,\sigma_3(Q)}{2}} > 0\,, \tag{4.29}$$

$$\sigma_2(Q) + \sqrt{\frac{\lambda_2(Q)\,\sigma_3(Q)}{2}} > 0\,, \tag{4.30}$$

$$\overline{\lambda}(Q) + \sqrt{\lambda_1(Q)\,\lambda_2(Q)} > 0\,, \tag{4.31}$$

where $\overline{\lambda}(Q) = \lambda_3(Q) + \min\left(0,\ \lambda_4(Q) + \lambda_5(Q),\ \lambda_4(Q) - \lambda_5(Q)\right)$.

(c) If $\sigma_1(Q) < 0$ and $\sigma_2(Q) < 0$, then

$$\overline{\lambda}(Q) + \frac{2}{\sigma_3(Q)}\left\{\sqrt{\left(\frac{\lambda_1(Q)\,\sigma_3(Q)}{2} - \sigma_1^2(Q)\right)\left(\frac{\lambda_2(Q)\,\sigma_3(Q)}{2} - \sigma_2^2(Q)\right)} - \sigma_1(Q)\,\sigma_2(Q)\right\} > 0\,. \tag{4.32}$$

If $\sigma_1(Q) < 0$ and $\overline{\lambda}(Q) < 0$, then

$$\sigma_2(Q) + \frac{1}{\lambda_1(Q)}\left\{\sqrt{\left(\lambda_1(Q)\,\lambda_2(Q) - \overline{\lambda}^2(Q)\right)\left(\frac{\lambda_1(Q)\,\sigma_3(Q)}{2} - \sigma_1^2(Q)\right)} - \sigma_1(Q)\,\overline{\lambda}(Q)\right\} > 0\,. \tag{4.33}$$

If $\sigma_2(Q) < 0$ and $\overline{\lambda}(Q) < 0$, then

$$\sigma_1(Q) + \frac{1}{\lambda_2(Q)}\left\{\sqrt{\left(\lambda_1(Q)\,\lambda_2(Q) - \overline{\lambda}^2(Q)\right)\left(\frac{\lambda_2(Q)\,\sigma_3(Q)}{2} - \sigma_2^2(Q)\right)} - \sigma_2(Q)\,\overline{\lambda}(Q)\right\} > 0\,. \tag{4.34}$$

[When all of $\sigma_1(Q)$, $\sigma_2(Q)$ and $\overline{\lambda}(Q)$ are negative, above three conditions are equivalent.]

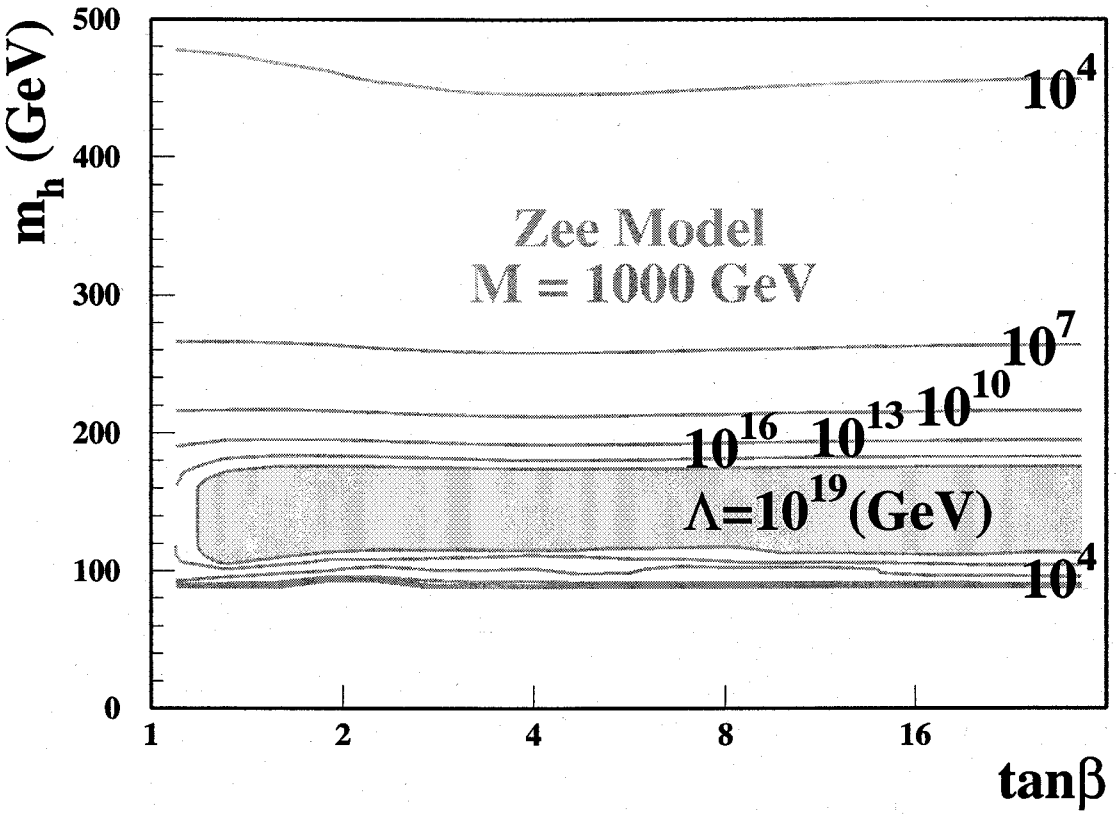

Figure 4.2: The allowed mass range of the lightest CP-even Higgs boson for $M = 1000$ GeV. Λ is the cut-off scale.

In addition to the above conditions, we also demand local stability of the potential at the electroweak scale, namely, we calculate the mass spectrum of all scalar fields at the extremum of the potential and make sure that all eigenvalues of the scalar-mass-squared are positive. We scan the remaining seven-dimensional space of λ_i and σ_i and examine whether a given mass of the lightest CP-even Higgs boson is allowed under the above conditions. In this way we obtain the allowed range of the mass of h in the space of $\tan\beta$ and M for each value of the cut-off scale Λ.

First, we discuss our result in the decoupling case, in which the soft-breaking scale M is much larger than the electroweak scale $\sim v$, and the masses of all the Higgs bosons but h are at the order of M.[8] In Fig. 4.2, the allowed range of m_h is shown as a function of $\tan\beta$

[8]In the decoupling regime ($M \to \infty$, which leads to $\alpha \to \beta - \frac{\pi}{2}$ and $\chi \to 0$), the masses of h and S_2 are dominated by the (1 1) component of the mass matrix in Eq. (4.7) and the (2 2) component of that in Eq. (4.9) respectively. The mass of h is determined by the self-coupling constants λ_i, while that of S_2

for $M = 1000$ GeV. (We take the pole mass of top quark $m_t = 175$ GeV, $\alpha_s(m_Z) = 0.118$ for numerical calculation.) The allowed ranges are shown as contours for six different values of Λ, i.e. $\Lambda = 10^{19}$, 10^{16},10^{13},10^{10},10^{7} and 10^{4} GeV. For most values of $\tan\beta$ except for small $\tan\beta$ region, the upper bound of m_h is about 175 GeV and the lower bound is between 110 GeV and 120 GeV for the cut-off scale Λ to be near the Planck scale. The numerical values in this figure are very close to those in the corresponding figure for the 2HDM discussed in Chapter 2 [10]. Compared to the corresponding lower mass bound in the SM, which is 145 GeV when using the one-loop RGE's, the lower mass bound in this model is reduced by about 30 GeV to 40 GeV. The reason is similar to the 2HDM case: the lightest CP-even Higgs boson mass is essentially determined by the value of λ_2 for $\tan\beta$ to be larger than about 2 , where λ_2 plays the role of the unique self-coupling constant of the Higgs potential in the SM[9]. On the right-hand side of the RGE for λ_2, cf. Eq. (B.5), there are additional positive-definite terms $\frac{2}{16\pi^2}(\lambda_3^2 + (\lambda_3+\lambda_4)^2 + \lambda_5^2 + \sigma_2^2)$ as compared to the RGE for the Higgs self-coupling constant in the SM. These additional terms can improve vacuum stability, and allow lower values of m_h. Therefore, one of the features of the model is to have a different mass range for the lightest CP-even Higgs boson as compared to the SM Higgs boson, for a given cut-off scale.

Next, we show our result for M to be around v. In Fig. 4.3, we present the m_h bound for $M = 100$ GeV. In this case, the allowed range of m_h is reduced as compared to that in the decoupling case, and lies around $m_h \sim M$ for large $\tan\beta$. Notice that we have not included phenomenological constraints from the $b \to s$, ρ parameter and the direct Higgs boson search experiment at LEP. As mentioned before, the mass bounds obtained from the RGE analysis are the same for the Model-I and Model-II models without these phenomenological constraints. However, it was shown in Section 3.2 [10] that the $b \to s$

depends not only on the self-coupling constants σ_i but also on the free mass parameter m_0. As noticed in the footnote 7, from m_h to M, the SM RGE are used in our analysis, even if the mass S_2 is smaller than M. The effect of S_2 on the mass bound of h is expected to be small, because at the one-loop level the primary effect is through the running of g_1, whose contribution to the right-handed side of the RGE for the Higgs-self coupling constant is small.

[9]However, $\tan\beta$ cannot be too large to ignore the contribution of the bottom quark in the case with the type-II Yukawa interaction.

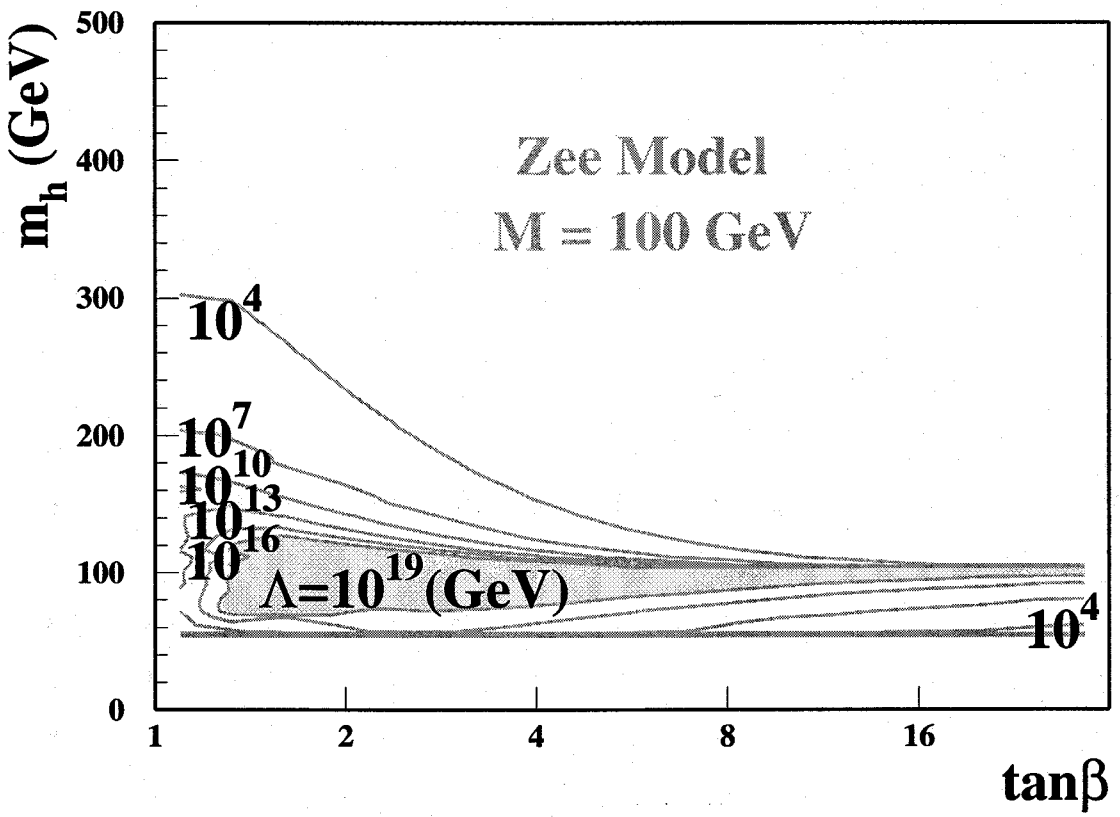

Figure 4.3: The allowed mass range of the lightest CP-even Higgs boson for $M = 100$ GeV.

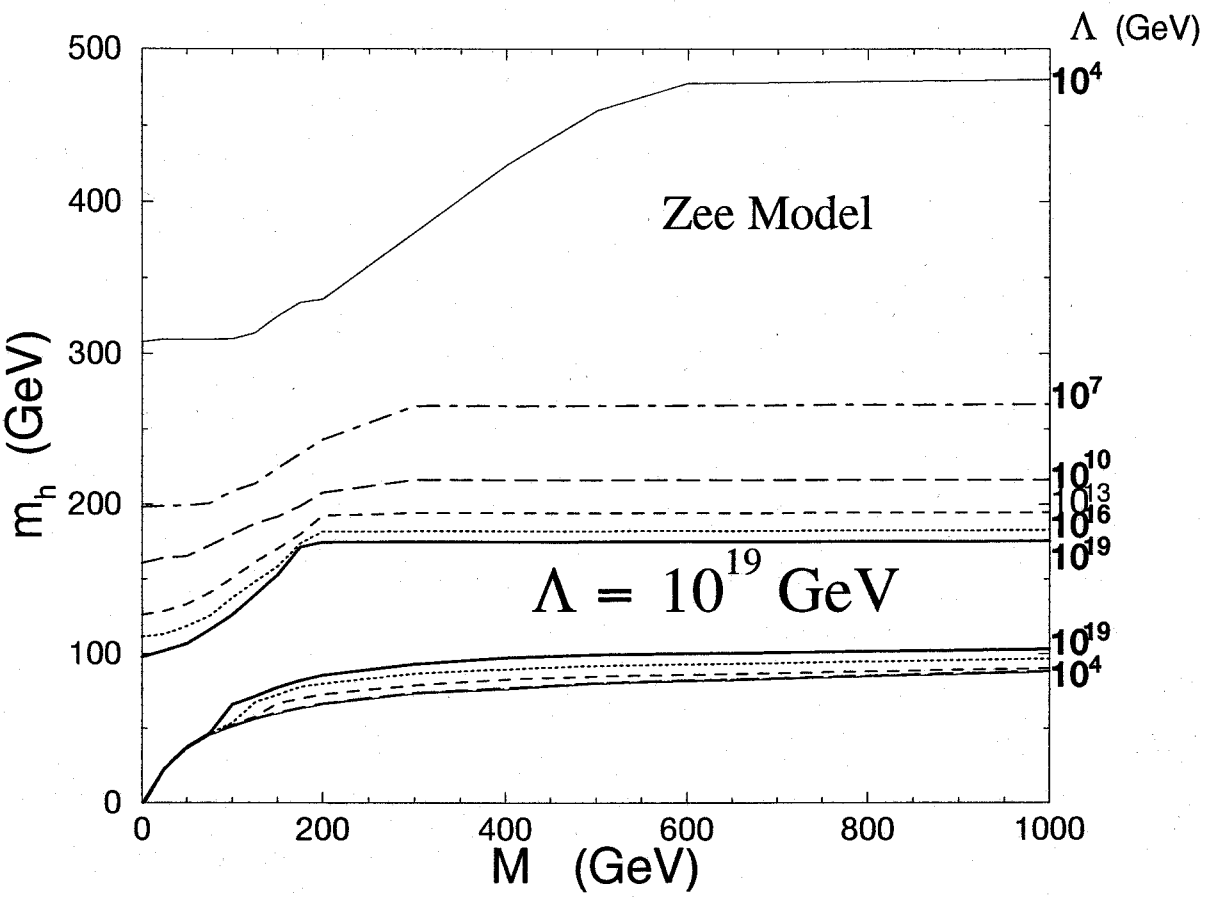

Figure 4.4: The allowed ranges of the lightest CP-even Higgs boson mass as a function of M for various Λ values.

data can put a strong constraint on the allowed range of the Higgs boson mass for $M \lesssim 200$ - 400 GeV in the Model-II 2HDM, whereas there is no appreciable effect in the Model-I model. This is because a small M implies a light charged Higgs boson in the 2HDM which can induce a large decay branching ratio for $b \to s\gamma$ in the Model-II model.[10] We expect a similar constraint from the $b \to s\gamma$ data on the Model-II Zee-model, when M is small.

In Fig. 4.4, we show the upper and lower bounds of m_h as a function of M for various values of Λ. For fixed M, we scan a range of $\tan\beta$ for $1 \leq \tan\beta \leq 16\sqrt{2}$ ($\simeq 22.6$). We find that the obtained m_h bounds are almost the same as those for the 2HDM[11]. The primary

[10]In addition, it has been known that the R_b data also give strong constraints on the charged Higgs bosons in the Model-I 2HDM [45].

[11]For the type-II 2HDM, the constraint from the $b \to s\gamma$ data should be included.

reason for this is that the new coupling constants σ_1, σ_2 and σ_3 do not appear directly in the mass formula of m_h, and therefore, do not induce large effects on the bounds of m_h.

We also investigate the allowed range of coupling constants σ_1, σ_2 and σ_3. For this purpose, we fix σ_1 (or σ_2, σ_3) as well as $\tan\beta$ and M to evaluate the upper and the lower bounds of m_h for each Λ value. In this way, we determine the possible range of σ_1 (or σ_2, σ_3) under the condition that the theory does not break down below the cut-off scale Λ. In Fig. 4.5, we present the allowed range of σ_1 and m_h for different choice of Λ in the case of $M = 1000$ GeV and $\tan\beta = \sqrt{2}$ or $16\sqrt{2}$. A similar figure is shown for the possible range of σ_2 in Fig. 4.6. We see that the maximal value of σ_1 and σ_2 is around 0.7 for $m_h = 110 - 170$ GeV if we take the cut-off scale to be 10^{19} GeV. For smaller value of Λ the allowed ranges of σ_i becomes larger. For example, σ_1 can exceed 1 for $\Lambda = 10^{13}$ GeV. We have calculated for other value of $\tan\beta$ and checked that these figures does not change greatly between $\tan\beta = 1.4$ and $16\sqrt{2}$. We also present the allowed range in σ_1 and σ_2 space for a fixed value of m_h in Fig. 4.7 ($m_h = 125$ GeV) and in Fig. 4.8 ($m_h = 140$ GeV). For either value of m_h with $\tan\beta = 16\sqrt{2}$, both σ_1 and σ_2 can be as large as 0.5 (2) for $\Lambda = 10^{19}$ (10^7) GeV. The allowed range of σ_3 and m_h for various values of Λ is given in Fig. 4.9. As shown, σ_3 has to be larger than zero, which is due to the vacuum stability condition. The maximal value of σ_3 is about 1 (3) for $\Lambda = 10^{19}$ (10^7) GeV and $M = 1000$ GeV. The impact of these new coupling constants to collider phenomenologies is given in the next section.

4.3 Two-photon decay width of the neutral Higgs boson

In this section, we study the phenomenological consequences of the Higgs boson mass and the coupling constants derived in the previous section. The important feature of the Higgs sector of the Zee-model is that there are additional weak doublet and singlet Higgs fields. The physical states of the Higgs particles are two CP-even Higgs bosons, one CP-odd Higgs boson and two pairs of charged Higgs bosons. Therefore, the Higgs phenomenology is quite close to the ordinary two Higgs doublet model. One unique difference is the existence of

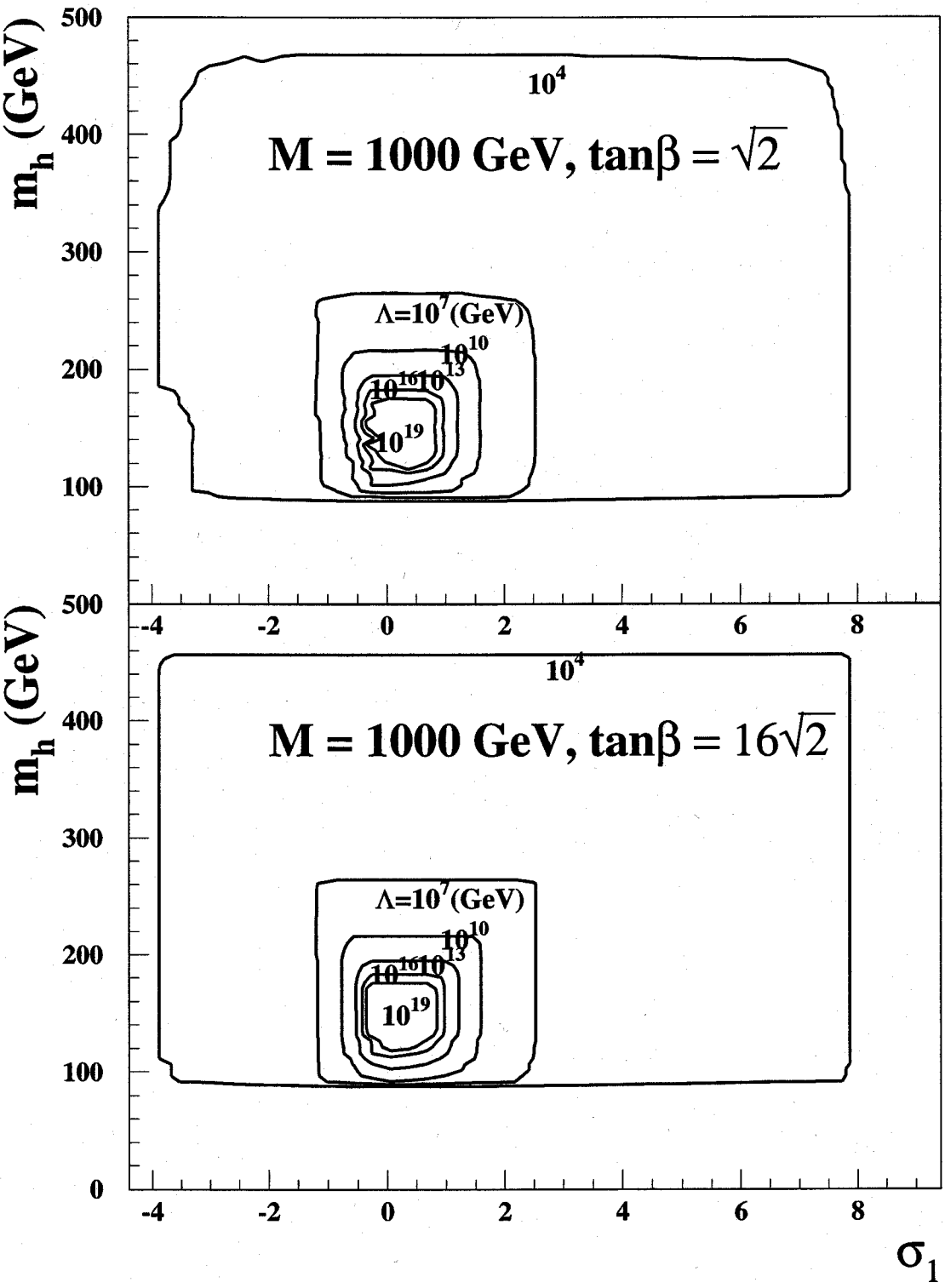

Figure 4.5: The allowed range of σ_1 and m_h for various Λ values.

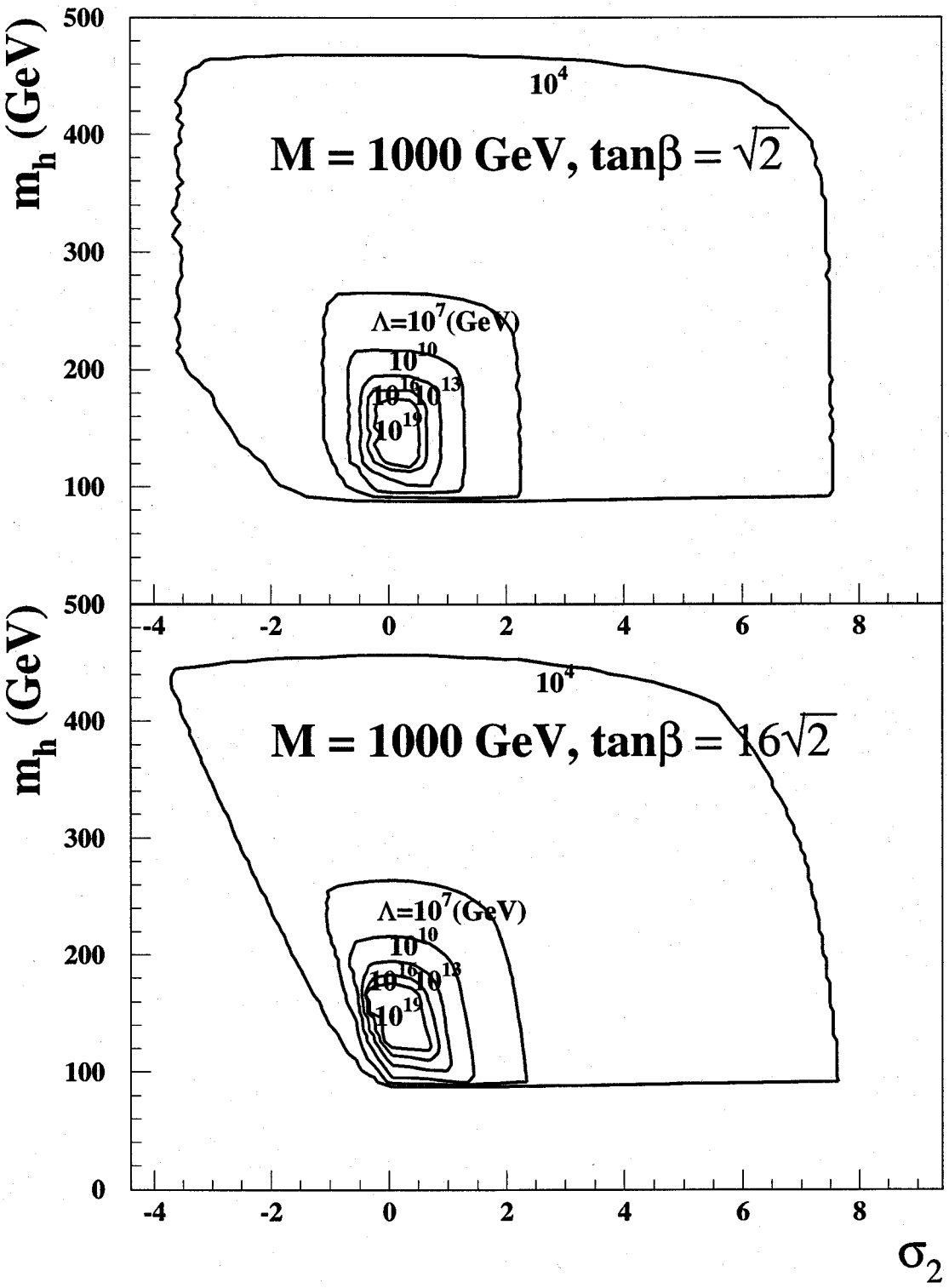

Figure 4.6: The allowed range of σ_2 and m_h for various Λ values.

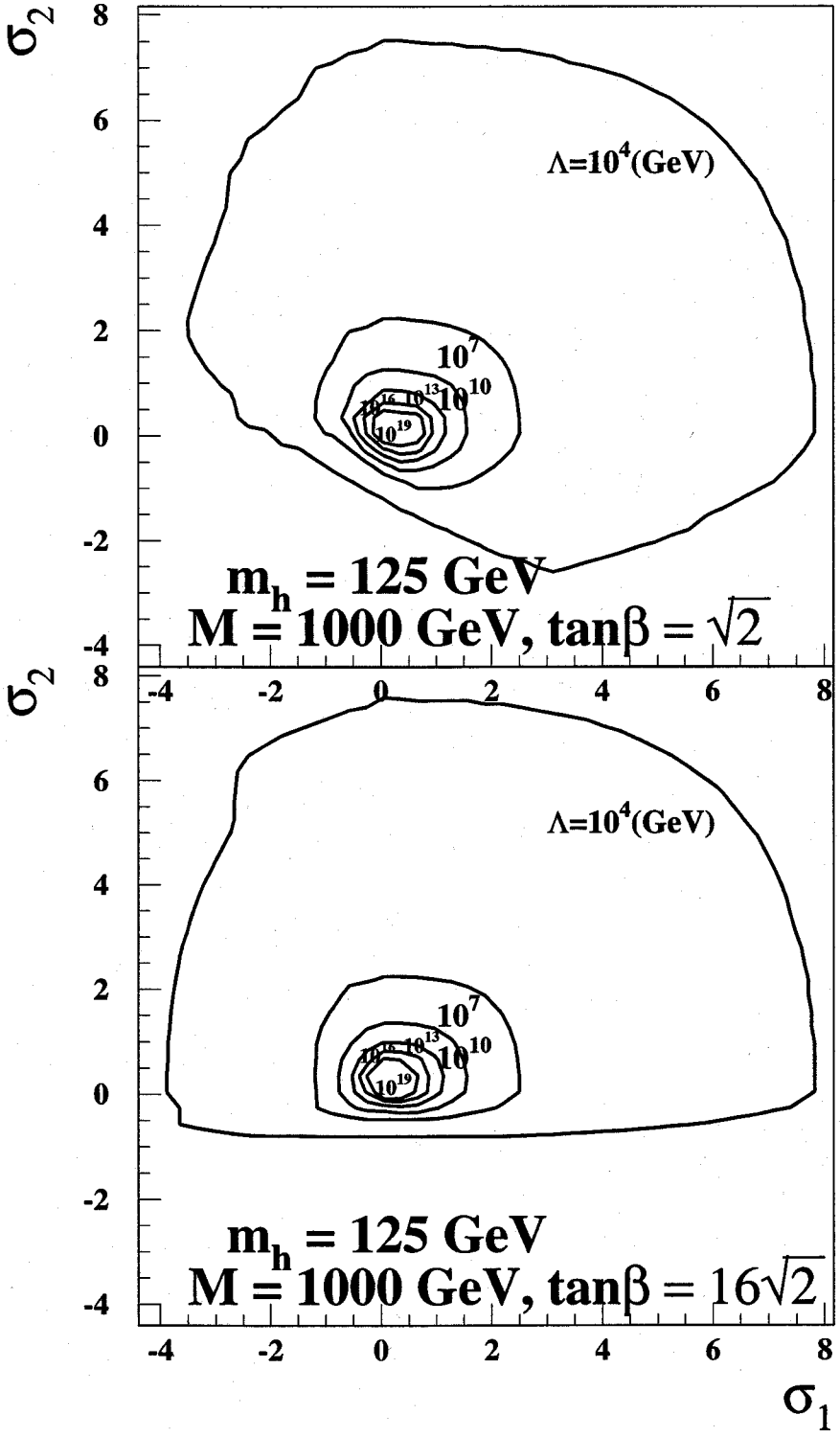

Figure 4.7: The allowed range of σ_1 and σ_2 for $m_h = 125$ GeV.

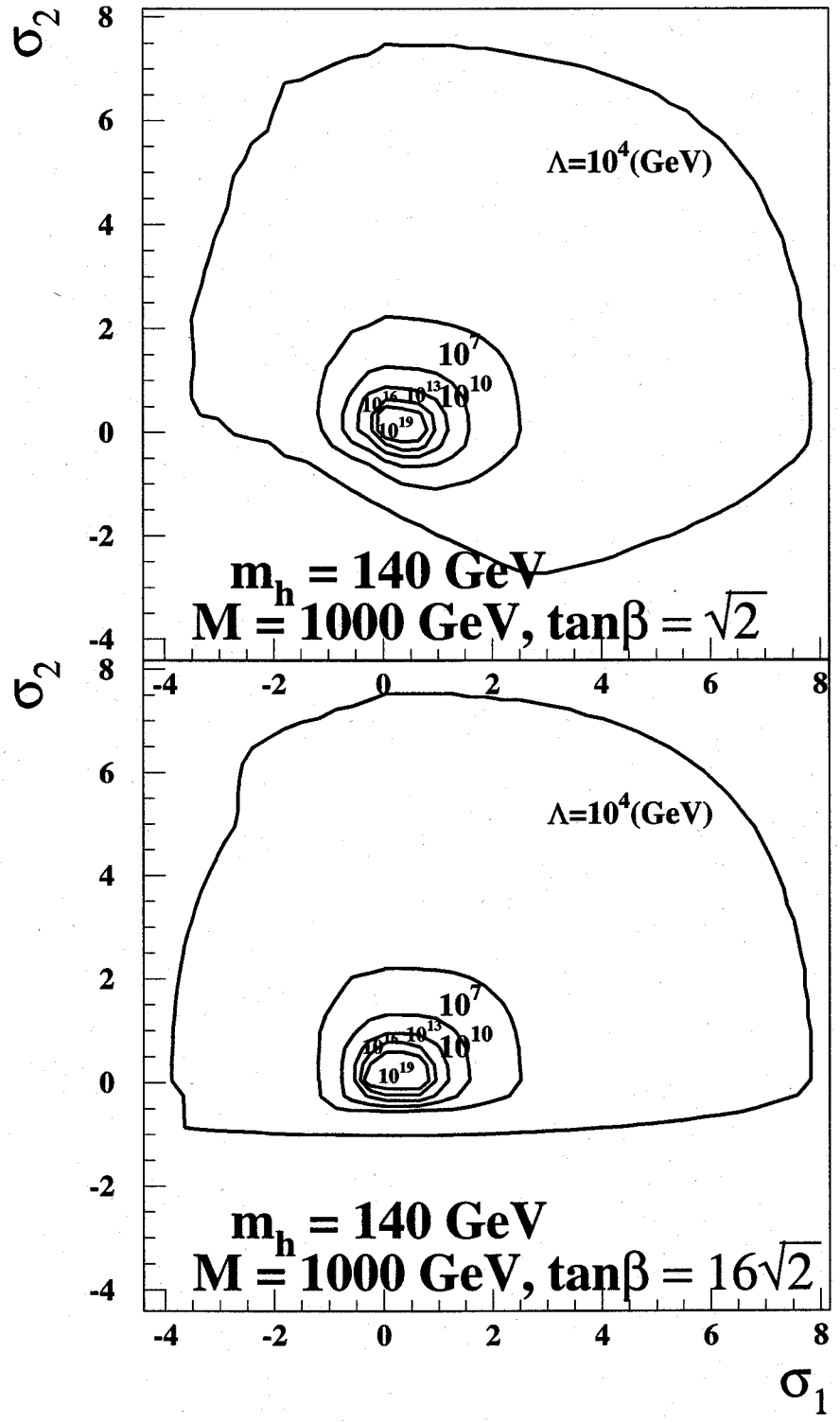

Figure 4.8: The allowed range of σ_1 and σ_2 for $m_h = 140$ GeV.

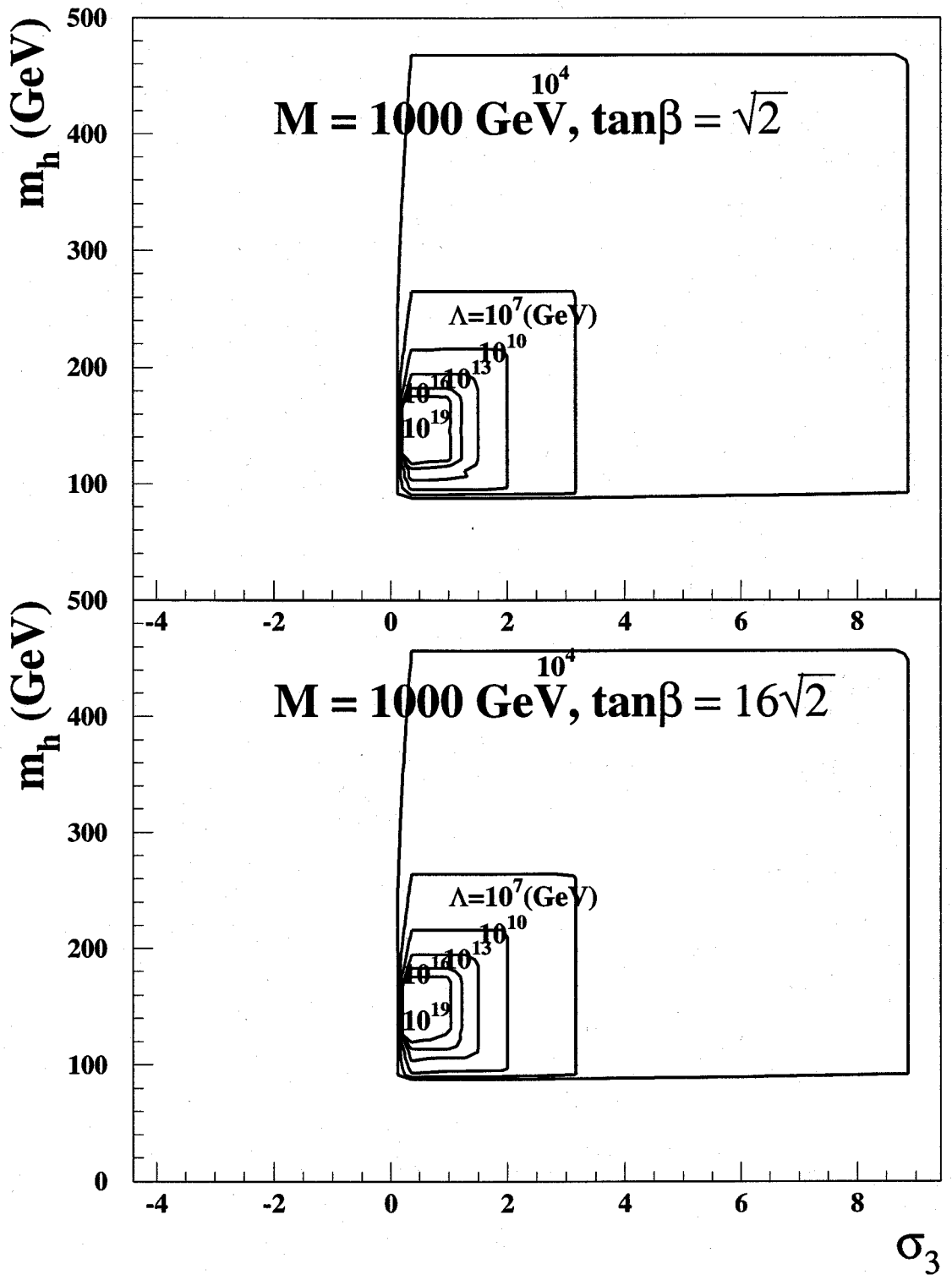

Figure 4.9: The allowed range of σ_3 and m_h for various Λ values.

the additional weak-singlet charged Higgs boson. The effect of this extra charged Higgs boson is especially important when M is much larger than the Z boson mass, i.e. in the decoupling regime. In such a case, the heavier CP-even Higgs boson, the CP-odd Higgs boson as well as one of the charged Higgs bosons have masses approximately equal to M, and these heavy states are decoupled from low energy observables. (Note that the condition of the applicability of the perturbation theory forbids the couplings among Higgs bosons to become too large. Hence, in the limit of large M, the heavy Higgs bosons decouple from the low energy effective theory.) The remaining light states are the lighter CP-even Higgs boson h and the lighter charged Higgs boson S_2 which mainly comes from the weak-singlet. In the previous section, we show that even in the decoupling case, there can be large difference in the allowed range of m_h between the Zee-model and the SM. Similarly, we expect that even in the decoupling case, the presence of the additional weak-singlet charged Higgs boson can give interesting effects in the Higgs phenomenology.

Since the lighter charged Higgs boson S_2 can couple to Higgs bosons and leptons, it can affect the phenomenology of the decay and the production of the neutral Higgs bosons at colliders through radiative corrections. In the following, we consider the decay width of $h \to$ as an example. For a SM Higgs boson, the partial decay width (or branching ratio) of $h \to$ is small: ~ 9.2 KeV (or 2.2×10^{-3}) for $m_h = 125$ GeV, and ~ 15.4 KeV (or 1.9×10^{-3}) for $m_h = 140$ GeV, with a 175 GeV top quark. Nevertheless, it is an important discovery mode of the Higgs boson at the LHC experiments for m_h less than about twice of the W-boson mass. Needless to say that a change in the branching ratio of $h \to$ would lead to a different production rate of $pp \to hX \to X$. At future e^+e^- LC's, the branching ratio of $h \to$ can be determined via the reaction $e^+e^- \to q\bar{q}$ and $e^+e^- \to \nu\bar{\nu}$ with a 16-22% accuracy [42]. At the photon-photon collision option of the future LC's, the partial decay width of $h \to$ can be precisely tested by measuring the inclusive production rate of the Higgs boson h, and a change in the partial decay width of $h \to$ will lead to a different production rate of h. In the Zee-model, such a change is expected after taking into account the loop contribution of the extra charged Higgs boson. We find that the deviation from the SM prediction can be sizable, and can be tested at the LHC and the LC.

The partial decay width of $h \to$ is calculated at the one loop order. Similar to our previous discussion, we limit ourselves to the parameter space in which $\tan\beta < 16\sqrt{2}$, and only keep top quark contribution from fermionic loop diagrams. Including the loop contributions from the W boson and the charged Higgs bosons S_1 and S_2 together with the top quark loop contribution, we obtain[17]

$$\Gamma(h \to \quad) = \frac{(\alpha m_h)^3}{256\pi^2 \sin^2\theta_W m_W^2} \left| \sum_{i=S_1,S_2,t,W} I_i \right|^2 , \tag{4.35}$$

with

$$\begin{aligned} I_{S_1} &= R_{S_1} F_0(r_i) , \\ I_{S_2} &= R_{S_2} F_0(r_i) , \\ I_t &= \frac{4}{3} \frac{\cos\alpha}{\sin\beta} \Big) F_{1/2}(r_i) , \\ I_W &= \sin(\beta-\alpha) F_1(r_i) , \end{aligned}$$

where $r_i = \frac{4m_i^2}{m_h^2}$ and m_i is the mass of the internal lines in the loop diagram. R_{S_1} and R_{S_2} are given by

$$\begin{aligned} R_{S_1} &= \frac{v^2}{2}\frac{1}{m_{S_1}^2}\Big[\cos^2\chi\Big\{-\lambda_1 \sin\alpha \sin^2\beta\cos\beta + \lambda_2 \cos\alpha \sin\beta \cos^2\beta \\ &\quad + \lambda_3\left(\cos\alpha\sin^3\beta - \sin\alpha\cos^3\beta\right) - \frac{1}{2}(\lambda_4+\lambda_5)\cos(\alpha+\beta)\sin 2\beta\Big\} \\ &\quad + \sin^2\chi\{-\sigma_1\sin\alpha\cos\beta + \sigma_2\cos\alpha\sin\beta\} + \sqrt{2}\sin\chi\cos\chi\frac{\mu}{v}\sin(\alpha-\beta)\Big] \end{aligned} \tag{4.36}$$

$$\begin{aligned} R_{S_2} &= \frac{v^2}{2}\frac{1}{m_{S_2}^2}\Big[\sin^2\chi\Big\{-\lambda_1 \sin\alpha \sin^2\beta\cos\beta + \lambda_2 \cos\alpha \sin\beta \cos^2\beta \\ &\quad + \lambda_3\left(\cos\alpha\sin^3\beta - \sin\alpha\cos^3\beta\right) - \frac{1}{2}(\lambda_4+\lambda_5)\cos(\alpha+\beta)\sin 2\beta\Big\} \\ &\quad + \cos^2\chi\{-\sigma_1\sin\alpha\cos\beta + \sigma_2\cos\alpha\sin\beta\} - \sqrt{2}\sin\chi\cos\chi\frac{\mu}{v}\sin(\alpha-\beta)\Big] \end{aligned} \tag{4.37}$$

and

$$F_0(r) = r\left(1 - rf(r)\right) , \tag{4.38}$$

$$F_{1/2}(r) = -2r\left(1 + (1-r)f(r)\right) , \tag{4.39}$$

$$F_1(r) = 2 + 3r + 3r\left(2-r\right)f(r) , \tag{4.40}$$

with

$$f(r) = \begin{cases} \left[\sin^{-1}\left(\sqrt{1/r}\right)\right]^2 & \text{if } r \geq 1 \\ -\frac{1}{4}\left[\ln\frac{1+\sqrt{1-r}}{1-\sqrt{1-r}} - i\pi\right]^2 & \text{if } r < 1 \end{cases} . \tag{4.41}$$

In the decoupling case of the model, namely $M^2 \gg \lambda_i v^2$, the above formulae are greatly simplified. This limit corresponds to $\alpha \to \beta - \frac{\pi}{2}$ and $\chi \to 0$, so that the light charged Higgs boson $S_2^\pm$ is identical to the weak-singlet Higgs boson $\omega^\pm$. Thus, we have

$$R_{S_2} \to \frac{v^2}{2}\frac{1}{m_{S_2}^2}\left(\sigma_1 \cos^2\beta + \sigma_2 \sin^2\beta\right) , \tag{4.42}$$

and the top-quark and W boson loop contributions reduce to the SM value. We like to stress that the weak-singlet Higgs boson does not directly couple to the quark fields in the limit of $\chi \to 0$. Therefore, it does not affect the decay rate of $b \to s\gamma$ at the one-loop order. Similarly, being a weak singlet, it also gives no contribution to the ρ parameter. Hence the low-energy constraint from either the $b \to s\gamma$ decay or the ρ parameter on the Zee-model in the limit of $\chi \to 0$ is similar to effects of that on the 2HDM.

Let us look at the one-loop effect of the weak-singlet charged Higgs boson on the decay width of $h \to \gamma\gamma$ in the decoupling case. Recall that in Fig. 4.8, the size of the new couplings σ_1 and σ_2 can be as large as 2 simultaneously, if the cut-off scale is at the order of 10^7 GeV. For the Zee-model to be a valid low energy effective theory up to 10^{19} GeV, σ_1 and σ_2 can not be much larger than 0.6 either for $\tan\beta = 1.4$ or 22.6. To illustrate the implications of this result, we show in Fig. 4.10 (a) and Fig. 4.10 (b) the ratio (r) of the $h \to \gamma\gamma$ width predicted in the Zee-model to that in the SM, $r = \Gamma_{\rm Zee}(h \to \gamma\gamma)/\Gamma_{\rm SM}(h \to \gamma\gamma)$, as a function of the coupling constant σ_2 and the charged Higgs boson mass m_{S_2}. Here, for simplicity, we have set $\sigma_1 = \sigma_2$ so that the $\tan\beta$ dependence drops in the decoupling case, cf. Eq. (4.42). For illustrations, we consider two cases for the mass of the lighter CP-even Higgs boson: $m_h = 125$ GeV and $m_h = 140$ GeV. As shown in the figures, the ratio r can be around 0.8 for $\sigma_1 = \sigma_2 \equiv \sigma \approx 0.5$ and $m_{S_2} \approx 100$ GeV. This reduction is due to the cancellation between the contribution from the S_2-boson loop and the W-boson loop contributions. To have a similar reduction rate in $\Gamma_{\rm Zee}(h \to \gamma\gamma)$ for a heavier S_2, the coupling constant σ_2 (and σ_1) has to be larger. Next, as is shown in Figs. 7 and 8, σ_1 and σ_2 do not have to have the same values in general, and they can be less than zero. In the cases with the negative values of σ_1 and σ_2, the contribution of the S_2-loop

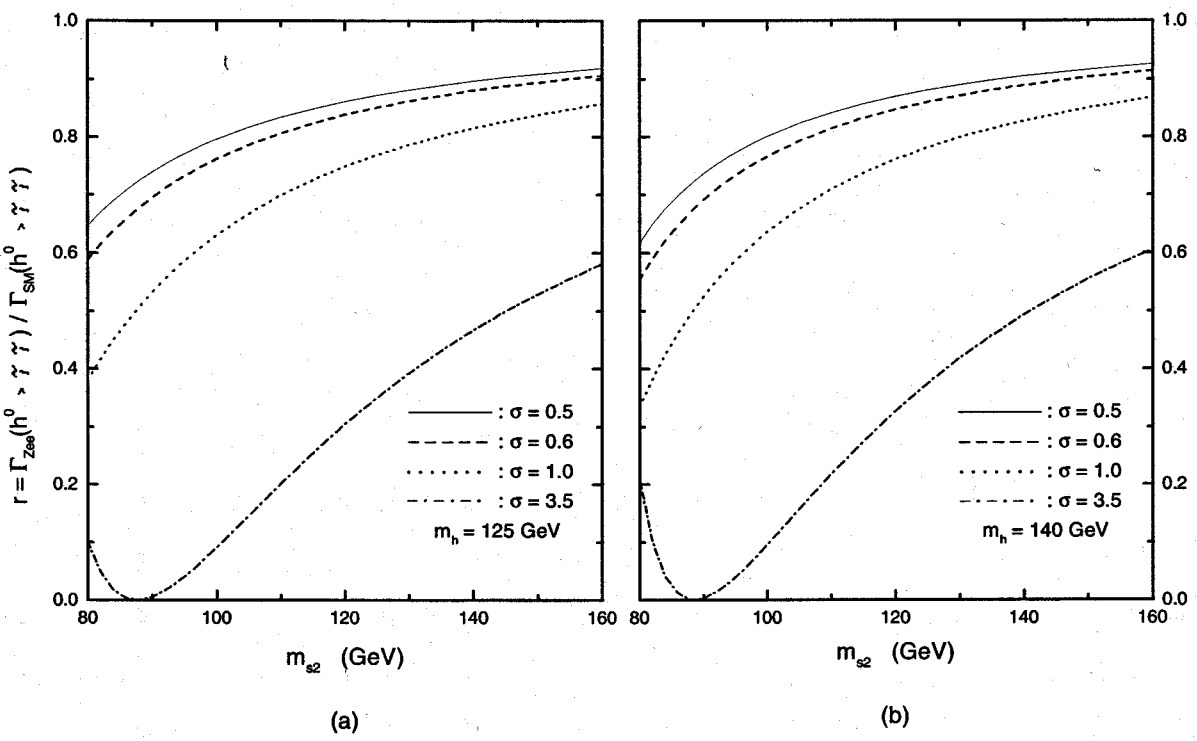

Figure 4.10: (a) The ratio r as a function of the charged Higgs boson mass m_{S_2}, for various values of the coupling constants $\sigma_1 = \sigma_2 \equiv \sigma$ and $m_h = 125$ GeV. The two smaller σ's are consistent with the cut-off scales $\Lambda = 10^{19}$ GeV and $\Lambda = 10^{16}$ GeV, respectively. The two larger σ's are allowed for $\Lambda = 10^4$ GeV. (b) A similar plot with $m_h = 140$ GeV.

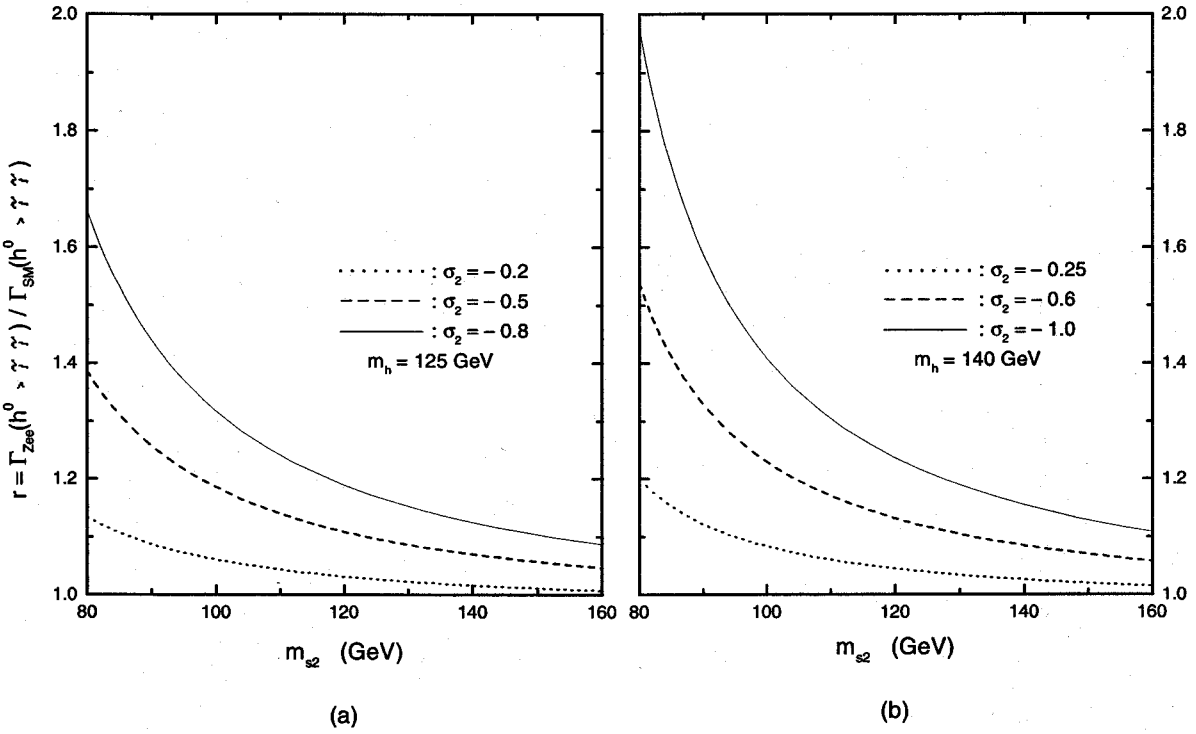

Figure 4.11: (a) The ratio r as a function of the charged Higgs boson mass m_{S_2} for negative values of the coupling constants σ_2 with $m_h = 125$ GeV, $\sigma_1 = 0$ and $\tan\beta = 16\sqrt{2}$. The value $\sigma_2 = -0.2$, -0.5 or -0.8 is consistent with the cut-off scale $\Lambda = 10^{19}$, 10^7 or 10^4 GeV, respectively. (b) A similar plot with $m_h = 140$ GeV, $\sigma_1 = 0$ and $\tan\beta = 16\sqrt{2}$. The value $\sigma_2 = -0.25$, -0.6 or -1 is consistent with the cut-off scale $\Lambda = 10^{19}$, 10^7 or 10^4 GeV, respectively.

diagram and that of the W-loop diagram have the same sign, so that r can be larger than 1. Such an example is shown in Fig. 4.11 (a), where the ratio r for $m_h = 125$ GeV is shown as a function of m_{S_2} at various negative σ_2 values with $\sigma_1 = 0$ and $\tan\beta = 16\sqrt{2}$. We consider the case with $\sigma_2 = -0.2$, -0.5 or -0.8, which is consistent with the cut-off scale $\Lambda = 10^{19}$, 10^7 or 10^4 GeV, respectively. In the case of $\Lambda = 10^{19}$ GeV (10^4 GeV), the deviation from the SM prediction can be about +6% (+30%) for $m_{S_2} = 100$ GeV. In Fig. 4.11 (b), the similar plot of the ratio r is shown for $m_h = 140$ GeV with $\sigma_1 = 0$ and $\tan\beta = 16\sqrt{2}$. Each case with $\sigma_2 = -0.25$, -0.6 or -1 is consistent with $\Lambda = 10^{19}$, 10^7 or 10^4 GeV, respectively. The correction is larger in the case with $m_h = 140$ GeV than in the case with $m_h = 125$ GeV for a given Λ. The deviation from the SM prediction can amount to about +8% (+40%) for $\Lambda = 10^{19}$ GeV (10^4 GeV) when $m_{S_2} = 100$ GeV. Larger positive corrections are obtained for smaller m_{S_2} values. Such a deviation from the SM prediction can be tested at the LHC and the LC.

Before concluding this section, we remark that if m_h is larger than $2m_{S_2}$ such that the decay mode $h \to S_2^+ S_2^-$ is open, then the total decay width of h can be largely modified from the SM prediction for large $\sigma_{1,2}$. In terms of R_{S_2}, the partial decay width of $h \to S_2^+ S_2^-$ is given by

$$\Gamma(h \to S_2^+ S_2^-) = \frac{c^2 v^2}{16\pi m_h}\sqrt{1 - \frac{4m_{S_2}^2}{m_h^2}}\,, \tag{4.43}$$

where $c^2 = (2m_{S_2}^2 R_{S_2}/v^2)^2$. In Fig. 4.12 (a), we show the partial decay width $\Gamma(h \to S_2^+ S_2^-)$ for $m_{S_2} = 80, 100, 150, 200$ GeV with $\sigma_1 = \sigma_2 = 1$, cf. Eq. (4.42), for the allowed range of m_h from 100 GeV to 500 GeV. In Fig. 4.12 (b), the total width ($\Gamma_h^{\rm total}$) of the SM Higgs boson is shown as a function of m_h for each value of m_{S_2}. This is to illustrate the possible size of the difference between the total width of the lightest CP-even Higgs boson h in the Zee-model and that of the SM Higgs boson[12]. Clearly, the impact of the $S_2^+ S_2^-$ decay channel is especially large in the small m_h region. We note that $\Gamma_h^{\rm total}(SM)$ can be determined to the accuracy of 10-20% at the LHC and the LC if $m_h < 2m_Z$, and to that of a couple of per cents if $m_h > 2m_Z$ [46]. (m_Z is the mass of the Z boson.) Hence,

[12]In doing this analysis, we have in mind a low cut-off scale $\Lambda = 10^4$ GeV, which allows a wide range of values for σ's, m_{S_2} and m_h.

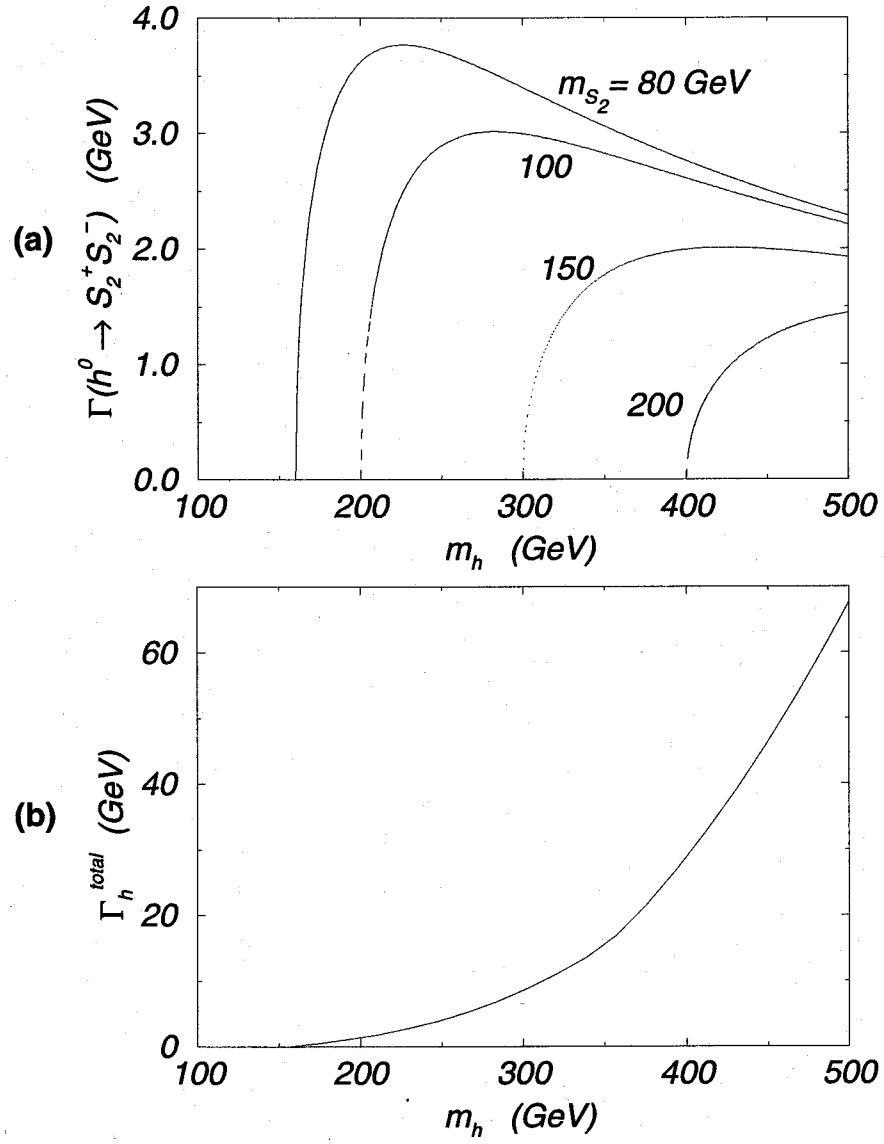

Figure 4.12: (a) The partial decay width $\Gamma(h \to S_2^+ S_2^-)$ for $m_{S_2} = 80, 100, 150, 200$ GeV with $\sigma_1 = \sigma_2 = 1$ for the allowed range of m_h from 100 GeV to 500 GeV. The total decay width of the SM Higgs boson is given in (b) just for comparison.

measuring the total decay width of the lightest neutral Higgs boson can provide further test of the Zee-model for $m_h > 2m_{S_2}$. The change in the total width of h also modifies the decay branching ratio of $h \to ZZ$, hence the Zee-model will predict a different rate of $h \to ZZ \to \mu^+\mu^-\mu^+\mu^-$ for a given m_h. (In the SM, the branching ratio of $h \to ZZ$ is about 1/3 for $m_h > 200$ GeV.) Needless to say that for $m_h > 2m_{S_2}$, the production mode of $h \to S_2^+ S_2^- \to \ell^+\ell'^-\not{E}_T$ can also be useful for testing the Zee-model. Further discussion for this possibility will be given in Chapter 5.

4.4 Phenomenology of charged-Higgs bosons

In the Zee-model, two kind of charged Higgs bosons appear. If there is no mixing between them ($\chi = 0$), the mass eigenstates $S_1^\pm$ and $S_2^\pm$ correspond to the 2HDM-like charged Higgs and the singlet Higgs $\omega^\pm$, respectively. The case with $\chi = 0$ occurs in the limit of $M^2 \gg v^2$, μ^2 and m_0^2; i.e. in the decoupling limit. The detection of $S_2^\pm$ can be a clear indication of the Zee-model. As to be shown later, its phenomenology is found to be drastically different from that of the 2HDM-like charged Higgs bosons $S_1^\pm$[47]. Here, we discuss how the effect of this extra charged boson can be explored experimentally. Throughout this section we consider only cases with $\chi = 0$, for simplicity.

The S_2^- boson decays into a lepton pair $e_i^- \overline{\nu}_{e_j}^c$ with the coupling constant f_{ij}. The partial decay rate, $\Gamma_{ij}^{S_2} = \Gamma(S_2^- \to e_i^- \overline{\nu}_{e_j}^c)$, is calculated as

$$\Gamma_{ij}^{S_2} = \frac{m_{S_2}}{4\pi} {f_{ij}}^2 \left(1 - \frac{m_{e_i}^2}{m_{S_2}^2}\right)^2, \tag{4.44}$$

and the total decay width is given by

$$\Gamma_{\text{total}}^{S_2} = \sum_{i,j=1}^{3} \Gamma_{ij}^{S_2}. \tag{4.45}$$

The life time of S_2^+, τ, is then given by the inverse of $\Gamma_{\text{total}}^{S_2}$. By taking into account the hierarchy pattern of f_{ij} in Eqs. (4.23) and (4.24) and by assuming $m_{S_2} = 100$ GeV and

$|f_{12}| = 3 \times 10^{-4}$, the total decay width and the life time can be estimated as[13]

$$\Gamma^{S_2}_{\rm total} \sim \Gamma^{S_2}_{12} + \Gamma^{S_2}_{21} \sim 1.6\,{\rm KeV}, \tag{4.46}$$

$$\tau \sim 1/\Gamma^{S_2}_{\rm total} \sim 10^{-18}{\rm sec}. \tag{4.47}$$

This corresponds that $S_2^\pm$ decay after traveling a distance of $\sim 10^{-10}$ m, which is significantly shorter than the detector scale. Therefore, $S_2^\pm$ decays promptly after its production, and can be detected at collider experiments.

The main production channel at the LEP-II experiment may be the pair production process $e^+e^- \to S_2^+ S_2^-$, similar to the production of the 2HDM-like charged Higgs boson S_1^+. The matrix-element squares for the $S_i^+ S_i^-$ production ($i = 1, 2$) are calculated as

$$\left|\mathcal{M}(e^-_{L(R)} e^+_{R(L)} \to S_i^+ S_i^-)\right|^2 = \left\{ \frac{Q_e e^2}{s} - \frac{1}{c_W^2}(I^3_{S_i} - s_W^2 Q_{S_i}) \frac{(I^3_e - s_W^2 Q_e) g^2}{s - m_Z^2} \right\}^2 s^2 \beta^2_{S_i} \sin^2\Theta, \tag{4.48}$$

where $Q_e = -1$ and $I^3_e = -\frac{1}{2}$ (0) for the incoming electron e^-_L (e^-_R); $Q_{S_i} = -1$ and $I^3_{S_i} = -\frac{1}{2}$ (0) for $i = 1$ (2); $\beta_{S_i} = \sqrt{1 - 4m^2_{S_i}/s}$, $s_W = \sin\theta_W$, $c_W = \cos\theta_W$, and Θ is the scattering angle of S_i^- in the e^+e^- center-of-mass (CM) frame whose energy is $\sqrt{s}$. For the other electron-positron helicity states ($e^-_L e^+_L$ and $e^-_R e^+_R$), the cross sections are zero. Thus the total cross section for the $S_2^+ S_2^-$ pair production is given by

$$\sigma(e^+e^- \to S_2^+ S_2^-) = \frac{1}{96\pi} e^4 \beta^3_{S_2} s \left[\left(\frac{1}{s} + \frac{s_W^2}{c_W^2} \frac{1}{s - m_Z^2} \right)^2 + \left\{ \frac{1}{s} - \left(\frac{1}{2} - s_W^2 \right) \frac{1}{c_W^2} \frac{1}{s - m_Z^2} \right\}^2 \right] \tag{4.49}$$

Hence, the production rates of S_1^- and S_2^- are different. We note that the ratio of cross sections for $S_1^+ S_1^-$ and $S_2^+ S_2^-$ production, $\sigma(e^+e^- \to S_2^+ S_2^-)/\sigma(e^+e^- \to S_1^+ S_1^-)$, is 0.8 at $\sqrt{s} = 210$ GeV assuming that the masses of $S_1^\pm$ and $S_2^\pm$ are the same. This ratio is independent of the masses of S_1^- and S_2^- for a fixed CM energy. (Only the difference between $S_1^+ S_1^- Z$ and $S_2^+ S_2^- Z$ coupling constants determines this ratio.)

The lower mass bound of the 2HDM-like charged boson $S_1^\pm$ can be obtained by studying its $\tau\nu$ and cs decay modes, completely in the same way as the charged Higgs boson search in the minimal supersymmetric standard model (MSSM) [48]. Similar experimental

[13]The size of the decay width depend on the value of f_{12}. If we take $m_{S_1} > 500$ GeV or $\mu < 100$ GeV, f_{12} can become one order of magnitude larger than 3×10^{-4}, while still being consistent with the phenomenological bounds discussed in Sec. 4.1.

constraints may be obtained for the extra charged bosons $S_2^\pm$. The situation, however, turns out to be fairly different from the $S_1^\pm$ case. First of all, decays of $S_2^\pm$ are all leptonic. Secondly, the branching ratios of various $S_2^\pm$ decays are estimated as

$$B(S_2^- \to e^- \not{E}_T) \sim 0.5, \tag{4.50}$$

$$B(S_2^- \to \mu^- \not{E}_T) \sim 0.5, \tag{4.51}$$

$$B(S_2^- \to \tau^- \not{E}_T) \sim \mathcal{O}\left(\frac{m_\mu^4}{m_\tau^4}\right) \sim 10^{-5}, \tag{4.52}$$

where we have used the relation Eqs. (4.23) and (4.24). Clearly, the branching ratio into the $\tau^- \not{E}_T$ mode is very small, so that it is not useful for detecting $S_2^\pm$ at all. This is different from the case of detecting the ordinary 2HDM-like charged Higgs boson, which preferentially decays into heavy fermion pairs (e.g. $\tau\nu$ and cs). Instead of the decay into $\tau^\pm \nu^c$, the decay into $e^\pm \nu^c$ and $\mu^\pm \nu^c$ can provide a strong constraint for the $S_2^\pm$ mass. In fact, the branching ratio for $S_2^- \to \ell^- \not{E}_T$ (ℓ^-: e^- and μ^-) is almost 100 %, so that we have $\sigma(e^+e^- \to S_2^+ S_2^- \to \ell^+\ell'^- \not{E}_T) \sim \sigma(e^+e^- \to S_2^+ S_2^-)$, where ℓ^- (ℓ'^-) represents e^- and μ^- (not τ^-). Let us compare this with the cross section $\sigma(e^+e^- \to W^+W^- \to \ell^+\ell'^- \not{E}_T) = \sigma(e^+e^- \to W^+W^-) \cdot B(W^- \to \ell^- \not{E}_T)^2$, where $B(W^- \to \ell^- \not{E}_T) = B(W^- \to e^- \not{E}_T) + B(W^- \to \mu^- \not{E}_T) \sim 21\%$. As seen in Fig. 4.13, the cross section $\sigma(e^+e^- \to S_2^+ S_2^- \to \ell^+\ell'^- \not{E}_T)$ is comparable with $\sigma(e^+e^- \to W^+W^- \to \ell^+\ell'^- \not{E}_T)$. Therefore, by examining the LEP-II data for $\ell^+\ell'^- \not{E}_T$ ($\ell^+\ell'^- = e^+e^-$, $e^\pm\mu^\mp$ and $\mu^+\mu^-$, in contrast to $\tau^+\tau^-$ for the $S_1^\pm$ case), the experimental lower bound for the $S_2^\pm$ boson can be determined. We may examine such mass lower bound from the smuon search results at the LEP experiments[49, 50] with massless neutralinos. For example, from the data of the final state $\mu^+\mu^- \not{E}_T$ accumulated at the experiments up to $\sqrt{s} = 202$ GeV[50], we can conclude that the lower mass bound of $S_2^\pm$ is likely to be 80-85 GeV for the $\chi = 0$ cases. [We note that the right-handed smuon ($\tilde{\mu}_R^\pm$) in the MSSM carries the same $SU(2) \times U(1)$ quantum number as the weak-singlet charged Higgs boson ($S_2^\pm$ for $\chi^\pm \sim 0$).]

Finally, we comment on $S_2^\pm$-production processes at hadron colliders and future LC's. At hadron colliders, the dominant production mode is the pair production through the Drell-Yan-type process. The cross sections for $p\bar{p} \to S_2^+ S_2^-$ at the Tevatron Run-II energy ($\sqrt{s} = 2$ TeV) and $pp \to S_2^+ S_2^-$ at the LHC energy ($\sqrt{s} = 14$ TeV) are shown as a function

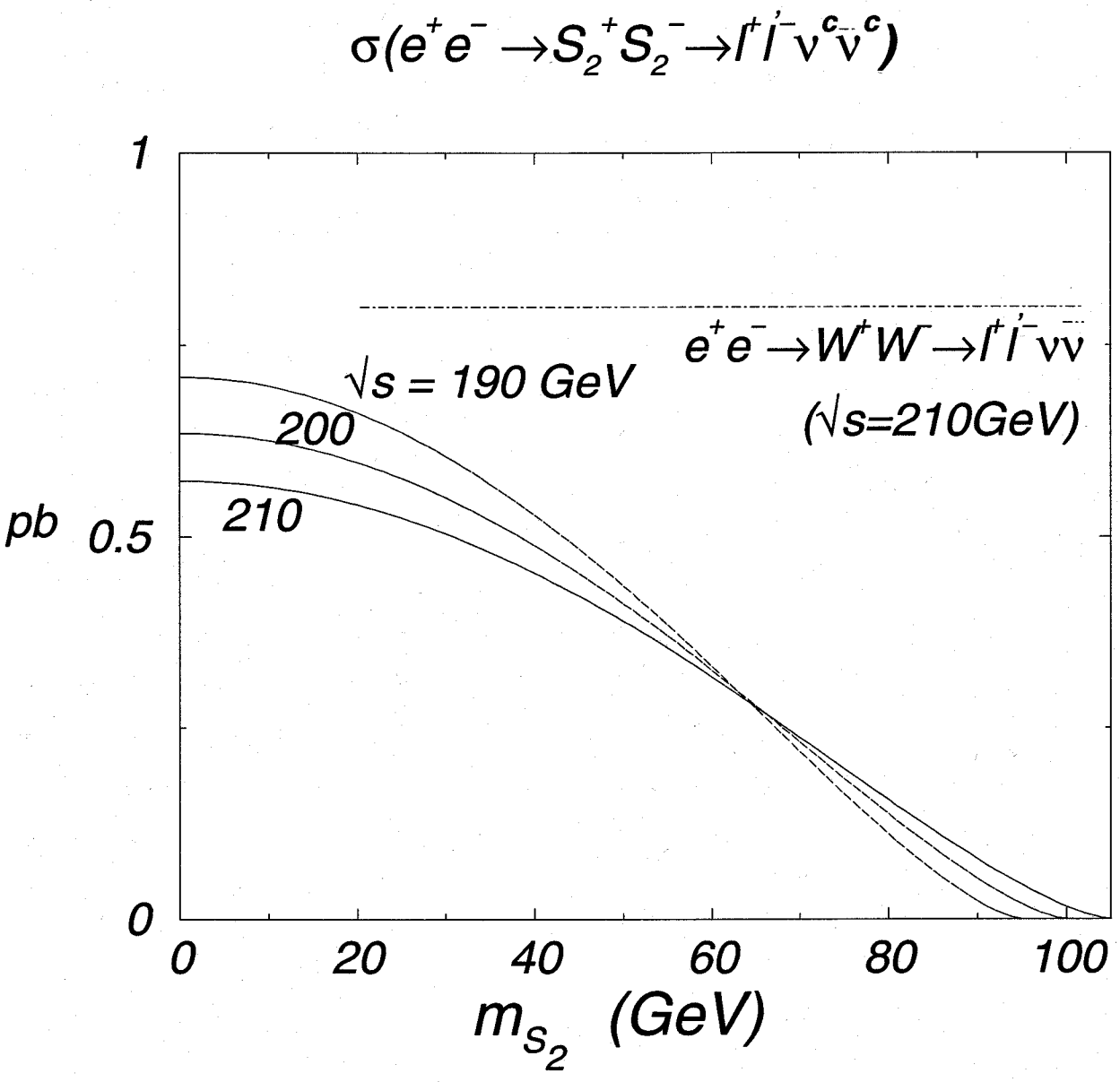

Figure 4.13: The cross section of the leptonic decay process $e^+e^- \to S_2^+S_2^- \to \ell^+\ell'^-\not{E}_T$ ($\ell\,(\ell') = e$ and μ) at $\sqrt{s} = 190$, 200, 210 GeV. The process $e^+e^+ \to W^+W^- \to \ell^+\ell'^-\not{E}_T$ at $\sqrt{s} = 210$GeV is shown for comparison.

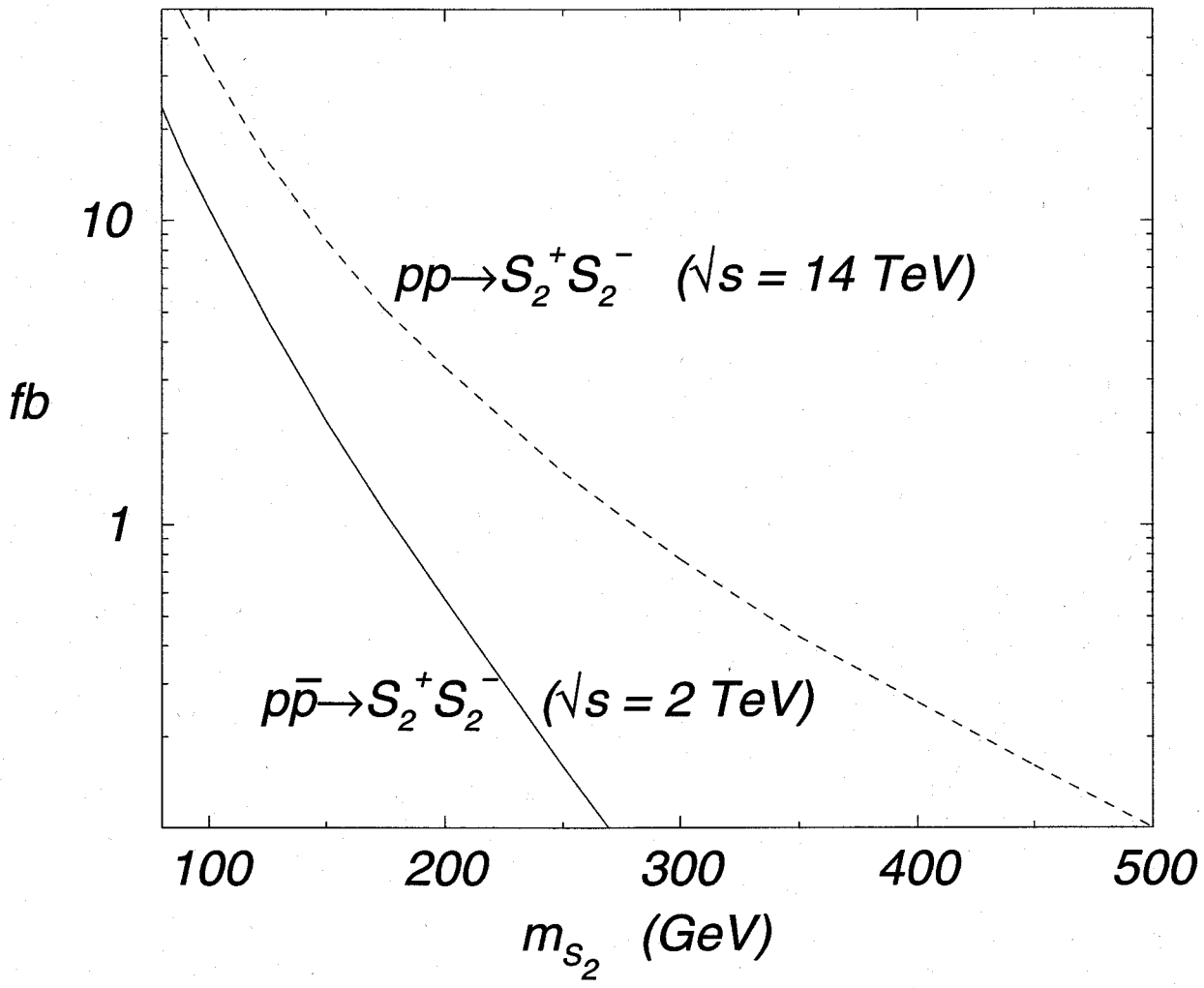

Figure 4.14: The total cross sections of $p\bar{p} \to S_2^+ S_2^-$ at $\sqrt{s} = 2$ TeV (solid curve) and $pp \to S_2^+ S_2^-$ at $\sqrt{s} = 14$ TeV (dotted curve) as a function of m_{S_2}.

of m_{S_2} in Fig. 4.14 for $\chi = 0$. At future LC's, the $S_2^\pm$ boson may be discovered through the above-discussed pair-production process from the electron-positron annihilation if $\sqrt{s}/2 > m_{S_2}$. In Fig. 4.15, we show the total cross section of $e^+e^- \to S_2^+ S_2^-$ for $\chi = 0$ as a function of m_{S_2} for $\sqrt{s} = 300$, 500, and 1000 GeV.

4.5 Summary of Zee model analysis

In this chapter, the Higgs sector of the Zee-model has been investigated, in which neutrino masses are generated radiatively. This model contains extra weak-doublet Higgs field and

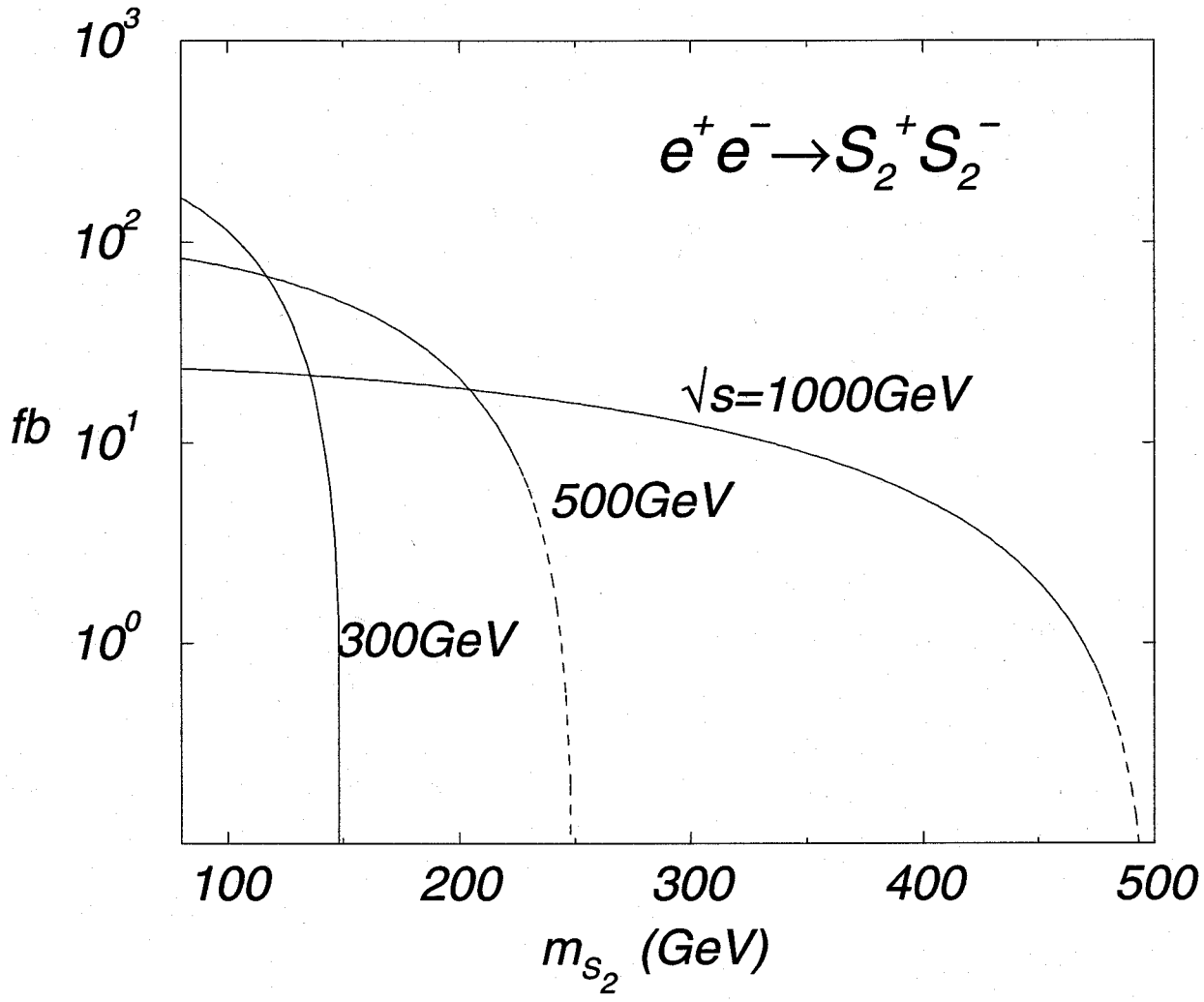

Figure 4.15: The total cross section of $e^+e^- \to S_2^+ S_2^-$ as a function of m_{S_2} at $\sqrt{s} = 300$, 500 and 1000 GeV.

singlet charged Higgs field.

We have studied indirect effects of these extra Higgs bosons on the theoretical mass bounds of the lightest CP-even Higgs boson, which are obtained from the requirement that the running coupling constants neither blow up to a very large value nor fall down to a negative value, up to a high-energy cut-off scale Λ. For $\Lambda = 10^{19}$ GeV, the upper bound of m_h is given by 175 GeV, which is almost the same value as the SM prediction. In the decoupling regime ($M \gg m_Z$), the lower bound is found to be about 100 GeV for $\Lambda = 10^{19}$ GeV, which is much smaller than the lower bound in the SM, and is almost the same as that in the 2HDM. For smaller Λ values, the bounds are more relaxed, similar to that of the SM. We have also investigated the allowed range of the coupling constants relevant to the weak-singlet Higgs field.

The most striking feature of the Zee-model Higgs sector is the existence of the weak-singlet charged Higgs boson. We have examined the possible impact of the singlet charged-Higgs boson on the neutral Higgs boson search through radiative corrections. We found that its one-loop contributions to the $h \to \gamma\gamma$ width can be sizable. In the allowed range of the coupling constants, the deviation from the SM prediction for this decay width can be +20% or near +10%, for $m_{S_2} = 100$ GeV and $\Lambda = 10^{19}$, depending on the sign of the coupling constants σ_i. The magnitude of the deviation is larger for lower Λ values or for $m_h = 125 - 140$ GeV, $m_{S_2} = 100$ GeV, and $\Lambda = 10^4$ GeV.

In the decoupling limit (i.e. when $M^2 \gg v^2$, so that $\alpha \to \beta - \pi/2$ and $\chi \to 0$), we expect that the production cross section for $gg \to h$, $e^+e^- \to \nu\bar{\nu}h$ and $e^+e^- \to Z^0h$ in the Zee-model are the same as those in the SM. However, a sizable change in the decay branching ratio of $h \to \gamma\gamma$ can alter the production rate of pp (or $p\bar{p}$) $\to hX \to \gamma\gamma X$ at the LHC, where this production rate can be determined with a relative error of 10-15% [41]. Also, such a deviation in the branching ratio of $h \to \gamma\gamma$ directly affects the cross section of $e^+e^- \to \nu\bar{\nu}h$ (and Z^0h)$\to \nu\bar{\nu}\gamma\gamma$, which can be measured with an accuracy of 16-22% at the LHC and the e^+e^- LC (with $\sqrt{s} = 500$ GeV and the integrated luminosity of 1 ab^{-1}) [42]. Therefore, the Zee-model with low cut-off scales can be tested through the $h \to \gamma\gamma$ process at the LHC and the e^+e^- LC's. At the future photon colliders, the enhancement (or reduction) of the $h \to \gamma\gamma$ partial decay rate will manifest itself in the

different production rate of h from the SM prediction. A few per cent of the deviation in $\Gamma(h \to \gamma\gamma) \cdot B(h \to b\bar{b})$ can be detected at photon collider [43], so that the effects of the singlet charged Higgs boson can be tested even if the cut-off scale Λ is at the Planck scale.

The collider phenomenology of the singlet charged Higgs boson has turned out to be completely different from that of the 2HDM-like charged Higgs boson. The singlet charged Higgs boson mainly decays into $\ell^{\pm} \not{E}_T$ (with $\ell^{\pm} = e^{\pm}$ or $\mu^{\pm}$), while the decay mode $\tau^{\pm} \not{E}_T$ is almost negligible, because of the relation $|f_{12}| \gg |f_{13}| \gg |f_{23}|$. This hierarchy among the coupling constants f_{ij} results from demanding bi-maximal mixings in the neutrino mass matrix of the Zee-model to agree with the neutrino oscillation data. On the other hand, the 2HDM-like charged Higgs boson decays mainly into either the $\tau\nu$ mode or the cs mode, through the usual Yukawa-interactions. Hence, to probe this singlet charged Higgs boson using the LEP-II data, experimentalists should examine their data sample with $e^+e^- \not{E}_T$, $e^+\mu^- \not{E}_T$, $\mu^+e^- \not{E}_T$ or $\mu^+\mu^- \not{E}_T$, while the experimental lower mass bound of the 2HDM-like charged Higgs boson is obtained from examining the $\tau\tau \not{E}_T$, $\tau \not{E}_T\, jj$ and $jjjj$ events. Using the published LEP-II constraints on the MSSM smuon production (assuming the lightest neutrinos to be massless), we estimate the current lower mass bound for this singlet charged Higgs boson to be about 80-85 GeV. The Tevatron Run-II, LHC and future LC's can further test this model.

Finally, we comment on a case in which the singlet charged Higgs boson ($S_2^{\pm}$ for $\chi = 0$) is the lightest of all the Higgs bosons. For $m_h/2 > m_{S_2} > m_Z$, the Higgs sector of the Zee-model can be further tested by measuring the production rate of pp (or $p\bar{p}$) $\to hX \to S_2^+ S_2^- X \to \ell^+\ell'^- \not{E}_T\, X$. The branching ratio for $h \to S_2^+ S_2^- \to \ell^+\ell'^- \not{E}_T$ can be large. For instance, for $m_h = 210$ GeV and $m_{S_2} = 100$ GeV, this branching ratio is about 12% for each $\ell^+\ell'^- = e^+e^-$, $e^+\mu^-$, μ^+e^- or $\mu^+\mu^-$. Moreover, the total decay width of h can be largely modified when the decay channel $h \to S_2^+ S_2^-$ is open. In this case, the decay branching ratios of $h \to W^+W^-$, ZZ are also different from the SM predictions.

In conclusion, the distinguishable features of the Zee-model from the SM and the 2HDM can be tested by the data from LEP-II, the Tevatron Run-II and future experiments at LHC and LC's.

Chapter 5

Conclusion

We have analyzed properties of the Higgs bosons in the various extensions of the SM, so that when the Higgs boson is discovered, we can test the models for the physics beyond the SM.

For each model, the allowed range of the Higgs boson mass is obtained by requiring that the running coupling constants neither blow up nor cause vacuum unstableness below Λ. In the SM, the allowed range of the Higgs boson mass is calculated as 143 - 175 GeV, if the cut-off scale is taken as the Planck scale (10^{19} GeV) and $m_t = 175$ GeV. For the MSSM the mass upper bound is less than 120 GeV. In the 2HDM, with a softly-broken discrete symmetry, while the upper bound has been found to be almost the same as in the SM, the lower bound turns out to be much reduced, because of the interaction between many Higgs fields. In the decoupling regime, the lower bounds is about 100 GeV for $\Lambda = 10^{19}$ GeV, which is lower by 40 GeV than the SM result. In the mixing regime, m_h is no longer bounded from below. The Higgs boson mass bounds of the Zee-model in which neutrino masses are generated radiatively, are almost same as those of the 2HDM. If the Higgs boson is discovered with the mass around 100 GeV at Tevatron or LHC experiment in near future and its property is quite similar to the SM Higgs boson, the 2HDM and Zee-model with very high cut-off scale are candidates of models which predict such light Higgs boson along with the MSSM and its extensions.

For the Zee-Model, the singlet charged Higgs boson can significantly modify the partial decay width of $h \to \gamma\gamma$ via radiative corrections, and its collider phenomenology can also

be drastically different from that of the charged Higgs bosons in the usual 2HDMs.

Acknowledgements

First of all, I would like to greatly thank Prof. Yasuhiro Okada, who is my supervisor. Until he lead me into the Higgs world three years ago, he have supported my work throughout. Although he is a hard worker and always busy, he have helped my work with wide and deep knowledge about the particle physics. However busy he is, He readily answer my question in detail. Also, he often encourages me with a lot of jokes.

I thank to Dr. Shinya Kanemura for his great help all over the analyses. I have collaborated with him for about three years. While he had stayed in KEK, he always cared about my work and helped me with his great knowledge about Higgs physics. Although his move to Karlsruhe was a big loss for me, he have supported me with e-mail after that.

I thank to Dr. Guey-Lin Lin, Jie-Jun Tseng and Prof. C.-P. Yuan. In the Zee-model analysis, I have collaborated with them. They know about production and decay process of the collider very much. Latter part of Zee-model analysis is made up with their great help. Also, Jie-Jun came to Japan to make sure RGE analyses.

I would like to thank Kenzo Inoue for useful comments about the 2HDM vacuum stability condition and so on.

I thank to Toru Goto and Junji Hisano. They introduced high performance alpha workstations and readied operating system, compiler and some useful tools and have managed numerical calculation environment. My numerical calculation of the RGE was depend on their work. Also they sometimes gave me comments.

Appendix A

One-loop RGE's for dimensionless coupling constants in the SM and the 2HDM

In the SM, the Higgs self-coupling constant λ_{SM}, is given by

$$16\pi^2\mu\frac{d\lambda_{SM}}{d\mu} = 24\lambda_{SM}^2 - 3\lambda_{SM}(3g^2+g'^2)+\frac{3}{4}g^4+\frac{3}{8}(g^2+g'^2)^2+12\lambda_{SM}y_t^{SM^2}-6y_t^{SM^4}. \quad \text{(A.1)}$$

The RGE's for the 2HDM Higgs couplings are [21]

$$16\pi^2\mu\frac{d\lambda_1}{d\mu} = 12\lambda_1^2+4\lambda_3^2+4\lambda_3\lambda_4+2\lambda_4^2+2\lambda_5^2-3\lambda_1(3g^2+g'^2)+\frac{3}{2}g^4+\frac{3}{4}(g^2+g'^2)^2, \quad \text{(A.2)}$$

$$16\pi^2\mu\frac{d\lambda_2}{d\mu} = 12\lambda_2^2+2\lambda_3^2+2(\lambda_3+\lambda_4)^2+2\lambda_5^2-3\lambda_2(3g^2+g'^2)+\frac{3}{2}g^4+\frac{3}{4}(g^2+g'^2)^2$$
$$+12\lambda_2y_t^2-12y_t^4, \quad \text{(A.3)}$$

$$16\pi^2\mu\frac{d\lambda_3}{d\mu} = (\lambda_1+\lambda_2)(6\lambda_3+2\lambda_4)+4\lambda_3^2+2\lambda_4^2+2\lambda_5^2+\frac{9}{4}g^4+\frac{3}{4}g'^4-\frac{3}{2}g^2g'^2$$
$$-3\lambda_3(3g^2+g'^2)+6\lambda_3y_t^2, \quad \text{(A.4)}$$

$$16\pi^2\mu\frac{d\lambda_4}{d\mu} = 2(\lambda_1+\lambda_2)\lambda_4+4(2\lambda_3+\lambda_4)\lambda_4+8\lambda_5^2+3g^2g'^2-3\lambda_4(3g^2+g'^2)+6\lambda_4y_t^2, \quad \text{(A.5)}$$

$$16\pi^2\mu\frac{d\lambda_5}{d\mu} = \lambda_5\left\{2(\lambda_1+\lambda_2)+8\lambda_3+12\lambda_4-3(3g^2+g'^2)+6y_t^2\right\}. \quad \text{(A.6)}$$

The RGE's for the gauge-coupling constants and the top-Yukawa-coupling constants are given in ref. [21].

$$\mu\frac{d}{d\mu}g_1 = \frac{1}{16\pi^2}\left(\frac{20}{9}N_g+\frac{1}{6}N_H\right)g_1^3 \quad \text{(A.7)}$$

$$\mu\frac{d}{d\mu}g_2 = \frac{1}{16\pi^2}\left(-\frac{22}{3}+\frac{4}{3}N_g+\frac{1}{6}N_H\right)g_2^3 \tag{A.8}$$

$$\mu\frac{d}{d\mu}g_3 = \frac{1}{16\pi^2}\left(-11+\frac{4}{3}N_g\right)g_3^3 \tag{A.9}$$

$$\mu\frac{d}{d\mu}y_t = \frac{1}{16\pi^2}\left\{-\left(\frac{17}{12}g_1^2+\frac{9}{4}g_2^2+8g_3^2\right)y_t+\frac{9}{2}y_t^3\right\}$$

where, N_g is the number of flavor and N_H is the number of the Higgs doublet.

Appendix B

One-loop RGE's for dimensionless coupling constants in the Zee-Model

Here, we summarize the relevant RGE's to our study. For the gauge coupling constants, we have

$$\mu\frac{d}{d\mu}g_1 = \frac{1}{16\pi^2}\frac{22}{3}g_1^3 \tag{B.1}$$

$$\mu\frac{d}{d\mu}g_2 = \frac{1}{16\pi^2}(-3)\,g_2^3 \tag{B.2}$$

$$\mu\frac{d}{d\mu}g_3 = \frac{1}{16\pi^2}(-7)\,g_3^3 \tag{B.3}$$

The RGE's for the Higgs-self-coupling constants of the doublets are calculated at one-loop level as

$$\begin{aligned}\mu\frac{d}{d\mu}\lambda_1 = \frac{1}{16\pi^2}\Big\{&12\lambda_1^2+4\lambda_3^2+4\lambda_3\lambda_4+2\lambda_4^2+2\lambda_5^2+2\sigma_1^2\\&-\left(3g_1^2+9g_2^2\right)\lambda_1+\left(\frac{3}{4}g_1^4+\frac{3}{2}g_1^2g_2^2+\frac{9}{4}g_2^4\right)\Big\}\end{aligned} \tag{B.4}$$

$$\begin{aligned}\mu\frac{d}{d\mu}\lambda_2 = \frac{1}{16\pi^2}\Big\{&12\lambda_2^2+4\lambda_3^2+4\lambda_3\lambda_4+2\lambda_4^2+2\lambda_5^2+2\sigma_2^2+12y_t^2\lambda_2-12y_t^4\\&-\left(3g_1^2+9g_2^2\right)\lambda_2+\left(\frac{3}{4}g_1^4+\frac{3}{2}g_1^2g_2^2+\frac{9}{4}g_2^4\right)\Big\}\end{aligned} \tag{B.5}$$

$$\begin{aligned}\mu\frac{d}{d\mu}\lambda_3 = \frac{1}{16\pi^2}\Big\{&2\left(\lambda_1+\lambda_2\right)\left(3\lambda_3+\lambda_4\right)+4\lambda_3^2+2\lambda_4^2+2\lambda_5^2+2\sigma_1\sigma_2+6y_t^2\lambda_3\\&-\left(3g_1^2+9g_2^2\right)\lambda_3+\left(\frac{3}{4}g_1^4-\frac{3}{2}g_1^2g_2^2+\frac{9}{4}g_2^4\right)\Big\}\end{aligned} \tag{B.6}$$

$$\mu\frac{d}{d\mu}\lambda_4 = \frac{1}{16\pi^2}\Big\{2\left(\lambda_1+\lambda_2\right)\lambda_4+4\left(2\lambda_3+\lambda_4\right)\lambda_4+8\lambda_5^2+6y_t^2\lambda_4$$

$$
\begin{aligned}
& -\left(3g_1^2+9g_2^2\right)\lambda_4+3g_1^2g_2^2\Big\} && \text{(B.7)}\\
\mu\frac{d}{d\mu}\lambda_5 &= \frac{1}{16\pi^2}\Big\{2\lambda_1+2\lambda_2+8\lambda_3+12\lambda_4+6y_t^2 \\
& -\left(3g_1^2+9g_2^2\right)\Big\}\lambda_5 && \text{(B.8)}
\end{aligned}
$$

and those with respect to the additional singlet charged Higgs are given by

$$
\begin{aligned}
\mu\frac{d}{d\mu}\sigma_1 &= \frac{1}{16\pi^2}\Big\{4\sigma_1^2+2\sigma_1\sigma_3+6\lambda_1\sigma_1+(4\lambda_3+2\lambda_4)\,\sigma_2+8f_{ij}f_{ij}\sigma_1 \\
& -\left(\frac{15}{2}g_1^2+\frac{9}{2}g_2^2\right)\sigma_1+3g_1^4\Big\} && \text{(B.9)}\\
\mu\frac{d}{d\mu}\sigma_2 &= \frac{1}{16\pi^2}\Big\{4\sigma_2^2+2\sigma_2\sigma_3+6\lambda_2\sigma_2+(4\lambda_3+2\lambda_4)\,\sigma_1+6y_t^2\sigma_2+8f_{ij}f_{ij}\sigma_2 \\
& -\left(\frac{15}{2}g_1^2+\frac{9}{2}g_2^2\right)\sigma_2+3g_1^4\Big\} && \text{(B.10)}\\
\mu\frac{d}{d\mu}\sigma_3 &= \frac{1}{16\pi^2}\Big\{8\sigma_1^2+8\sigma_2^2+5\sigma_3^2+16f_{ij}f_{ij}\sigma_3-128\,tr\,f^4 \\
& -12g_1^2\sigma_3+24g_1^4\Big\} && \text{(B.11)}
\end{aligned}
$$

Finally, the RGE's for the Yukawa-type coupling constants are obtained at one-loop level as

$$
\begin{aligned}
\mu\frac{d}{d\mu}y_t &= \frac{1}{16\pi^2}\left\{-\left(\frac{17}{12}g_1^2+\frac{9}{4}g_2^2+8g_3^2\right)y_t+\frac{9}{2}y_t^3\right\} && \text{(B.12)}\\
\mu\frac{d}{d\mu}f_{ij} &= \frac{1}{16\pi^2}\left\{-\left(\frac{3}{2}g_1^2+\frac{9}{2}g_2^2\right)f_{ij}+4f_{kl}f_{kl}f_{ij}-4f_{ik}f_{kl}f_{lj}\right\} && \text{(B.13)}
\end{aligned}
$$

where

$$
\begin{aligned}
tr\,f^4 &\equiv \sum_{i,j,k,l=1-3} f_{ij}f_{jk}f_{kl}f_{li}, \\
f_{ij}f_{ij} &\equiv \sum_{i,j=1-3} f_{ij}f_{ij}.
\end{aligned}
$$

Appendix C

Vacuum stability in the Zee-Model

Higgs potential

Higgs potential (ϕ^4 term) is written as follows.

$$V^{(4)} = \frac{\lambda_1}{2}X^2 + \frac{\lambda_2}{2}Y^2 + \frac{\sigma_3}{4}Z^2 + \overline{\lambda_3}XY + \sigma_1 XZ + \sigma_2 YZ \tag{C.1}$$

where,

$$\overline{\lambda_3} \equiv \lambda_3 + \min\left(0, \lambda_4 - \lambda_5, \lambda_4 + \lambda_5\right),$$

$$X \equiv |\phi_1|^2,\ Y \equiv |\phi_2|^2,\ Z \equiv \left|\omega^-\right|^2.$$

Using

$$\begin{cases} X = r\sin\theta\sin\varphi \\ Y = r\sin\theta\cos\varphi \\ Z = r\cos\theta \end{cases} \qquad \begin{matrix} \varphi : 0 - \frac{\pi}{2} \\ \theta : 0 - \frac{\pi}{2} \end{matrix}$$

this potential is also written as,

$$\begin{aligned} V^{(4)} \;=\; & \frac{r^2}{2}\Big\{\lambda_1 \sin^2\theta\sin^2\varphi + \lambda_2\sin^2\theta\cos^2\varphi + \frac{\sigma_3}{2}\cos^2\theta \\ & + 2\overline{\lambda_3}\sin^2\theta\sin\varphi\cos\varphi + 2\sigma_1\sin\theta\cos\theta\sin\varphi + 2\sigma_2\sin\theta\cos\theta\cos\varphi\Big\} \end{aligned} \tag{C.2}$$

Vacuum stability condition

The vacuum stability conditions is satisfied, if the quartic terms of the scalar potential do not have a negative coefficient in any direction,

$$V^{(4)}(r,\theta,\varphi) > 0. \tag{C.3}$$

By classifying into some case, we lead formulae those are independent of r, θ, φ.

1.

In the case that all of the σ_1, σ_2, $\overline{\lambda_3}$ are positive, the requirement that $V^{(4)}$ should be positive in the direction ($\cos\theta = 0$, $\cos\varphi = 0$) implies $\lambda_1 > 0$. For the direction ($\cos\theta = 0$, $\sin\varphi = 0$), the condition $\lambda_2 > 0$ is lead, and for the direction ($\sin\theta = 0$), the condition $\sigma_3 > 0$ is lead. Namely, the vacuum stability condition is lead as follows.

$$\sigma_1 > 0,\ \sigma_2 > 0,\ \overline{\lambda_3} > 0: \quad \begin{cases} \lambda_1 > 0 \\ \lambda_2 > 0 \\ \sigma_3 > 0 \end{cases} \tag{C.4}$$

2.

Next, we study the case that one of the σ_1, σ_2, $\overline{\lambda_3}$ is negative and others are positive. For example, we treat "$\sigma_1 > 0$, $\sigma_2 > 0$, $\overline{\lambda_3} < 0$" case. The $V^{(4)}$ is rewritten as

$$\begin{aligned} V^{(4)} &= \frac{r^2}{2}\left\{\lambda_1 \sin\theta\sin\varphi + \frac{\overline{\lambda_3}}{\lambda_1}\sin\theta\cos\varphi\right)^2 + \left(\lambda_2 - \frac{\overline{\lambda_3}^2}{\lambda_1}\right)\sin^2\theta\cos^2\varphi \\ &\quad + \frac{\sigma_3}{2}\cos^2\theta + 2\sigma_1\sin\theta\cos\theta\sin\varphi + 2\sigma_2\sin\theta\cos\theta\cos\varphi\Big\} > 0 \end{aligned} \tag{C.5}$$

The requirement that $V^{(4)}$ is positive for the direction ($\cos\theta = 0$, $\cos\varphi = 0$) lead the condition $\lambda_1 > 0$. for the direction ($\cos\theta = 0$, $\sin\varphi + \frac{\overline{\lambda_3}}{\lambda_1}\cos\varphi = 0$), the condition $\lambda_2 - \frac{\overline{\lambda_3}^2}{\lambda_1} > 0$ is lead, and for the direction ($\sin\theta = 0$), the condition $\sigma_3 > 0$ is lead. Namely, the vacuum stability condition is lead as follows.

$$\sigma_1 > 0,\ \sigma_2 > 0,\ \overline{\lambda_3} < 0: \quad \begin{cases} \lambda_1 > 0 \\ \lambda_2 - \frac{\overline{\lambda_3}^2}{\lambda_1} > 0 \\ \sigma_3 > 0 \end{cases} \tag{C.6}$$

By the same way, in the case "$\sigma_1 > 0,\ \sigma_2 < 0,\ \overline{\lambda_3} > 0$", the vacuum stability condition is lead as follows.

$$\sigma_1 > 0,\ \sigma_2 < 0,\ \overline{\lambda_3} > 0: \quad \begin{cases} \lambda_1 > 0 \\ \lambda_2 > 0 \\ \frac{\sigma_3}{2} - \frac{\sigma_2^2}{\lambda_2} > 0 \end{cases} \tag{C.7}$$

In the case "$\sigma_1 < 0,\ \sigma_2 > 0,\ \overline{\lambda_3} > 0$", the vacuum stability condition is lead as follows.

$$\sigma_1 < 0,\ \sigma_2 > 0,\ \overline{\lambda_3} > 0: \quad \begin{cases} \lambda_1 > 0 \\ \lambda_2 > 0 \\ \frac{\sigma_3}{2} - \frac{\sigma_1^2}{\lambda_1} > 0 \end{cases} \tag{C.8}$$

3.

Next, we study the case that two of the σ_1, σ_2, $\overline{\lambda_3}$ is negative and the other is positive. For example, we pick up "$\sigma_1 > 0,\ \sigma_2 < 0,\ \overline{\lambda_3} < 0$" case. The $V^{(4)}$ is rewritten as

$$\begin{aligned} V^{(4)} = \frac{r^2}{2}\Bigg\{\Bigg(\lambda_1 - \frac{\overline{\lambda_3}^2}{\lambda_2}\Bigg)\sin^2\theta\sin^2\varphi + \lambda_2 \quad \sin\theta\cos\varphi + \frac{\overline{\lambda_3}}{\lambda_2}\sin\theta\sin\varphi + \frac{\sigma_2}{\lambda_2}\cos\theta\Bigg)^2 \\ + \quad \frac{\sigma_3}{2} - \frac{\sigma_2^2}{\lambda_2}\Bigg)\cos^2\theta + 2 \quad \sigma_1 - \frac{\overline{\lambda_3}\sigma_2}{\lambda_2}\Bigg)\sin\theta\cos\theta\sin\varphi\Bigg\} > 0 \end{aligned} \tag{C.9}$$

This case further classified into two cases as $\sigma_1 - \frac{\overline{\lambda_3}\sigma_2}{\lambda_2}$ is positive or negative.

3-1.

First, we study $\sigma_1 - \frac{\overline{\lambda_3}\sigma_2}{\lambda_2} > 0$ case. For the direction ($\cos\theta = 0,\ \cos\varphi + \frac{\overline{\lambda_3}}{\lambda_2}\sin\varphi = 0$), the vacuum stability condition $\lambda_1 - \frac{\overline{\lambda_3}^2}{\lambda_2} > 0$ is lead, the direction ($\cos\theta = 0,\ \sin\varphi = 0$), the condition $\lambda_2 > 0$ is lead. For the direction ($\sin\theta\cos\varphi + \frac{\sigma_2}{\lambda_2}\cos\theta = 0,\ \sin\varphi = 0$), the vacuum stability condition $\frac{\sigma_3}{2} - \frac{\sigma_2^2}{\lambda_2} > 0$ is lead. Namely, the vacuum stability condition is as follows.

$$\sigma_1 > 0,\ \sigma_2 < 0,\ \overline{\lambda_3} < 0,\ \sigma_1 - \frac{\overline{\lambda_3}\sigma_2}{\lambda_2} > 0: \quad \begin{cases} \lambda_1 - \frac{\overline{\lambda_3}^2}{\lambda_2} > 0 \\ \lambda_2 > 0 \\ \frac{\sigma_3}{2} - \frac{\sigma_2^2}{\lambda_2} > 0 \end{cases} \tag{C.10}$$

3-2.

Second, for the case $\sigma_1 - \frac{\overline{\lambda_3}\sigma_2}{\lambda_2} < 0$, we transform $V^{(4)}$ as

$$
\begin{aligned}
V^{(4)} \;=\; & \frac{r^2}{2}\left\{\left(\lambda_1 - \frac{\overline{\lambda_3}^2}{\lambda_2}\right)\left(\sin\theta\sin\varphi + \frac{\sigma_1 - \frac{\overline{\lambda_3}\sigma_2}{\lambda_2}}{\lambda_2 - \frac{\overline{\lambda_3}^2}{\lambda_2}}\cos\theta\right)^2\right. \\
& +\lambda_2\left(\sin\theta\cos\varphi + \frac{\overline{\lambda_3}}{\lambda_2}\sin\theta\sin\varphi + \frac{\sigma_2}{\lambda_2}\cos\theta\right)^2 \\
& \left.+\left(\frac{\sigma_3}{2} - \frac{\sigma_2^2}{\lambda_2} - \frac{\left(\sigma_1 - \frac{\overline{\lambda_3}\sigma_2}{\lambda_2}\right)^2}{\lambda_1 - \frac{\overline{\lambda_3}^2}{\lambda_2}}\right)\cos^2\theta\right\} > 0. \qquad \text{(C.11)}
\end{aligned}
$$

For the direction ($\cos\theta = 0$, $\cos\varphi + \frac{\overline{\lambda_3}}{\lambda_2}\sin\varphi = 0$), the vacuum stability condition $\lambda_1 - \frac{\overline{\lambda_3}^2}{\lambda_2} > 0$ is lead. For the direction ($\cos\theta = 0$, $\sin\varphi = 0$), the condition $\lambda_2 > 0$ is lead. For the direction ($\sin\theta\sin\varphi + \frac{\sigma_1 - \frac{\overline{\lambda_3}\sigma_2}{\lambda_2}}{\lambda_2 - \frac{\overline{\lambda_3}^2}{\lambda_2}}\cos\theta = 0$, $\sin\theta\cos\varphi + \frac{\overline{\lambda_3}}{\lambda_2}\sin\theta\sin\varphi + \frac{\sigma_2}{\lambda_2}\cos\theta = 0$), the condition $\frac{\sigma_3}{2} - \frac{\sigma_2^2}{\lambda_2} - \frac{\left(\sigma_1 - \frac{\overline{\lambda_3}\sigma_2}{\lambda_2}\right)^2}{\lambda_1 - \frac{\overline{\lambda_3}^2}{\lambda_2}} > 0$ is lead. Namely, vacuum stability condition is lead as follows.

$$
\sigma_1 > 0,\ \sigma_2 < 0,\ \overline{\lambda_3} < 0,\ \sigma_1 - \frac{\overline{\lambda_3}\sigma_2}{\lambda_2} < 0: \quad \begin{cases} \lambda_1 - \frac{\overline{\lambda_3}^2}{\lambda_2} > 0 \\ \lambda_2 > 0 \\ \frac{\sigma_3}{2} - \frac{\sigma_2^2}{\lambda_2} - \frac{\left(\sigma_1 - \frac{\overline{\lambda_3}\sigma_2}{\lambda_2}\right)^2}{\lambda_1 - \frac{\overline{\lambda_3}^2}{\lambda_2}} > 0 \end{cases} \qquad \text{(C.12)}
$$

By the same way, for the case "$\sigma_1 < 0$, $\sigma_2 > 0$, $\overline{\lambda_3} < 0$", the vacuum stability condition is lead.

$$
\sigma_1 < 0,\ \sigma_2 > 0,\ \overline{\lambda_3} < 0,\ \sigma_2 - \frac{\overline{\lambda_3}\sigma_1}{\lambda_1} > 0: \quad \begin{cases} \lambda_1 > 0 \\ \lambda_2 - \frac{\overline{\lambda_3}^2}{\lambda_1} > 0 \\ \frac{\sigma_3}{2} - \frac{\sigma_1^2}{\lambda_1} > 0 \end{cases} \qquad \text{(C.13)}
$$

$$
\sigma_1 < 0,\ \sigma_2 > 0,\ \overline{\lambda_3} < 0,\ \sigma_2 - \frac{\overline{\lambda_3}\sigma_1}{\lambda_1} < 0: \quad \begin{cases} \lambda_1 > 0 \\ \lambda_2 - \frac{\overline{\lambda_3}^2}{\lambda_1} > 0 \\ \frac{\sigma_3}{2} - \frac{\sigma_1^2}{\lambda_1} - \frac{\left(\sigma_2 - \frac{\overline{\lambda_3}\sigma_1}{\lambda_1}\right)^2}{\lambda_2 - \frac{\overline{\lambda_3}^2}{\lambda_1}} > 0 \end{cases} \qquad \text{(C.14)}
$$

For the case "$\sigma_1 < 0,\ \sigma_2 < 0,\ \overline{\lambda_3} > 0$", the vacuum stability condition is lead.

$$\sigma_1 < 0,\ \sigma_2 < 0,\ \overline{\lambda_3} > 0,\ \overline{\lambda_3} - \frac{2\sigma_1\sigma_2}{\sigma_3} > 0 : \quad \begin{cases} \lambda_1 - \frac{2\sigma_1^2}{\sigma_3} > 0 \\ \lambda_2 - \frac{2\sigma_2^2}{\sigma_3} > 0 \\ \sigma_3 > 0 \end{cases} \tag{C.15}$$

$$\sigma_1 < 0,\ \sigma_2 < 0,\ \overline{\lambda_3} > 0\ \overline{\lambda_3} - \frac{2\sigma_1\sigma_2}{\sigma_3} < 0 : \quad \begin{cases} \lambda_1 - \frac{2\sigma_1^2}{\sigma_3} > 0 \\ \lambda_2 - \frac{2\sigma_2^2}{\sigma_3} - \frac{\left(\overline{\lambda_3} - \frac{2\sigma_1\sigma_2}{\sigma_3}\right)^2}{\lambda_1 - \frac{2\sigma_1^2}{\sigma_3}} > 0 \\ \sigma_3 > 0 \end{cases} \tag{C.16}$$

4.

If all of σ_1, σ_2, $\overline{\lambda_3}$ are negative, the vacuum stability condition is lead by the same way as in one of above three case that two of σ_1, σ_2, $\overline{\lambda_3}$ are negative, i.e. "$\sigma_1 > 0,\ \sigma_2 < 0,\ \overline{\lambda_3} < 0$", "$\sigma_1 < 0,\ \sigma_2 > 0,\ \overline{\lambda_3} < 0$" or "$\sigma_1 < 0,\ \sigma_2 < 0,\ \overline{\lambda_3} > 0$". The conditions from above three ways are identical.

The formulae of vacuum stability condition

Collecting those conditions, the vacuum stability condition at energy scale Q in the Zee-model is rewritten as follows.

1.

$$\lambda_1(Q) > 0, \quad \lambda_2(Q) > 0, \quad \sigma_3(Q) > 0\,. \tag{C.17}$$

2.

$$\sigma_1(Q) + \sqrt{\frac{\lambda_1(Q)\,\sigma_3(Q)}{2}} > 0\,, \tag{C.18}$$

$$\sigma_2(Q) + \sqrt{\frac{\lambda_2(Q)\,\sigma_3(Q)}{2}} > 0\,, \tag{C.19}$$

$$\overline{\lambda}(Q) + \sqrt{\lambda_1(Q)\,\lambda_2(Q)} > 0\,, \tag{C.20}$$

where $\overline{\lambda}(Q) = \lambda_3(Q) + \min(0,\ \lambda_4(Q) + \lambda_5(Q),\ \lambda_4(Q) - \lambda_5(Q))$.

3. If $\sigma_1(Q) < 0$ and $\sigma_2(Q) < 0$, then

$$\overline{\lambda}(Q) + \frac{2}{\sigma_3(Q)} \left\{ \sqrt{\left(\frac{\lambda_1(Q)\,\sigma_3(Q)}{2} - \sigma_1^2(Q) \right) \left(\frac{\lambda_2(Q)\,\sigma_3(Q)}{2} - \sigma_2^2(Q) \right)} - \sigma_1(Q)\,\sigma_2(Q) \right\} > 0\,. \tag{C.21}$$

If $\sigma_1(Q) < 0$ and $\overline{\lambda}(Q) < 0$, then

$$\sigma_2(Q) + \frac{1}{\lambda_1(Q)} \left\{ \sqrt{\left(\lambda_1(Q)\,\lambda_2(Q) - \overline{\lambda}^2(Q) \right) \left(\frac{\lambda_1(Q)\,\sigma_3(Q)}{2} - \sigma_1^2(Q) \right)} - \sigma_1(Q)\,\overline{\lambda}(Q) \right\} > 0\,. \tag{C.22}$$

If $\sigma_2(Q) < 0$ and $\overline{\lambda}(Q) < 0$, then

$$\sigma_1(Q) + \frac{1}{\lambda_2(Q)} \left\{ \sqrt{\left(\lambda_1(Q)\,\lambda_2(Q) - \overline{\lambda}^2(Q) \right) \left(\frac{\lambda_2(Q)\,\sigma_3(Q)}{2} - \sigma_2^2(Q) \right)} - \sigma_2(Q)\,\overline{\lambda}(Q) \right\} > 0\,. \tag{C.23}$$

[When all of $\sigma_1(Q)$, $\sigma_2(Q)$ and $\overline{\lambda}(Q)$ are negative, above three conditions are equivalent.]

Bibliography

[1] S. Weinberg, *Phys. Rev. Lett.* **19** (1967) 1264.

[2] ALEPH Collabolation, PLB **487** (2000) 253; S. Jin, a talk given at ICHEP 2000, http://ichep2000.hep.sci.osaka-u.ac.jp/scan/0728/pa11/jin/index.html

[3] "Report of the Higgs Working Group" from the Physics at Run II Supersymmetry/Higgs Workshop, (hep-ph/0010338).

[4] CMS Technical Proposal, CERN/LHCC/94-38 (1994); ATLAS Technical Proposal, CERN/LHCC/94-93 (1994); ATLAS Technical Design Report, CERN/LHCC/99-15 (1999).

[5] N. Cabibbo, L. Maiani, G. Parisi and R. Petronzio, *Nucl. Phys.* B **158** (1976) 295; M. Lindner, *Z. Phys.* C **31** (1986) 295.

[6] Y. Okada, M. Yamaguchi and T. Yanagida, *Prog. Theor. Phys.* **85** (1991) 1; J. Ellis, G. Ridolfi and F. Zwirner, *Phys. Lett.* B **257** (1991) 83; H.E. Haber and R. Hempfling, *Phys. Rev. Lett.* **66** (1991) 1815.

[7] Y. Okada, M. Yamaguchi and T. Yanagida, *Phys. Lett.* B **262** (1991) 54; H.E. Haber and R. Hempfling, *Phys. Rev.* D **48** (1993) 4280.

[8] R. Hempfling and A. Hoang, *Phys. Lett.* B **331** (1994) 99; M. Carena, J.R. Espinosa, M. Quirós and C.E.M. Wagner, *Phys. Lett.* B **355** (1995) 209; M. Carena, M. Quirós and C.E.M. Wagner, *Nucl. Phys.* B **461** (1996) 407; H. Haber, R. Hempfling and A. Hoang, *Z. Phys.* C **75** (1997) 539; S. Heinemeyer, W. Hollik and G. Weiglein, KA-TP-17-1998, DESY 98-194, CERN-TH/98-405, (hep-ph/9812472).

[9] M. Drees, *Int. J. Mod. Phys.* A **4** (1989) 3635; J. Ellis, J.F. Gunion, H.E. Haber, L. Roszkowski and F. Zwirner, *Phys. Rev.* D **39** (1989) 844; L. Durand and J.L. Lopez, *Phys. Lett.* B **217** (1989) 463; J.R. Espinosa and M. Quirós, *Phys. Lett.* B **279** (1992) 92; P. Binétruy and C.A. Savoy, *Phys. Lett.* B **277** (1992) 453; T. Moroi and Y. Okada, *Phys. Lett.* B **295** (1992) 73; G. Kane, C. Kolda and J. Wells, *Phys. Rev. Lett.* **70** (1993) 2686; W.T.A. ter Veldhuis, Purdue preprint, PURD-TH-92-11; J.R. Espinosa and M. Quirós, *Phys. Lett.* B **302** (1993) 51; U. Ellwanger,*Phys. Lett.* B **303** (1993) 271; P.N. Pandita,*Phys. Lett.* B **318** (1993) 338; *Z. Phys.* C **59** (1993) 575; T. Elliot, S.F. King and P.L. White, *Phys. Lett.* B **305** (1993) 71; *Phys. Rev.* D **49** (1994) 4435.

[10] S. Kanemura, T. Kasai, Y. Okada, *Phys. Lett.* B **471** (1999) 182.

[11] S. Kanemura, T. Kasai, G.-L. Lin, Y. Okada, J.J. Tseng, and C.-P. Yuan, (hep-ph/0011357).

[12] A. Zee, *Phys. Lett.* B **93** (1980) 339; *Phys. Lett.* B **161** (1985) 141.

[13] P. Higgs, *Phys. Rev. Lett.* **12** (1964) 132; P. Higgs, *Phys. Rev. Lett.* **13** (1964) 508.

[14] Y. Nambu and G. Jona-Lasinio, *Phys. Rev.* **122** (1961) 345; Y. Nambu and G. Jona-Lasinio, *Phys. Rev.* **124** (1961) 246.

[15] The LEP Electroweak Working Group, http://www.cern.ch/LEPEWWG/

[16] J. Ellis, S. Kelley, D. Nanopoulos *Phys. Lett.* B2601311991; U. Amaldi, W. Boer, H. Fürstenau, *Phys. Lett.* B2604471991; P. Langacker, M. Luo, *Phys. Rev.* D448171991.

[17] J.F. Gunion, H.E. Haber, G. Kane and S. Dawson, *The Higgs Hunter's Guide*, Addison-Wesley Publishing Company, New York, (1990).

[18] S. Glashow and S. Weinberg, *Phys. Rev.* D **15** (1977) 1958.

[19] D. Kominis and R.S. Chivukula, *Phys. Lett.* B **304** (1993) 152.

[20] S. Kanemura, T. Kubota and E. Takasugi, *Phys. Lett.* B **313** (1993) 155.

[21] H. Komatsu, *Prog. Theor. Phys.* **67** (1982) 1177.

[22] R.A. Flores and M. Sher, *Ann. Phys. (NY)* **148** (1983) 295.

[23] M. Sher, *Phys. Rep.* **179** (1989) 273; S. Nie and M. Sher, *Phys. Lett.* B **449** (1999) 89.

[24] A. Akeroyd, A. Arhrib, E. Naimi, FR-HEP-00-06, KEK-TH-00-699, KEK-TH-699, hep-ph/0006035.

[25] J. Preskill, S.P. Trivedi, and F. Wilczek, *Nucl. Phys.* B **363** (1991) 207.

[26] T. Appelquist and J. Carrazone, *Phys. Rev.* D **11** (1975) 2856.

[27] S. Kanemura and H-A. Tohyama, *Phys. Rev.* D **57** (1998) 2949; S. Kanemura, KEK Preprint 97-160, (hep-ph/9710237).

[28] K. Inoue, A. Kakuto and Y. Nakano, *Prog. Theor. Phys.* **63** (1980) 234.

[29] S. Bertolini, *Nucl. Phys.* B **272** (1986) 77; W. Hollik, *Z. Phys.* C **32** (1986) 291.

[30] K. Hagiwara, D. Haidt and S. Matsumoto, *Eur. Phys.* C **2** (1998) 95.

[31] CLEO Collaboration, CLEO CONF 98-17, ICHEP98 1011.

[32] M. Ciuchini, G. Degrassi, P. Gambini and G.F. Giudice, *Nucl. Phys.* B **527** (1998) 21; P. Ciafaloni, A. Romanino and A. Strumia, *Nucl. Phys.* B **524** (1998) 361; F. Borzumati and G. Greub, *Phys. Rev.* D **58** (1998) 074004; T.M. Aliev and E.O. Iltan, *Phys. Rev.* D **58** (1998) 095014.

[33] G. Altarelli and I. Ishidori, *Phys. Lett.* B **337** (1994) 141; J.A. Casas, J.R. Espinosa, and M. Quirós, *Phys. Lett.* B **342** (1995) 171; *ibid.* B **382** (1996) 374; J.R. Espinosa and M. Quirós, *Phys. Lett.* B **353** (1995) 257; M. Quirós, IEM-FT-153/97, in *Perspectives on Higgs Physics II, Ed. G.L. Kane*, World Scientific, Singapore; T. Hambye and K. Riesselmann, *Phys. Rev.* D **55** (1997) 7255.

[34] Super-Kamiokande Collaboration, Y. Fukuda et al., *Phys. Rev. Lett.* **81** (1998) 1562.

[35] S.T. Petcov, *Phys. Rev.* D **115** (1982) 401; J. Liu, *Phys. Lett.* B **216** (1989) 367; B.K. Pal, *Phys. Rev.* D **44** (1991) 2261; W. Grimus, and G. Nardulli, *Phys. Lett.* B **271** (1991) 161; A.Y. Smirnov and Z.-J. Tao, *Nucl. Phys.* B **426** (1994) 415; P.H. Frampton and S.L. Glashow, *Phys. Lett.* B **461** (1999) 95; G.C. McLaughlin and J.N. Ng, *Phys. Lett.* B **464** (1999) 232; A.S. Jaurabh and S.D. Rindani, *Phys. Lett.* B **464** (1999) 239; K. Cheung, O.C.W. Kong, *Phys. Rev.* D **61** (2000) 113012; K. Cheung, O.C.W. Kong, (hep-ph/0003276); Y. Koide and A. Ghosal, *Phys. Rev.* D **63** (2001) 037301.

[36] C. Jarlskog, M. Matsuda, S. Skadhauge, M. Tanimoto, *Phys. Lett.* B **449** (1999) 240.

[37] C. Jarlskog, M. Matsuda, S. Skadhauge, M. Tanimoto, (hep-ph/0005147).

[38] A.Yu. Smirnov, M. Tanimoto, *Phys. Rev.* D **55** (1997) 1665.

[39] G.C. McLaughlin and J.N. Ng, *Phys. Lett.* B **455** (1999) 224.

[40] J. Casas, V. Clemente, A. Ibarra, M. Quirós, *Phys. Rev.* D **62** (2000) 053005.

[41] D. Zeppenfeld, R. Kinnunen, A. Nikitenko, and E. Richiter-Was, *Phys. Rev.* D **62** (2000) 013009.

[42] E. Boos, J.-C. Brient, D.W. Reid, H.J. Schreiber, and R. Schanidze, hep-ph/0011366; Rick van Kooten, Talk at the Berkley Linear Collider Meeting in March 2000 (http://needmore.physics.indiana.edu/~rickv/nlc/talks/Berkeley_2000/Berkeley_2000.html)

[43] M. Melles, Talk given at LCWS 2000 (Fermilab, October 2000), hep-ph/0012195.

[44] Z. Maki, M. Nakagawa and S. Sakata, *Prog. Theor. Phys.* **28** (1962) 870.

[45] H.E. Haber and H.E. Logan, *Phys. Rev.* D **62** (2000) 015011.

[46] V. Drollinger and A. Sopczak, hep-ph/0102342.

[47] S. Kanemura, T. Kasai, G.-L. Lin, Y. Okada, J.J. Tseng, and C.-P. Yuan, (hep-ph/0010233).

[48] C. Tully, LEPC Seminar – September 5, 2000,
http://lephiggs.web.cern.ch/LEPHIGGS/talks/.

[49] M. Dima, talk given at LCWS 2000 (Fermilab, October 2000)
http://www-lc.fnal.gov/lcws2000/;
The ALEPH collaboration, *Phys. Lett.* B **407** (1997) 377.

[50] M. Antonelli, talk given at ICHEP 2000 (Osaka Japan, July-August 2000)
http://ichep2000.hep.sci.osaka-u.ac.jp/.